Electronic Thesis and Dissertation Repository

12-4-2020 9:00 AM

Evidence of an Antigen Presenting Cell Phenotype in Granular Cell Tumours

Benjamin J W A Rogala, *The University of Western Ontario*

Supervisor: Darling, Mark, *The University of Western Ontario*
Joint Supervisor: Khan, Zia, *The University of Western Ontario*
Co-Supervisor: Lapointe, Henry, *The University of Western Ontario*
A thesis submitted in partial fulfillment of the requirements for the Master of Science degree in Pathology
© Benjamin J W A Rogala 2020

Follow this and additional works at: https://ir.lib.uwo.ca/etd

Part of the Oral Biology and Oral Pathology Commons

Abstract

Granular Cell Tumours (GCTs) are rare subepithelial lesions that are believed to develop from Schwann cells and are characterized by large polygonal cells with abundant lysosomes. Pilot studies from our laboratory showing unexpected HLA-DR immunoreactivity in GCTs lead us to hypothesize that GCTs have an antigen presenting cell (APC) phenotype.

To test our hypothesis, we assessed immunoreactivity of GCT lesions to APC phenotype markers, including CD68, HLA-DR, CD163, CD40 and CD11c. In addition, we assessed markers of neural crest cell (NCC) origin S100, SOX10, NSE and GAP43. Samples subjected to these studies included 23 cases of GCTs and 10 cases of Schwannomas, used as comparators. To confirm the key findings, we detected transcript levels of select genes using quantitative polymerase chain reaction..

We identified a new NCC marker for GCTs, GAP43. We also provide evidence of an APC phenotype of GCTs, as determined from CD68 and HLA-DR immunoreactivity. Due to the limited nucleic acid yield from paraffin-embedded GCT sections, we were unable to draw conclusions from transcript assessment.

Keywords: Granular Cell Tumour, Schwannoma, S100, SOX10, Neuron Specific Enolase, GAP43, HLA-DR, CD68, CD163, CD40, CD11c, SOX2, SOX9, Nestin, GFAP, beta-Tubulin-3, and beta-actin, NF

Summary for Lay Audience

Granular Cell tumours (GCT) are rare benign nodular lesions that develop in the connective tissue below the skin. Our current understanding is that these tumours develop from tissue-supporting cell types called Schwann cells. Schwann cells support the peripheral nervous system. Based on pilot work completed in our lab, GCTs appear express a protein that is commonly found on immune cells. Based on these studies, we hypothesized that the cells making up GCTs have a cellular appearance or behaviour similar to cells in the body whose job is to identify foreign material, such as bacteria or viruses. To test our hypothesis, we obtained tumour tissues and examined whether these tissues express other proteins that would strengthen an immune cell-like property. We were able to identify one additional protein that is primarily found in immune cells: CD68. A panel of other proteins tested were not found. While there are similarities in the appearance of the granular cells and immune cells, the evidence is not conclusive. One key finding, however, is that GCTs express a new protein called GAP43 which is important in the growth of new nerves and is found in Schwann cells following nerve injury. The presence of GAP43 protein in the granular cells of GCTs provides strong evidence that GCTs develop from Schwann cells. Future studies from our lab will focus on whether granular cells are more like mature or immature Schwann cells.

Dedication

I dedicate this thesis to my wife Jennifer and son Griffin

Acknowledgments

I would like to acknowledge all of those who made this thesis possible. I am grateful to my supervisor Dr. Mark Darling and co-supervisors Dr. Zia Khan and Dr. Henry Lapointe. I would also like to acknowledge the other members of my thesis committee Dr. Christina McCord and Dr. Brett Wehrli for their valuable input. Lisa Jackson-Boeters made this thesis possible with her technical support. I would also like to thank Meera Shah who assisted me with the IHC investigations during her honours thesis. Funding support was obtained from the Canadian Association of Oral and Maxillofacial Surgery through their resident research grant program. Finally I would like to thank my wife Jennifer who has supported me through this endeavor.

TABLE OF CONTENTS

List of Tables

List of Figures

List of Abbreviations:

(abbreviations are in alphabetical order)

APC	Antigen presenting cells
β-Tub3	Beta Tubulin-III
BDNF	Brain-derived neurotrophic factor
BPNST	Benign peripheral nerve sheath tumour
Caspr	Contactin-associated protein, also known as Paranodin
cDNA	Complimentary DNA
CD68	Cluster of differentiation-68, also known as Macrosialin
CEN	Congenital Epulis of newborn
CGOT	Central Granular Cell Odontogenic Tumour
CT	Computerized tomography
FFPE	Formalin-fixed, paraffin-embedded
GAP	GTPase-activating/accelerating protein
GAP43	Growth associated protein 43
GCA	Granular Cell Ameloblastoma
GCAF	Granular Cell Ameloblastic Fibroma
GCT	Granular Cell Tumour
GFAP	Glial fibrillary acidic protein
H&E	Hematoxylin and eosin
HLA-DR	Human leukocyte antigen – DR isotype
IHC	Immunohistochemistry
Krox20	Zinc-finger transcription factor
LAMP	Lysosomal-associated membrane protein
M-GCT	Malignant Granular Cell Tumour

merlin	Moesin-ezrin-radixin-like protein
MPNST	Malignant peripheral nerve sheath tumours
MRI	Magnetic resonance imaging
NC	Neural crest
NCAM	Neural cell adhesion molecule
NCC	Neural crest cell
NF	Neurofibroma
NF1	Neurofibromatosis type 1
NF2	Neurofibromatosis type 2
NGF	Nerve growth factor
NRG-1	Neuregulin-1
NSE	Neuron specific enolase
NTC	No Template Control
PAS	Neural cell adhesion molecule
PNST	Peripheral nerve sheath tumour
PTPN11	protein tyrosine phosphatase non-receptor type-11
P0	Myelin protein 0
P2	Myelin protein 2
p75^{NTR}	protein 75 low affinity nerve growth factor receptor /neurotrophin receptor
RSC	Repair Schwann cell
RT-qPCR	Reverse Transcriptase Quantitative Polymerase Chain Reaction
SC	Schwann cell
SCC	Squamous Cell Carcinoma
SCP	Schwann cell precursor
SHP-2	Src homology region 2-containing protein tyrosine phosphatase-2
V-ATPase	Vacuolar H+-ATPase
WHO	World Health Organization

<div align="center">

Chapter 1

</div>

1.0   Introduction

Granular Cell Tumours (GCTs) are thought to be derived from cells originating from the neural crest, specifically Schwann cells. While there is a body of evidence to support a neural crest origin for GCTs, little has been done to explore the granular appearance of GCTs. A serendipitous discovery in our lab of a case of GCT that stained for Human Leukocyte Antigen – DR isotype (HLA-DR) during an investigation of Langerhans cell lesions of the tongue, led us to theorize that GCTs granular appearance is an Antigen Presenting Cell (APC) phenotype.   In the introduction I will provide a comprehensive review of our current understanding of GCT tumorigenesis, neural crest cell embryology and differentiation to Schwann cells, and provide a review of our current understanding of Schwann cell derived benign peripheral nerve sheath tumours. I will also introduce and discuss the experimental setup and the rationale behind specific markers investigated.

1.1.0 Granular cell tumours

Granular cell tumours (GCT) are relatively rare soft tissue lesions whose etiology has been a focus of interest for many years. The current understanding is that the granular cells of GCTs originate from Schwann cells (SCs), based primarily on the immunohistochemistry profile of GCT and Schwannomas. In this chapter I will review the epidemiology and current understanding of GCT origin and tumourigenesis with a focus on intraoral lesions.

1.1.1 Epidemiology of Granular cell tumours

Granular cell tumours are relatively uncommon sub-epithelial entities usually presenting as a solitary benign lesion; however multifocal and malignant cases are reported[1]. It is estimated that 50% of all GCTs occur in the head and neck region, with the tongue being the most common site representing 23 to 28% of all lesions and 65 to 85% of intraoral lesions[1]. Other common sites include the connective tissue of cutaneous epithelium, breast, esophagus, tracheobronchial tree, gastrointestinal tract, biliary tree and genitourinary tract[1]. Although exceptionally rare, there have been case reports of plexiform variants of GCT within peripheral nerves [2]. Literature on GCT epidemiology is poor and mostly from case series. The largest case series was published in 1980 by Lack who reviewed the epidemiological data for 110 individuals with GCTs. He identified the age range to be 16 to 58 years with a mean age of 32. He showed a gender predilection of males to females of 2:1, and a race predilection of white to black individuals of 3:1. Six of the cases had multiple GCTs[3]. A 1969 report by Vance and Hudson reviewed data from 48 cases of GCT. They found the youngest patient was 11 months, with the oldest being 68 and a mean of 37 years old. He identified a female predilection of 2:1, and that 75% of cases occurred in black individuals[4]. A third large case series was published by Khansur who identified 37 lesions over a 20-year period at their institution. In this case series, age ranged from 6 months to 73 years with a median age of 31. Two patients presented with multiple lesions, and 3 cases demonstrated a familial occurrence. There was no gender predilection; and the race predilection was 2:1 for black to white individuals[5]. Based on scarce evidence, the estimated incidence of multiple GCT ranges widely. However, literature on GCTs of the aerodigestive tract suggests multiple lesions occur in 2-10% of cases[6]. There are also reports suggesting an incidence of 7-29% for multiple cutaneous GCTs, seeming to occur in younger-aged patients [7]. Despite the variability of the reported epidemiology data, the World Health Organization (WHO) cites the most common age group to be the fourth and sixth decade. It also cites a predilection for females over males of 2:1[8].

The size of GCTs at the time of diagnosis varies widely depending on the site of presentation, and they are generally thought to be slow-growing indolent lesions. In the oral cavity, the mean size at presentation and treatment is 2 cm, with the majority of lesions being treated before 3 cm in size[1]. Tumours larger than 5 cm in diameter are suspicious for malignant transformation[9]. Clinically, they present as unassuming subepithelial firm round nodules and are generally asymptomatic, however large legions can be obstructive such as in the esophagus, or biliary tree[10]. Following surgical excision, GCTs tend not to reoccur. Recurrence rates have been cited as 20% for incompletely excised lesions and at 2-8% of lesions with surgically clear margins[11]. In cases of reoccurrence with surgically clear margins, it is theorized that tumour extensions likely remained rather than a true recurence[12]. Given the low recurrence rate and benign nature of GCTs narrow margin excision is the recommended treatment, and while not required, consideration may be given for intraoperative frozen section. Additionally they are nondescript on imaging and, especially for larger lesions, may be interpreted as an invasive lesion on computerized tomography (CT) or magnetic resonance imaging (MRI)[13].

1.1.2 Histology of Granular Cell Tumours

Gross examination of a GCT is consistent with a tan/pale colored, rubbery, and poorly circumscribed nodule without a capsule. Histologically, these lesions are composed of larger than average polygonal or lozenge shaped cells of varying size with abundant cytoplasmic eosinophilic granules and small eccentric nuclei. The granules are periodic acid Schiff (PAS)-positive and diastase-resistant[3]. The granules additionally stain positively with Luxol fast blue stain[1]. There is no recognized architectural arrangement of GCTs, but tumour cells are arranged in clusters or sheets with thin/scant bands of connective tissue interspersed. The periphery of the tumour is poorly delineated and at times, appear to merge both with the overlying epithelium and with the underlying skeletal muscle giving an infiltrative appearance. Additionally, there is often detached clusters of cells that can be found a distance from the bulk of the tumour, likely representing tumour extensions rather than budding lesions[1]. There are also varying reports of the prevalence of small nerve at the periphery of lesions suggesting there is an association between GCTs and

perineural cells, and may implicate a lesion that occurs following axonal injury[1]. Nearly 50% of cases show evidence of pseudoepitheliomatous hyperplasia, an inflammatory reaction of the epithelium, with increased epithelial thickness and elongated rete ridges. It may be mistaken for squamous cell carcinoma (SCC) by a pathologist unfamiliar with the lesion, confounded by the rarity of GCTs and the relatively high incidence of SCC [14,15]. Cytology after fine needle biopsy is challenging and can often be confused with other tumour cells with granularity such apocrine metaplasia/carcinoma in breast cancer which may result in unnecessary surgery[16].

1.1.3 Tumourigenesis of Granular Cell Tumours

GCTs were first described by Weber and Virchow in 1854 using light microscopy as a lesion characterized by clusters of large cells of an unknown origin with eosinophilic granular cytoplasm [13]. Their work was expanded on by a Russian Pathologist Abrikossoff who identified several lesions with a similar appearance arising within the tongue. He theorized that the lesions arose from myoblasts of the underlying skeletal muscle, and named the tumour myoblastenmyome or myoblastoma[1]. As microscopy techniques became more sophisticated, including the development and use of electron microscopy (EM), myogenous origin has since been disproven. The first evidence to refute a myogenous origin came from EM studies showing GCTs to be invariably separated from skeletal muscle by bands of collagen without a transitional zone and no evidence of myofibrils[17]. EM also identified that the granules of GCTs were most consistent with lysosomes/autophagic vacuoles, and secondary intermediate lysosomes including some vacuoles that contained virus like particles suggesting a possible histiocytic origin[17,18]. Other EM studies identified vacuoles containing lipoproteins and syringolipids, which were presumed to be degraded myelin, and microtubules. Given the proximity of such a cell to axons near the tumours periphery indicated a possible common precursor to Schwannomas[17,19]. Finally a third theory developed using EM was that GCTs arose from undifferentiated mesenchymal precursors of fibroblasts that had phagocytized cellular debris[17].

4

While EM raised many questions, it was not able to provide many answers. Much of what we now know about GCTs etiology has come from immunohistochemical staining (IHC). One of the first groups of IHC antibodies to be studied marked skeletal muscle: myoglobin, myosin, actin and desmin, all of which consistently stain negative giving further evidence to refute a myogenic origin[20,21]. Investigating the theory that GCTs were of neural sheath origin, Mukai completed IHC staining for S100 and myelin protein P0 and P2. S100 belongs to a small molecular-weight protein family, initially thought to be only found in in neural tissue. He found positive staining in 18/18 GCTs for S100, P0 and P2, with P0 and P2 staining the PAS-positive granules. Give that histocytes generally stain negative for S100, he provided evidence that granular cell tumours were likely derived from SCs and theorized that the GCT cells produced myelin rather than phagocytizing myelin debris[21]. Stewart also assessed immunoreactivity of S100, in addition to enzymes common to histiocyte vacuoles: muramidase and alpha-1 antitrypsin. S100 was diffusely positive, while muramidase and alpha-1 antitrypsin were negative suggesting that GCTs arose from neve sheath cells[20]. More recently, GCTs have been found to stain positive with a number of other antibodies associated with nerve sheath cells including SOX10, p75[NTR] and Neuron Specific enolase (NSE), a nonspecific glycolytic enzyme thought to be associated with neural inflammation[12]. Additionally GCTs are reported to stain for vimentin, and weakly or negatively for glial fibrillary acid protein (GFAP) provide evidence that the microtubules seen on EM are likely structural proteins common to glial cells[22]. Other IHC antibodies thought to indicate a neural origin that have been found to stain positive include: Calretinin, a calcium binding protein, and PGP9.5 protein, a hydrolase enzyme thought to be expressed primarily by neural tissue[22], although both have been since been proven to be non specific[23,24.] There is also evidence of IHC staining for neural cell adhesion molecule neural cell adhesion molecule (NCAM), a cell-cell binding protein integral to the structure of nerves.

In contrast to the cell markers suggesting a neural origin, GCTs show immunoreactivity to endomesenchymal antigens. Gurzu found that GCTS stained positive for antibodies to macrosialin (CD68), a transmembrane glycoprotein associated with lysosome membranes. Five of the 15 cases in their series demonstrated positive staining for the proto-oncogene tyrosine-protein kinase receptors c-kit and RET. Five cases showed loss of staining for NCAM. Given that

the cells were S-100 positive, NCAM negative but positive for c-kit and RET, he theorized that GCTs were "glial like" but of endomesenchymal origin[12]. GCTs have also been shown to stain for CD63, a tetraspanin glycoprotein localized to lysosomes and cell membranes of cells with autophagosomal action, in addition to being a tumour marker of a variety of different tumours of both endodermal and ectodermal origin[25]. Another antibody identified to stain positive was anti-3, which is reactive for the microtubule-associated protein 1 light chain 3, a specific marker for autophagay[26]. Serendipitously, in an unpublished study our lab identified positive staining of a GCT section for the antigen presenting cell marker HLA-DR while investigating Langerhans cells of the tongue. This surprising finding has only been reported in one other investigation[27]. While the likely cell of origin are SCs, HLA-DR and CD68 immunoreactivity suggest an antigen presenting cell (APC) phenotype for GCTs. Additionally, considering the available evidence provided by IHC it is not clear if GCTs are true neoplasms or reactive in nature.

While thought to originate from neuroectodermal cells, there is limited understanding of the cellular events that result in GCT formation.   Resulting from reports of patients with multiple GCTs, researchers have tried to identify a possible genetic cause for GCTs. There are three reported cases of multiple GCTs in a patient with a diagnosis of LEOPARD syndrome, [28,29], and 7 case reports of patients diagnosed with Noonan syndrome presenting with multiple GCTs[30]. LEOPARD syndrome and Noonan syndrome are related conditions that arise from an activating mutation of the protein tyrosine phosphatase non-receptor type-11 (PTPN11) gene on chromosome 12 (12q24.13).   LEOPARD syndrome characteristics include: clinical cluster of lentigos, electrocardiographic conduction defects, pulmonary stenosis, abnormal genitalia, intellectual impairment, short stature and deafness[31]; while Noonan syndrome is characterized by a characteristic facial dysmorphism with cardiac defects, short stature, broad or webbed neck, and a variable learning disability[32].   PTPN11 is an oncogene that codes for an auto-inhibitory protein Src homology region 2-containing protein tyrosine phosphatase-2 (SHP-2) which is part of the Ras/MAPK signalling pathway. Normally, binding of a phosphorylated tyrosine residue disinhibits SHP-2, resulting in signalling for cell growth, proliferation, differentiation and migration. Thus, the activating mutation of PTPN11 results in sustained activity of the Ras/MAPK

signalling pathway and sustained growth signals[33]. While there is a correlation between Noonan and LEOPARD syndrome and multiple GCTs, PTPN11 mutations do not appear to be causative in the tumourigenesis as additional studies have not found a PTPN11 mutation in solitary granular cell tumours [34]. There is also at least one report of a mother and child with diagnosis' of NF1, both presenting multiple cutaneous GCT[35], however there does not appear to be a strong correlation between GCTs and NF1 mutations. More recently, after the onset of our investigation, a novel mutation in ATP6AP1 and ATP6AP2 genes associated with endosome acidification have been identified by Pareja et al. using whole-exon sequencing[36]. In the initial cohort of 17 GCTs, they were unable to identify any known oncogenic genes or pathogenic fusion genes. They did however discover novel inactivating mutations of ATP6AP1 and ATP6AP2 in 12 of the 17 tumours. They then subjected 65 additional GCTs to targeted gene sequencing and identified somatic mutations of ATP6AP1 in 36/65 cases and ATP6AP2 in 6/65 cases. In total, 72% of the GCTs demonstrated either ATP6AP1 or ATP6AP2 mutations. They also investigated gene sequencing data of 6285 cases of malignancy from among 14 cancers in the Cancer Genome Atlas, and 103 cases of histologically similar lesions including Schwannomas, paragangliomas, adrenocortical carcinomas, oncocytomas, hibernomas, and chromophobe renal carcinomas. From these lesions, they identified ATP6AP1/ ATP6AP2 mutations in 0.03 and 0.05% of the malignancies, respectively and no mutations of ATP6AP1/ ATP6AP2 in the other soft tissue lesions[36]. ATP6AP1 and ATP6AP2 genes are found on the X chromosome, Xq28 and Xp11.4 respectively, and code for accessory proteins of vacuolar H+-ATPase (V-ATPase). V-ATPase, composed of the subunits V0 and V1, is found in the membranes of endosomes and functions to acidify secretory vesicles and lysosomes. The accessory proteins coded by ATP6AP1 and ATP6AP2 are required for V-ATPase insertion during endosomes formation at the Golgi apparatus and have an additional role in vesicle trafficking[37]. Pareja was successful in achieving a granular cell transformation of an immortal Schwann cell line, human embryonic kidney (HEK)-293 cell line and non-tumourigenic mammary epithelial MCF-10 cell line through in vitro depletion of ATP6AP1 and ATP6AP2. These granular cells also demonstrated reduced acidification of vesicles as a result of reduced V-ATPase function. They theorized that the accumulation of endosomes was a function of both altered vesicle trafficking and a loss of endosomal function as a

consequence of altered pH[36]. Following the work of Pareja, there has been additional research into other potential mutations that could affect the function of V-ATPase. Sekimizu et al. performed gene sequencing on 51 GCTs and identified mutations of genes encoding for V-ATP subunits and accessory genes in 33/51 cases (65%)[38]. ATP6AP1 mutations were identified in 23 cases and ATP6AP2 mutation identified in 2 cases. Additionally there were found to be mutations of 1 other V-ATPase accessory protein, in addition to mutations of 6 different V-ATPase subunits of both V1 and V0[38]. Collectively, the evidence suggests that the genotype-phenotype correlation is related to V-ATPase dysfunction. The mechanism of tumourigenesis following mutations that disrupt V-ATPase activity is still unclear, however it has been theorized that changes in endosomal function results in altered cell signalling in an independent fashion giving GCTs oncogenic properties[36]. These findings provide evidence of a mutation that likely contributes to an APC phenotype of granular cell tumour.

1.1.4 Malignant Granular Cell Tumours

Malignant GCTs (m-GCT) are classified as high-grade sarcomas due to their aggressive behavior, lack of response to treatment and poor clinical outcomes. While thought to develop from benign GCTs, it is also possible they are a different tumour with a similar phenotype[39]. Reports suggest that malignant variants represent 2% of all GCTs and 0.2% of soft tissue sarcomas[40]. Metastasis has been reported to lymph nodes, lung, bone, nerve, and peritoneum[41]. The accepted classification system for determining malignant transformation is the Fanburg criteria. Fanburg et al, reviewed 73 cases of atypical GCTs under light microscopy in an attempt to identify features that could be used to classify GCTs as malignant or lesions with high risk of malignancy[39]. They proposed 6 histological criteria: necrosis, spindling, nuclei with large nucleoli, increased mitotic activity (2 or more atypical mitoses/10 fields at 200x magnification), high nucleus to cytoplasm ratio, and pleomorphism. They concluded that lesions meeting 3 or more criteria should be diagnosed as malignant and, 2 or less as benign with atypical features. Of the 73 lesions in their report, 46 were classified as malignant, with 28/46 of the malignant cases having metastasized and 0/27 of the atypical cases having metastasized. IHC of the malignant cases showed no

significant difference between malignant and benign cases for S100, vimentin, and NSE, commonly used markers for GCTs. They also stained tumours with Ki67, a marker of cell proliferation, and found a statistically significant worse prognosis if Ki67 was >10%. Other authors suggest that metastasis should be the sole criteria for diagnosing a malignant GCT (M-GCT), while recognizing the Fanburg criteria as a risk stratification method[42]. In the largest review of M-GCT involving 113 patients, the median age was 54 and 77% of patients were female. The average reported size of malignant lesions was larger than reported for benign lesions at 4 cm, although 53 of the cases did not report tumour size. A true value for rate of metastasis could not be calculated due to poor reporting. There was a significant difference in patient survival for tumours larger than 5 cm, with 5 year survival of 51.3% for lesions >5 cm and 90% for lesions < 5 cm. Survival at 5 years was 0% for patients with reported distant metastasis[43]. In another study, the 3 year survival was 39% for metastatic disease[39]. M-GCT of the oral cavity is extremely rare, although there is one case report from India that diagnosed an 11 cm M-GCT in the base of tongue causing ankyloglossia without metastasis[44]. The rarity of oral M-GCT is cited to be related to tumour size at the time of diagnosis [44]. Thus far, surgical excision is the only curative choice as radiation and chemotherapy have not demonstrated increased survival with worse patient outcomes[43]. There has been one case of M-GCT that underwent whole genome sequencing. This study identified a total of 12 genetic mutations in the single case of M-GCT, most of which had an unknown significance at the time of the report, including a mutation of ATP6AP1. There was one known loss of function mutation of the tumour suppressor gene BRD7, a subunit of PBAF-specific SWI/SNF chromatin remodeling complex, known to be a regulator of BRCA1[45]. While the study only looked at 1 case of M-GCT it is of interest that they identified a mutation of ATP6AP1, in addition to BRD7 a gene that has been shown to be a tumour suppressor gene in breast cancer[46]. Further investigations can hopefully elicit a possible targeted therapy for GCT, which may be patient specific depending on the genotype of the tumour cells.

1.2 Embryology of neural crest cells

Despite vast knowledge of the development, migration, and differentiation of neural crest cells (NCCs) from the neural crest to their respective cell populations, it is still somewhat poorly understood. I will provide a brief summary of the process of migration and differentiation with a focus on peripheral perineural glial cells.

1.2.1 Formation of the neural crest

At approximately day 16 of human embryo development, the single layered blastula is reorganized into the trilaminar gastrula, via a process called gastrulation, forming the ectoderm, mesoderm and endoderm. This process also defines the rostral and caudal ends of the developing embryo, and the midline axis at the notochord. During the third week of development, neurulation occurs forming the neural plate from ectodermal cells located below the notochord, which then invaginates to form the neural tube. During the folding process, the dorsal marginal ectodermal cells are pulled inward to form the neural crest (NC) sandwiched between the non-neural ectoderm and the neural tube. The neural tube will later develop to become the brain and spinal cord while the neural crest remains as a pluripotent cell population that will continue to migrate and form a wide variety of cell populations[47].

1.2.2 Migration of neural crest cells

Neural crest cells (NCC) undergo the most varied and complex migration of all cell types in the developing embryo and are often referred to as a fourth germ later due to its significance. Much of the early work in the study of NCC migration was done by LeDourain in the 1960s who grafted quail NCCs into chicken embryos, generating a chimera. Using light microscopy and later antibody labelling, LeDourain identified several different clusters of NCC at different levels of the embryo

10

axis and termed the clusters cranial, vagal, trunk and lumbrosacral populations[48]. The cranial level cells contribute to cranial sensory ganglia, the cartilaginous precursors of the facial skeleton, dental papilla, the dermis, smooth muscle, adipose tissues of the head and neck, and the salivary glands. Vagal and sacral neural crest cells populate the gut, forming the enteric nervous system and the outflow tract of the heart in addition to the vagus nerve, while the trunk neural crest cells form sensory and sympathetic ganglia and the adrenal medulla. Cells from all levels contribute to the formation of the sympathetic and parasympathetic nervous system, pigmented cells of the epidermis and peripheral glial cells[49,50].

1.2.3 Neural crest cell differentiation

There is some debate regarding the terminal differentiation of NCCs, with evidence to support both fate restriction and retained multipotency. Fate restriction refers to a process where the terminal cell lines are determined prior to migration, and retained multipotency suggests that the terminal cell line is determined following migration while the stem cell characteristics are retained late into cellular maturation. Regardless of which theory one attest to, there is evidence to suggest that the environment to which stem cells migrate to plays a key role in determining their terminal cell type fate. During NCC differentiation, there are both permissive and repulsive extracellular matrix cues that result in differential gene activation[51], initiating the progression of NCCs towards their terminal cell type fate[52]. In the case of Schwann cells (SC), the process of NCCs differentiating to Schwann cell precursors (SCP) is a process referred to as peripheral gliogenesis[53]. One of the key transcription factors identified in peripheral gliogenesis and differentiation of other NCC cell lines is SOX10, a member of the RY-related Homeobox box (SOX) family of transcription factors. SOX10 interacts with a number of other proteins in a context-specific fashion to promote differential gene transcription playing a key role in determining cell line fates[52,53,54]. A functional role of SOX10 in gliogenesis is supported by evidence that knock out mice lack peripheral glial cells resulting in a neurodegenerative condition[55]. In humans, there

are a number of conditions that result from heterozygous SOX10 mutations, such as Hirschprung's Disease and Waardenburg Syndrome in which there are myelination defects of peripheral nerves[56]. The signalling cascades involved in NCC maturation are complex, but key ligands have been identified as playing important roles. One of these signaling molecules in peripheral gliogenesis is neuregulin-1 (NRG-1), a growth factor which supresses neuronal development and promotes glial specification[57]. NRG-1 is a protein ligand of the ErbB receptors tyrosine kinases (ErbB1-4) transmembrane epidermal growth factor family receptors. ErbB3/4 activity has been shown to result in upregulation of SOX10 expression[52] although the intracellular mechanism for promoting SOX10 is unclear[55]. An example of a transcription factor that is differentially expressed during peripheral gliogenesis is SOX2, another member of the SOX family. SOX2 has been found to be upregulated in SCP but downregulated in both NCCs and absent in mature SCs. SOX2 acts to inhibit the induction of Krox20, a zinc finger transcription factor required for myelination of axons and promotes proliferation of SCP[58]. In contrast to SOX2, SOX10 is persistently expressed in cells with neural, glial and melanocyte fates while other NCC derived cell lines downregulate SOX10 in their mature cell lines[53]

1.3 Schwann cell

Schwann cells are the principal glial cells of the peripheral nervous system. I will outline their function and the steps in progressing from SCPs to immature Schwann cells and maturation to myelinating SCs and non-myelinating SCs.

1.3.1 Schwann cell precursors to myelinating Schwann cells

Schwann cells develop from SCPs located in the boundary cap region, which are clusters of NCCs on the surface of the neural tube, at the exit points of the developing peripheral nerve roots[59]. The first step in differentiation from SCPs to immature SCs is a process referred to as radial

sorting. During radial sorting, SCPs polarize, undergo functional and structural changes and align themselves parallel to developing axons[52]. There is evidence to suggest that this process is regulated by signaling cues from the developing axon rather than being intrinsic to the SCP or that axonal growth is guided by the SCPs. Neural derived ligands include brain-derived neurotrophic factor (BDNF) and nerve growth factor (NGF) whose substrate is protein 75 low affinity nerve growth factor receptor /neurotrophin receptor (p75[NTR]) and NRG-1[60]. During radial sorting, SCP will either associate with a single large caliber developing axon in a 1:1 ratio resulting in a pro-myelinating SC fate or associate with a number of small caliber axons resulting in non-myelinating remark SC[53]. The pro-myelinating SC then develop finger like lamellipodia cytoplasmic projections that start to ensheath the developing axon in 40 or more layers, while at the same time synthesizing the cytoskeleton, and laying down an extracellular matrix forming a basal lamina[52]. Components of the cytoskeleton include glial fibrillary acidic protein (GFAP) and vimentin. As the cells mature, vimentin remains as an integral structural protein while GFAP is downregulated[61]. Late pro-myelinating SC at this point in maturation are organized into adaxonal, paranodal, internodal and abaxonal cellular compartments. The adaxonal surface is in tight contact with the axon, and is rich in adhesion molecules interacting with ligands of the axon. At each end of the cell is the paranodal region that binds to the associated axon through tight junctions resulting in the nodes of ranvier[62]. The outer abaxonal compartment contains the nucleus, is rich in cellular organelles and also binds to the basal lamina via integrin proteins[62]. The internodal compartment eventually becomes the tightly wrapped myelin rich compartment during cell maturation from pro-myelinating SC to myelinating SC [63]. As the cell matures there is a shift to down regulate transcription factors and cell signals that inhibit myelin formation and upregulate pro-myelination transcription factors and signals. One of the key cellular events is the downregulation of SOX2, which removes the zinc-finger transcription factor (Krox20) inhibition. Krox20 is a pro-myelinating transcription factor that functions synergistically with SOX10 and the pro-myelinating POU domain transcription factors Oct6 (Pou3f1) and BRn2 (Pou3f2)[64,59]. A target of SOX10 are the histone deacetylase HDAC1 and HDAC2, that promote pro-myelinating genes such as myelin protein zero (P0). HDAC1/2 knockout mice show arrest of SCP in the pro-myelinating state[65]. On a larger scale, SCP migration and organization also play an

important role in the formation of nerve fascicles. Another role of SCPs is to help guide sprouting axons to make contact with their targets via clusters of SCP that advance at the leading edge of axonal growth cones during development of the peripheral nervous system[53].

1.3.2 Function of Schwann cells

As the principle glial cells of the peripheral nervous system, Schwann cells have many different roles, with similar but different roles for: myelinating SCs, non-myelinating remark cells, and other specialized non-myelinating SC. Each myelinating SC spans approximately 100 um along a single axon and functions to increase conduction velocity along axons by ten times via a process known as saltatory conduction[66]. During salutatory conduction action potentials propagate at unmyelinated gaps between adjacent SC, nodes of Ranvier, while the dense myelin sheath of the internodal cellular compartment acts to insulate the action potential restricting sodium influx to the high voltage channels of the nodes of ranvier[67]. The paranodal region appears to have a role in inducing the expression of these high voltage electrolyte channels by the neuron and tightly binds to the axon via contact-associated paranodin cell adhesion molecule (caspr) among other proteins restricting ion influx to the nodal regions[68]. Myelin of the internodal compartment has a high lipid content, and is enriched with galactosphingolipids, saturated long-chain fatty acids, and cholesterol[69]. The primary structural protein of myelin is myelin protein zero (P0) belonging to a family of membrane adhesion molecules. each P0 spans the cellular membrane to ensure tight coiling of the internodal compartment via interaction of transmembrane hydrophobic domains while binding to other P0 domains in the intracellular compartment[70]. In addition to P0 there are a number of other myelin proteins found in higher concentration in the peripheral nervous system relative to the central nervous system including myelin protein 2 (P2), peripheral myelin protein 22 (PMP22) and myelin basic protein with similar structural roles to P0[71].   Other functions of myelinating SCs include regulation of axonal diameter and neurofilament spacing. SCs also provide metabolic support for their associated neuron as several studies report that mitochondrial dysfunction in SC results in degeneration of the axon, but not the SC[72].

14

Populations of Non-myelinating SC include remark cells, presynaptic SC, and satellite glia cells of peripheral ganglia. Each Remark cells associates with several non-myelinated axons via cellular extensions that cluster non myelinated axons into bundles referred to as remark bundles[73]. Perisynaptic SCs encase neuromuscular junctions; and satellite glia cover the surfaces of nerve cell bodies in sensory, sympathetic and parasympathetic ganglia. Both groups appear to have roles in maintain synapses and regulating the perisynaptic environment through uptake of neurotransmitters[74].

1.3.3 Role of Schwann cells in nerve injury

In the peripheral nervous system, axons are bundled together in an organized multilayered fashion to form nerves. Each axon and their associated SCs are encased in a fibrous endoneurium known as funiculi. Funiculi are then bundled together and are encased in a second fibrous layer, the perineurium, resulting in the formation of fascicles. Fascicles are then bundled and encased in the outer fibrous membrane, the epineurium, an extension of the fusion of arachnoid and pia matter as a nerve exits the spinal foramen[75,73]. Nerve injuries are generally classified according to level of discontinuity of the respective nerve. Axonotmesis, axonal discontinuity with an intact endoneurium, has an excellent prognosis for re-establishing contact at the distal synapse. Injuries that result in discontinuity of axons and their fibrous sheath, neurotmesis, have a significantly worse prognosis for regaining function as a result of poor selectivity of axon-target reconnection[76]. Following loss of axonal continuity, there is death of the distal segment in a process known as Wallerian degeneration. As myelinating SCs lose contact with their associated axon, there is a change in the cellular environment that no longer favors the myelinating phenotype of SCs, and myelinating SCs dedifferentiate to repair Schwann cells (RSC). Three key ligands that are implicated in this process include calcium, NRG-1, and Fibroblast Growth Factor-2 (FGF-2), all of which are found in increased concentration following Wallerian degeneration[77]. During dedifferentiation, the transcription factor c-jun is activated resulting in upregulating of both SOX2 and an additional transcription factor Pax-3.   Upregulation of SOX2 inhibits the pro-

myelinating transcription factors Oct-6 and Krox-20 inhibiting myelination. This results in both myelinating SC and non-myelinating SC dedifferentiating to RSC, a phenotype of SCs that is very similar to SCPs[73,77,78,79]. RSC undergo myelin autophagy, phagocytize degraded myelin sheath, and release cytokines that signal for macrophage ingress to assist in debriding neural and myelin debris. RSC then reorganize into repair tracts along the basal lamina called bunger bands effectively maintaining an environment for new axonal growth[75,77]. Simultaneously, the neuron undergoes a process referred to as the cell body response, switching from a transmission state to a growth state resulting in growth cone formation at the proximal stump[76]. Growth cones are characterized by several lamellipodia that respond to signals including both neurotrophic and neurotropic factors released from the cells of the bunger bands, such as glial derived neurotrophic factor (GDNF), NRG-1 and Growth associated protein 43 (GAP43) to promote axon elongation[76,78]. As the growth cone advances, signalling cues from the maturing axon result in redifferentiation of the RSC back to myelinating SC in a process that is similar to development[73,80].

1.4 Schwann cell neoplasms

Schwann cell neoplasms are classified as peripheral nerve sheath tumours (PNST) and include Schwannomas, neurofibromas (NF), and malignant peripheral nerve sheath tumours (MPNST). The cellular processes that result in PNST are poorly understood but thought to occur following nerve injury. More commonly, PNSTs will arise as isolated lesions, but much of what we know about the process that results in the formation of PNST comes from research of genetic conditions such as neurofibromatosis type 1 (NF1), neurofibromatosis type 2 (NF2), Carney complex type 1 and Schwannomatosis, conditions characterized by the formation of multiple PNST in a variety of anatomical locations[81]. I will discuss our understanding of the underlying cellular processes that result in PNST with focus on intraoral Schwannomas.

1.4.1 Neurofibromas

Neurofibromas have a propensity for forming in the dermal layer of the skin, but plexiform NFs deeply situated within nerves, most commonly in large nerves of the extremities, do occur[82]. Clinically, they are described as unencapsulated ovoid, grey or tan colored firm masses and are generally smaller than 2 cm in diameter. A distinguishing feature is the button-hole sign where the lesions retract into the underlying tissues on palpation and then reappear on release. In dermal NF, there is also a characteristic violaceous skin change[83]. Histologically, they are composed of varying numbers of SCs and fibroblasts with the SCs recognized as the neoplastic cell type making up 40-80% of the lesion[84]. There is great architectural variety and they are described as a of "bag of worms", due to the mix of spindly SCs, fibroblasts and axons; however, the spindle SCs and fibroblasts are found in clusters. The stroma is dense in poorly organized collagen bundles. Transected or damaged axons are often found adjacent to the lesion suggesting that they form following nerve injury. Dermal NF form in the subcutaneous tissue and have a Grenz zone, normal dermis between the lesion and the overlying epidermis. Approximately 90% of neurofibromas will appear sporadically as an isolated lesion, while the remainder occur in patients with NF1[82]. They are generally thought to be benign, however malignant transformation can occur resulting in MPNST. The age of onset is variable; however they most commonly develop in young adults in the 3rd to 5th decade of life. Patients with NF1 develop multiple NFs, both dermal and plexiform types. NF are often asymptomatic with chief complaints of pruritis, pain, or paresthesia, but the most common complaint is cosmetic appearance[85].

Much of what we know about the cellular process that result in the formation of NF comes from research in the condition NF1. NF1 effects 1 in 2500 to 3500 patients. The condition is either inherited in an autosomal dominant fashion with complete penetrance but variable expression or occurs as a de novo mutation in as many as 50% of cases[84]. While the characteristic lesion of NF1 is multiple dermal NF, they do also develop plexiform NF, have reduced intelligence, and other tumours including boney dysplasia, optic gliomas, Lisch nodules, glioblastomas, pheochromocytomas, and gastrointestinal stromal tumours among others[84]. Research in the

1990s identified a mutation on the long arm of chromosome 17 (17q11.2) that coded for a large gene called neurofibromin (NF1 gene)[86]. Complete deletion is rare, with nonsense, frameshift and missense mutations more commonly identified. There is also great variability in genotype-phenotype correlation[87]. DNA analysis of isolated NFs in patients without NF1 has also identified mutations in the NF1 gene; suggesting that mutation of NF1 is required for NF formation[88]. The NF1 gene has multiple functional domains, however mutations do not always result in NF formation suggesting that there are key domains that are still being explored[87]. The NF1 gene appears to be a tumour suppressor gene, as research suggests that a "second hit" to the wild type allele results in tumourgenesis. Loss of heterozygosity is also seen[88,87]. The Neurofibromin gene encodes for a protein with a similar structure to GTPase-accelerating protein (GAP). Neurofibromin protein binds to Ras GTPase, which is a hub protein associated with a wide variety of transmembrane receptors. Ras GTPase functions as a binary control for signal transduction by cycling between the inactive GDP-bound form and active GTP-bound form facilitated by GAP. By inhibiting the GAP-Ras GTPase interaction, neurofibromin effectively inhibits the conversion of GTP to GDP resulting in downregulation of Ras activity[84,89]. Mutation of neurofibromin results in upregulation of Ras signaling which results in cell proliferation and increased cell survival among other cellular functions[89,90]. NF1 Knockout mice variably develop NF, and it is yet unclear which cell stage of SC are responsible for NF formation[84]. Recently, there is evidence to suggest that in addition to NF1 mutation, other growth factor signals are required. One candidate is NRG1 and its ErbB receptors, as upregulation of RAS system in the context of high levels of NRG1 results in tumourgenesis[84,91]. This would suggest that NF develop from SC when there is high levels of NRG1 such as in repair SC or SCP[84]. Other investigations suggest that inflammation and cytokine release by mast cells, T cells and dendritic cells during nerve inflammation may also play a role in NF tumourigenesis upregulating proto-oncogenic transcription factors such as c-jun, FosB and c-Fos [92]. Progression to MPNST requires additional gene mutations that will not be discussed.

1.4.2 Schwannomas

I will review the histology epidemiology, and tumourigenesis of Schwannomas.

1.4.2.1 Histology of Schwannomas

Gross description of Schwannoma is consistent with a firm uniform rubbery tan colored lesion with an intact capsule. Cut sections are uniform and without any significant inclusions or cystic component[93]. In contrast to neurofibromas, with exception of plexiform Schwannomas, axons are rarely present within the lesion but are often found at the periphery[93]. There is a distinct histologic pattern of Schwannomas, first described by Nils Antoni in 1920 that helps to differentiate Schwannomas from other PNST and other spindle cell lesions. Antoni identified that Schwannomas are composed almost entirely of SC-like cells. Within the lesion, there are two distinct architectural patterns which he referred to as tissue type A and tissue type B that are now referred to as Antoni A and Antoni B regions[93]. Antoni A regions are highly cellular, and packed with polarized elongated spindle cells with a central bulge and tapered ends. Within Antoni A areas, Verocay identified that cells tended to stack in rows with nuclear palisades and alternating anuclear zones; an arrangement known as Verocay bodies[94]. Verocay body architecture is thought to be a result of SC signaling for cell-cell contact, similar to the way RSC polarize to form bunger bands. The anuclear zone has a dense lamina rich in laminin and deficient in other matrix components interspersed with filamentous cytoplasmic extensions[95,96]. The percent of the tumour representing Antoni B regions is quite variable, and can be scant or comprise large portions of the lesion. The Antoni B region is less cellular and does not appear to have any apparent organization. The cells are thin and wispy separated by microcystic spaces filled with basophilic mucin[93]. In some tumours, the microcystic components can convalesce to give the appearance of a more prominent cystic component on radiological assessment[97]. Unlike the Antoni A regions which are entirely composed of spindle cells, Antoni B areas often have a high number of small vessels with hyalinized walls, and evidence of thrombosis and intralesional hemorrhage in addition to macrophage and lymphocyte infiltration suggesting inflammation[93,98]. It is also not uncommon to identify atypical nuclei, accumulation of cytoplasmic granules and myelin debris in the Antoni B regions[99]. In addition to Antoni A and B, a third transitional region between the Antoni A and Antoni B regions has been described. This transitional zone shares

features of both Antoni A and Antoni B regions, with a dense disorganized cellular component and a haphazard basal lamina[93,94]. A subset of Schwannomas can be classified as ancient Schwannomas. These tumours demonstrate "ancient change" with an increased Antoni B component and inclusions including: calcifications, regions of necrosis, increased nuclear atypia, cyst formation, and xanthamatous change[93]. While not proven, it is accepted that the Antoni B region represents degenerated Antoni A regions which is supported by the multiple inclusions, cellular atypia of the Antoni B region, presence of a transitional zone, and tumour architecture of ancient Schwannomas[99].

1.4.2.2 Epidemiology of Schwannomas, with a focus on oral Schwannomas

Schwannomas (neurilemmoma) are uncommon slow growing encapsulated lesions comprised almost entirely of neoplastic SCs in a poorly collagenized stroma and are the most common PNST[84]. In contrast to neurofibromas, they tend to present at the periphery of nerves, displacing the fascicles rather than intertwining with them[84]. They can occur at any site in the body arising from cranial nerves III-XII, and autonomic or somatic nerves from the spinal nerve roots to terminal synapse[100]. Estimating the incidence of Schwannomas is difficult because the epidemiology literature is poor. There is one report from Finland that looked at all cases of peripheral Schwannoma from 1985 to 1995 in the Helsinki University Hospital catchment area and found an overall incidence of 1 in 50 000 per year[101]. The most common site for Schwannomas to form is the vestibular nerve, which has an incidence of 1 in 100 000 per year[102]. Approximately 25-48% of all Schwannomas are found in the head and neck region with the oral cavity being an uncommon site representing 1% of all Schwannomas[100]. There is limited published data on intraoral Schwannomas. The most common intra oral site appears to be the tongue at 50% prevalence, with soft tissue lesions of the hard palate, soft palate, mucosa and lip being reported[25,103,104]. A review of published cases of lingual Schwannoma between 1959 and 2016 identified 84 cases. The age range was between 7 and 77, with the highest incidence in the 3rd and 4th decade of life and a mean age of 28[105]. The average lesion size at the time of presentation and treatment was 2.4 cm. Schwannomas were generally asymptomatic.

Symptomatic patients reported pain, dysphagia, paresthesia, snoring and vocal changes. There does not appear to be a gender predilection identified as cases generally are thought to occur equally in males and females [105]. Approximately 90% of all cases of Schwannomas are solitary lesions with the remaining cases presenting as multiple Schwannomas in NF2, carney complex 1 and Schwannomatosis. Of the 3 genetic conditions, NF2 is the most common affecting 1 in 25000 births[106]. Variants of Schwannomas do occur including cellular Schwannoma with higher cellularity, plexiform Schwannomas with an infiltrative pattern, ancient Schwannomas with a hyalinized matrix, and melanotic or pigmented Schwannomas[84]. Malignant transformation to MPNST is extremely rare and seem to occur only in very large lesion, greater than 5 cm, based on case reports[107].

1.4.2.3 Cellular processes of Schwannomas tumourigenesis

Much of what we know about the cellular processes resulting in Schwannoma tumourigenesis comes from studying patients with NF2. Patients with NF2 have a mutation in the NF2 tumour suppressor gene, on chromosome 22 (22q12.2) which encodes for at least 10 protein variants [84]. Given the structural similarity to the protein 4.1 family ERM proteins (moesin, ezrin and radixin), the NF2 protein is referred to as the moesin-ezrin-radixin-like protein (merlin). NF2 is inherited in an autosomal dominant fashion with 50% of cases arising as de novo mutations[84]. Nonsense and frameshift deletions do occur, but the most common mutation is single or multiple exon deletion[108]. Additionally, one third of patients are mosaic for the mutation suggesting that germ line mutation is common[108]. Schwannoma tumourigenesis requires either a double hit to the native allele or more commonly loss of heterozygosity[109]. DNA analysis of patients with NF2 identifies a single wild type allele, while analysis of tumours cells identified two mutant copies[110]. In a report on 22 cases of solitary Schwannomas, only 50% of the Schwannomas demonstrated identifiable mutations of the NF2 gene, however merlin protein was unidentifiable on IHC and western blot in all tumours[111]. This can be interpreted as either the mutation was missed during genome sequencing due to the location of the mutation or that there are other possible

mutations that could result in a disruption of merlin other than the NF2 gene. Patients with NF2 are prone to bilateral vestibulocochlear nerve Schwannomas resulting in profound hearing loss, and vestibular disturbances. They also develop multiple Schwannomas in other sites of the body with a propensity for plexiform Schwannomas[84]. Other common diagnosis include the development of meningiomas, ependymomas and retinal hamartomas[84]. Merlin mutations have also been found in a variety of malignancies including colorectal cancer, prostate cancer, melanoma and thyroid cancer suggesting that it has a function in a variety of cells outside of the nervous system[108]. Nf2-/- mice models are embryonic lethal suggesting that merlin is important for development[112]. Merlin is a large protein without a catalytic domain that functions to inhibit cellular processes of proliferation, apoptosis, survival, motility, adhesion, and invasion [108,113]. One target of merlin is p75^{NTR}, a coreceptor with Trk receptor tyrosine kinases (TrKA, TrKB and TrkC), sortilin and Nogo[114]. Cell signalling cascades of p75^{NTR} can signal for survival or apoptosis depending on the coreceptor it associates with[115]. p75^{NTR} expression is downregulated in mature SCs, but is substantially upregulated following axonal injury[116]. Rapidly after nerve injury, P75^{NTR} forms a P75^{NTR}/TrkA complex, which activates signalling pathways that promote schwann cell survival, dedifferentiation and proliferation[117]. In the absence of reinnervation, there is a temporally mediated switch in the coreceptors of P75^{NTR} to sortilin. Switching of coreceptors is thought to be influenced by SC merlin phosphorylation, as progressive merlin phosphorylation occurs following axonal injury which corelates with switching of the P75^{NTR} coreceptor from TRkA to sortilin [114]. In a healthy state P75^{NTR}/sortilin activity signals proapoptotic signals by activating c-jun terminal kinase (JNK)[113]. In Schwannomas, the absence of merlin results in dysfunctional P75^{NTR} signalling resulting in Schwannoma cells evading proapoptotic signals[114]. An alternative theory about how Schwannoma cells survive despite proapoptotic signaling is thought to be a result of disinhibition of the ErbB family of receptors, and other receptor tyrosine kinases, as absence of merlin is associated with increased activity of these receptors[84]. A third target of merlin is the transmembrane hyaluronic acid receptor (CD44), which mediates contact inhibition following cell proliferation. In native repair SCs, merlin becomes phosphorylated when cell density is low, increasing CD44 signals for cell proliferation and replication. As cell density increases, merlin becomes hypo-phosphorylated and CD44 signalling switches to inhibit

growth[118]. In Schwannomas, a lack of merlin is thought to disrupt CD44 signalling downregulating the growth inhibition signals of CD44[84]. Collectively, there is a body of evidence that absence of merlin contributes to Schwannoma cell survival and tumour growth. The function of merlin and its target receptors is an active area of research with new targets being identified regularly. Continued research in the field will give further clarity of merlin's cellular function and new insight into is role in tumourigenesis of neural and non-neural tissues. The genetic cause of Schwannomatosis and Carney complex type 1, are less understood, but research suggests that merlin is likely to be involved in tumourigenesis of these conditions as well[84].

1.5 Immunohistochemical profile investigated

In this section I will provide a literature review of the antibodies used for immunohistochemical (IHC) staining to investigate a possible antigen presenting cell lineage for granular cell tumours in addition to a number of markers specific for NCCS and neuroectodermal cells that are used in this report.

1.5.1 S100

The S100 protein family consists of a total of 24 related EF-hand calcium-binding proteins that regulate a vast array of cellular functions. They are divided into 3 groups based on their function: exclusively intracellular regulatory effects, exclusively extracellular regulatory effects, serving autocrine or paracrine functions, and those that exert both intracellular and extracellular effects[119]. In their active form, S100 monomers form dimers or multimers, with the monomers classified as either alpha or beta subunits. When two alpha subunits or hands form a dimer, they are referred to as S100A, while two beta subunits are termed S100B. When one alpha and one beta subunit for a dimer, they belong to the S100A class of S100 proteins[120]. Upon calcium or zinc binding, structural reorganization exposes protein active sites[121,122]. They then interact with

a multitude of target proteins including cell surface receptors, enzymes, cytoskeleton subunits and transcription factors to regulate cell functions including proliferation, apoptosis, assembly of the cytoskeleton, differentiation, metabolism and cell migration[119]. S100 protein expression is tightly regulated to maintain cell homeostasis. High levels of S100 expression has been identified in neural crest cells and was once thought to have a high specificity for neural cell origin. Elevated S100 levels has been shown to be a nonspecific marker of inflammation in a number of conditions such as osteoarthritis[123] and cardiomyopathy[124] and in cancers such as, clear cell sarcoma[125] and lymphoma[126] and other tumours such as chondrocytomas[123] and pheochromocytoma[120]. S100 immunoreactivity has been identified in tumours of Langerhan cell origin while tumours of monocyte and histocyte origin do not stain for S100. Such differences in immunoreactivity provides utility in using S100 antibody to distinguishing Langerhans cell histiocytosis from other histiocytosis syndromes[127]. S100 is a common antibody used in the diagnosis of melanoma, and is positive in almost all cases[128]. While the significance of elevated S100 levels in other tumour types is still under investigation, it remains one of the most commonly used stains to differentiate neural crest-derived tumours from other spindle cell lesions such as myofibrosarcoma of fibroblast lesions[129]. In lesions that stain positive for S100, staining with SOX10 is often used for further differentiation of cells derived from the neural crest[130]. S100 has been shown to uniformly stain cells of Schwannomas, GCTs, and the Schwann cell component of neurofibromas. PMNST staining of S100 is seen in less than 50% of cases[130]. While monoclonal antibodies exist, the most commonly used S100 stains are polyclonal and have highest affinity for S100B as was used in this study.

1.5.2 SOX10

SOX10 is a transcription factor that has been identified as a key regulator in the differentiation of NCCs to their terminal cell fate and plays a particularly important role in the differentiation of mesenchymal NCCs to a glial fate[55]. It is generally recognized as a highly specific marker of NCC origin in IHC studies. In a large study of 5134 human neoplasms representing all tissue types, SOX10 was found to stain positive for all Schwann cell-derived tumours, and variably for MPNST.

It was universally absent in all mesenchymal tumours, with the exception of rhabdomyosarcoma. It was also absent in non-melanoma epithelial lesions, and all carcinomas with exception of basal cell type breast cancers[131]. This evidence suggests that SOX10 is a valuable stain in the diagnosis of NCC-derived tumours, specifically those derived from SCs and melanocytes. SOX10 does not stain mature Langerhans cells There is a plethora of reports confirming SOX10 staining in GCTs and Schwannomas[12].

1.5.3 Neuron specific enolase

Enolases are metalloenzymes that convert 2-phosphoglycerate to phosphoenolpyruvate during glycolysis. Enolases are formed from the dimerization of the subunits α, β and γ that form five different isozymes αα, αγ, αβ, ββ and γγ in a cell specific fashion[132]. The γ unit forms homologous γγ dimer or the heterogenous αγ dimer, both of which are highly expressed in neural tissues and collectively are termed NSE[133]. The γγ dimer is found in highest concentrations in neurons and the αγ dimer is higher in glial cells[134]. NSE has been localized to cell cytoplasm, and in inflammation, to the cell membrane[135]. An additional function of NSE includes activating plasmin from plasminogen, resulting in degradation of the extracellular matrix during inflammation such as in tumours[136].

Anti-NSE is a commonly used antibody to identify cells of a neural origin, neuroendocrine origin and neural crest origin. Since its discovery, it has become apparent that while the expression of NSE is mostly restricted to neural tissues in a healthy state, there is a vast array of tumours from different cell types that stain positive for NSE. This is thought to result from the upregulation of enolases in tumour cells by a process known as the Warberg effect (a response to hypoxia favoring glycolysis over oxidative phosphorylation)[136]. Non-neural tumours that stain for NSE include breast cancers, lung cancers, squamous cell carcinoma, renal cancers and gastric cancers. Such tumours will often stain with other neuroendocrine markers such as secretagogin and its theorized that the co-staining represents a tumour cell phenotype[133,137]. As a serology test, it is used to identify cardiac injury, neuroblastoma from cord blood and as a marker for intracranial

inflammation in CSF[133]. NSE has been shown to stain GCTs in multiple investigations[1] favoring a neural crest origin, although could also represent tumour cell inflammation.

1.5.4 Growth associated protein 43

GAP43 or neuromodulin is an intracellular growth associated protein that has a critical role in guiding axonal growth, regulating neural cytoskeleton organization, and transduction of intra- and extra-cellular growth of neurites. It is also referred to as a plasticity protein as it is induced following nerve injury and plays a role in new synapse formation of neural networks. During formation of new axons or regeneration of injured axons, signaling from growth ligands such as neurotrophins and NGF or BDNF upregulates the expression of GAP43[138]. Newly translated GAP43 becomes integrated in lipid rafts that are transported to the filipodia of growth cones[139]. Once integrated within the cell membrane, GAP43 releases the inhibitory protein calmodulin and bind to $Ca2^{2+}$ resulting in GAP43 activation via phosphorylation by protein kinase C. In its active state, GAP43 binds to actin filaments of the cytoskeleton at the leading edge of the filipodia providing structural connection of the cell membrane with the developing cytoskeleton[139]. It is thought that as new lipid rafts are inserted at the leading edge of filipodia, membrane tension results in elongation of the cytoskeleton; thus axonal elongation and growth cone formation are a response to external signals rather than an intrinsic property of neurons[139]. GAP43 expression is also induced during new synapse formation and is intrinsic to regions of the brain involved in learning such as the hippocampus suggesting that its role is critical in cell membrane architecture at synapses[139].

In addition to neurons, GAP43 expression has been localized to SCPs and RSCs but not mature SCs. It is not entirely clear what function GAP43 may have in glial cells, however in contrast to many of the other changes that occur during dedifferentiation of glial cells expression of GAP43 occurs late at 4 weeks in RSC[9]. There is one report investigating GAP43 expression in rat astrocytes. They found that following cortical injection of endotoxin lipopolysaccharide (LPS), resulting in axonal injury, significant inflammation and astrogliosis, there was upregulation of

GAP43 in the repair astrocytes. *In vitro* Astrocytes with a stellate phenotype were cultured in glial medium and transfected with GAP43 small interfering RNA, resulting in GAP43-knockdown. The GAP43 knockdown cells were then transferred to astrocyte conditioned medium where they were cultured with rat cortical neurons. They identified a significant decrease in axonal spread and the number of dendrites of the rat neurons. They also found that while GAP43 expression in the rat neurons was preserved, there was a significant reduction in neuron GAP43 phosphorylation. There was a significant increase in expression of inflammatory markers IL-6 and TNF-α in the GAP43-knockdown group, which corresponded with increased microgliosis. Collectively, they theorized a new role for GAP43 as a regulator of inflammation in glial cells that is beneficial for neuronal plasticity, favoring axonal growth[140].

There has been data to suggest that BPNST also express GAP43, and may be useful in diagnosing BPNST from among other spindle cell lesions. In a recent report, GAP43 staining was positive in MPNST, Schwannomas, NFs and desmoplastic melanomas; all other spindle cell lesions stained negative[141]. Of note, GAP43 was positive in 92% of the cases of MPNST while S100 was only positive in 62% suggesting that GAP43 may be a better tumour marker for MPNST and in turn, an excellent marker for tumours derived from nerve sheath. GAP43 IHC has also been shown to stain positive in cases of perineural invasion of malignancy such as Squamous Cell Carcinoma (SCC)[142]. There are also reports identifying GAP43 expression in papillary thyroid cancer[143] and some non-small cell lung cancers[144] and some breast cancers[145]. Of note, there seems to be a significant difference in the rate of brain metastasis in GAP43 positive non-small cell lung cancers and breast cancers when compared to cases that are GAP43 negative[144,145]. Additionally, breast cancers that have metastasized to non-neural sites, such as bone, seem to be negative for GAP43[145]. Such findings suggest that elevated GAP43 may preferentially facilitate tumour metastasis across the blood brain barrier, and that differences in cancer protein expression may play a role in determining sites of metastasis[144]. There are no prior reports investigating GAP43 expression in GCTs.

1.5.5 Human leukocyte antigen – DR isotype

The human leukocyte antigen – DR isotype (HLA-DR) is a major histocompatibility complex class II cell surface receptor that presents antigens to CD4+ T-lymphocytes during an adaptive immune response. The adaptive immune response is too complex to review here, however I will provide a brief summary of the events and the role of MHC class II molecules (MHC-II) in the process. MHC-II are composed of 2 polypeptide chains, α and β that each have a peptide-binding domain, an Ig-like domain, and a transmembrane region[146]. In contrast to MHC-I which are present on the cell surfaces of all nucleated cells, MHC-II are thought to be restricted to B lymphocytes, activated T lymphocytes and professional antigen presenting cells (APCs): monocytes, macrophages and dendritic cells[146]. In response to inflammatory cytokines, APCs migrate and phagocytize foreign material or antigens. The antigen is then processed inside the cell and binds to MHC-II molecules forming the MHC-II/antigen complex, which is then inserted into the cell membrane. The CD4 glycoprotein of CD4+ helper T-cells then recognizes the MHC-II molecule and binds to the MHC-II/antigen complex activating the helper T-cell. A second signal functions as a feedback loop in which B7 molecules (CD80 and CD86) of the APC binds to CD28 of the T-cell strengthening the activation signal. Other co-stimulating signals include interaction of the CD40 protein of APCs and CD154/CD40 ligand of helper T-cells[147]. Activated helper T-cells can then further activate macrophages and activate B-cells to secrete antibodies, in addition to activating cytotoxic T cells[148].

In contrast to the general knowledge that HLA class II molecules are restricted to professional antigen presenting cells, there is data to suggest that HLA-II can be expressed by nonprofessional APCs. One group of nonprofessional APCs that has been shown to express HLA-DR is esophageal epithelial cells in the disease state of eosinophilic esophagitis in response to the inflammatory marker interferon- γ. Interestingly, other MHC-II molecules such as HLA-DP or HLA-DQ were not expressed[149]. Other cell populations that can be induced to express MHC-II in response to inflammation include liver sinusoidal endothelial cells and hepatocytes[150], respiratory epithelium and gastrointestinal epithelium[151] and conjunctiva[152]. There are also reports identifying that

Schwann cells can express MHC-II in inflammatory neuropathies such as guillian-barre syndrome[153] and glial cells in gliomas[154]. HLA-DR expression has been reported in one report on GCTs[27], and HLA-DR expression has not been reported in Schwannomas.

1.5.6 CD68

CD68 is a transmembrane glycoprotein, also known as macrosialin or scavenger receptor class D member 1, belonging to the lysosomal-associated membrane proteins (LAMP) protein family. LAMP proteins are found in abundance in lysosomal membranes, making up 50% of the protein component. It is generally accepted as a marker for cells with phagocytic functions such as histiocytes, monocytes, giant cells, Kupffer cells, and osteoclasts, and it expression is thought to be regulated by a macrophage-specific promoter gene[155,156]. CD68 functions as a sorting protein playing a role in the formation of lysosomes, exocytosis and fusion with the plasma membrane. Lack of CD68 has been shown to result in abnormal lysosome transportation[157]. LAMP proteins are thought to be in highest concentration in late endosomes and to a lesser extent cell membranes[155]. CD68 has been shown to be expressed in lymphoid tissues and intestinal neutrophils during inflammatory processes but not in a healthy state, suggesting its expression is upregulated in permissive states[158]. CD68 expression has also been found in a number of tumours arising from fibroblast and endothelial cells[156] melanoma and renal cell carcinoma[159]. Such evidence supports the theory that CD68 is a marker of lysosomes, rather than cells of myeloid origin[156]. There is also recent evidence to suggest that non-macrophage cells have a different gene promoter and have a slightly different protein structure due to different sites of transcription initiation[155]. Anti-CD68 is well established as a IHC marker for granular cell tumours, co-staining with the PAS-positive granules[22]. There is contradictory evidence on Schwannoma CD68 staining, with some reports stating it to be strongly positive[160], and other reports suggesting it is focally positive in as few of 5% of cells, although notably as high as 85% of cells in tumours classified as ancient Schwannomas[161].

1.5.7 CD163

CD163 is a hemoglobin scavenger receptor thought to be relatively specific marker for macrophages, and a high CD163 expression occurs during macrophage activation in an inflammatory processes[162]. CD163 scavenges the hemoglobin-haptoglobin complexes and to a lesser extent, free hemoglobin, allowing for endocytosis and intracellular degradation of the inflammatory substrate indirectly serving an anti-inflammatory role[163]. More recently, additional roles of CD163 have been identified including immunomodulating effects via cell signal cascades following binding to viruses and bacteria, and functioning as a receptor for tumour necrosis factor (TNF), a weak contributor to apoptosis signals. CD163 has also been shown to be shed by cells exerting anti-inflammatory effects[164]. A recent report identified that glial cells and neurons can be induced to express CD163 following intracranial hemorrhage[165]. CD163 expression in Schwannomas and GCTs has not been investigated.

1.5.8 CD40

CD40 is a costimulatory protein found on the cell surface of professional APCs during an innate immune response and a member of the TNF-receptor superfamily. During the activation of CD4+ T cells, CD40 of APCs binds to CD154/CD40 ligand of helper T cells enhancing the activation of helper T cells. CD40 is also present on the cell surface of B cells, and ligating of B-cell CD40 with activated T-cell CD154 plays a role in class switching of memory B cells downstream of T cell activation. CD40 is also expressed by a number of cell types including epithelial cells, smooth muscle cells, fibroblasts and endothelial cells in inflammatory states[166]. Data of CD40 expression by GCTs and Schwannomas has not been reported.

1.5.9 CD11c

CD11c is an integrin alpha X chain protein that is thought to be highly expressed by macrophage, dendritic cells and leukocytes, although most widely thought to be a marker for myeloid dendritic

cells[167]. It is thought to primarily function as a fibrinogen receptor, playing important roles in monocyte adhesion and chemotaxis. It also functions as complement receptor 4 mediating phagocytosis of inactivated C3b particles, and has a poorly defined role in the innate immune response[168]. CD11c expression has not been investigated in GCTs or Schwann cells.

1.6 Quantitative polymerase chain reaction profile

I also used reverse transcriptase-quantitative polymerase chain reaction (RT-qPCR) to detect select transcripts in GCTs. Specifically, we investigated genes expressed by NCCs and SCs. In this section I will review the target genes, SOX2, SOX9, Nestin, GFAP, and Tubulin-3. SOX10, CD68 and NF2 will also be investigated but already been discussed earlier in the report

1.6.1 SOX2

SOX2, sex determining region Y box 2, is a transcription factor that is variably expressed by NCC and SCs. It is known as a master transcription factor due to its role in embryonic stem cells promoting pluripotency, and self-renewal of stem cell populations[169]. SOX2 expression is not a hallmark of any mature cell line and its expression varies according to cell maturity with higher levels of SOX2 transcription factor thought to represent less differentiated or more embryonic-like cells[170] In the context of SCs, SOX2 functions to inhibit the induction of Krox20 [58], effectively promoting a less differentiated cell stage. Cell maturation causes reduced SOX2 and activated Krox20[58]. A reverse process likely occurs following nerve injury, whereby SOX2 expression is upregulated, and Krox20 is inhibited as SCs have been shown to express SOX2 after nerve injury [171]. In summary, SOX2 has been found to be upregulated in SCP and RSCs but downregulated in both NCCs and absent in mature SCs with SOX2 functioning like a molecular rheostat for cell line maturity[169]. Another role of SOX2 in NCC populations is to inhibit early SCPs or NCCs from

developing into a melanocyte cell by inhibiting micropthalmia-associated transcription factor (MITF), a master regulator of melanocyte development, function and survival[172]. Recently, there have been a number of cancers identified including SCC and small cell lung cancers that express SOX2, with SOX2 transcription factor levels correlating with tumour aggression and worse prognosis[173]. If GCTs are found to express SOX2 mRNA, this would support an early SC stage or possibly repair SCs as the cell of tumourigenesis.

1.6.2 SOX9

SOX9 is recognized as being a relatively non-specific transcription factor that functions during development of all 3 germ cell layers. Like other SOX proteins, its function is dependent on forming complexes with other transcription factors and post-transcriptional changes that can have context-specific effects for promotion or inhibition of target gene translation[174]. Based on the amino acid sequence of the HMG domain, SOX9 can be grouped with SOX8 and SOX10 into the SOXE subgroup, which share similar functional properties[175]. SOX9 expression persists in many different cell types derived from both the ectoderm and endoderm at variable levels. In the context of neural crest cell, SOX9 is a target of sonic hedgehog, and is essential for the initial formation of the neural crest[174]. SOX9 also seems to play a supporting role in promoting SCP and their maturation to myelinating SCs as it is not sufficient to promote myelination in SOX10 knockout mice but is reported to have a role in mature SC survival[174]. SOX9 gene is reported to be upregulated in neurofibromas, and in MPNST relative to native SCs. In contrast, IHC studies identify Schwannomas to either stain negative for SOX9 or focally and weakly, suggesting that SOX9 may actually be a useful marker for NFs[174]. SOX9 is an excellent marker for early NCCs, its function and expression in mature cells can be variable. There is evidence to suggest that its expression is upregulated in NF but downregulated in Schwannomas. IF GCTs express SOX9 mRNA it would mostly support a dedifferentiated NCC cell phenotype.

1.6.3 Nestin

The neuroectodermal stem cell marker (Nestin) is a subunit of type IV intermediate filament and is coded by the NES gene. Nestin is generally believed to be expressed by immature cells during cytoskeleton formation, particularly by axons of the PNS and skeletal muscle. As cells mature, Nestin is replaced by cell specific intermediate filaments such as GFAP in glial cells. Nestin expression is also reported to be upregulated following glial cell dedifferentiation in response to neuron injury[176]. Nestin has been found to stain positive for GCTs and Schwannomas on IHC[177]. Given the IHC data, we would expect GCTs to express mRNA for Nestin.

1.6.4 GFAP

Glial fibrillary acidic protein is a type III intermediate filament protein coded by the GFAP gene. GFAP is thought to be expressed by all glial cells of the nervous system at some point during cellular maturation. Levels of GFAP remain high in the glial cell of the central nervous system such as astroctyes, while the predominant cytoskeleton components of mature peripheral glial cells is vimentin[59]. In SCs, GFAP expression is inducible upon cell dedifferentiation[178]. IF GCTs are found to express the GFAP mRNA, it would suggest that GCTs arise from immature SC lines.

1.6.5 Beta Tubulin-III

Beta-tubulin-III is one of seven B-tubulin isotype proteins, that belong to the microtubule family, and is coded by the TUBB3 gene[179]. It is expressed exclusively in cells of the nervous system while other subtypes are thought to represent other cell types[180]. β-Tubulin-III is found in highest levels in neurons during cellular differentiation and growth, and lower levels at cellular maturity. There are a number of neuroblastic tumours which have high levels of β-Tub3 such as retinoblastoma or medulloblastoma[179]. In addition to a number of neural derived tumours, non-neural tumours expressing β-Tub3 include adrenal pheochromocytoma and breast cancer[180]. Glial cells are thought to not express β-tubulin. IF β-Tub3 mRNA is detected it would suggest that there was neural tissue present within the selected tissue, confounding the results of the specimen.

Chapter 2

2 Hypothesis and Rational

2.1 Hypothesis

We hypothesize that *granular cell tumours exhibit an antigen presenting cell phenotype and are derived from Schwann cells*. To test our hypothesis, we utilized IHC to examine GCT and Schwannoma immunoreactivity to APC-associated markers. We expected there to be significant differences between the IHC staining profiles of Schwannomas and GCTs, providing evidence that while they may originate from a common cell type, they express different phenotypes. We also performed qPCR to detect select gene transcripts to bolster our IHC findings.

2.2 Rationale

The current understanding is that GCTs represent a tumour originating from SC lineage, although a number of different cell types have been considered as the cell of origin for GCTs including myoblasts[1], fibroblasts[17], Schwann cells[1], histiocytes[18] and endomesenchymal cells[12]. A SC lineage is supported by the similarity of IHC profile for markers of neural crest cells and neuroectodermal origin including SOX10, S100 and NSE. SOX10 seems to be a stronger tumour marker for NCC origin compared to S100[130]. NSE is now considered to be much less specific than we originally thought, as NSE seems to be restricted to healthy neural tissue, but is induced during tumourigenesis accounting for the increased energy demands and reliance of glycolysis as an energy source[133]. One significant difference between the IHC profile of GCTs and Schwannomas previously reported is their staining for CD68, with GCTs staining strongly and diffusely, and Schwannomas staining weakly and in only a small number of cells within the lesion. Staining of CD68 a lysosomal marker supports a possible APC phenotype. Additional evidence that the granular appearance of GCTs results from the accumulation of lysosomes is supported by work identifying mutations of the gene coding for accessory proteins of H+-ATPase , ATP6AP1 and ATP6AP2 providing evidence of the abnormal lysosome content of the granular cells [36]. The finding of a genetic mutation of GCTs suggests that the GCTs are true tumours and not reactive

lesions. The serendipitous discovery of HLA-DR staining of a GCT in our lab, during a study of Langerhans cell lesions of the tongue, provides additional support of an APC phenotype for GCTs. An APC phenotype could suggest that GCTs that have undergone a mesenchymal transformation. Testing our hypothesis would further our understanding of this rare and unusual tumour. Additional IHC stains could also aid in histological diagnosis of GCTs and separation from other lesions with a granular cell appearance.

2.3 Aims and objectives.

1) Investigate an APC phenotype of GCT using immunohistochemistry. We will use a number of different antibodies to detect antigens associated with an APC phenotype, including HLA-DR, CD68, CD163, CD40 and CD11c.
2) Investigate a possible NCC origin of GCTs by detecting GAP43 immunoreactivity, in addition to S100, SOX10 and NSE.
3) Detect mRNA of Nestin, SOX2, SOX9, SOX10, NF2 and GFAP to assess level of cell maturity.

Chapter 3

3.0   Material and Methods

In this chapter I will review the methods employed in this investigation to explore an APC phenotype for GCTs using IHC techniques, and the NCC developmental phenotype of GCTs using RT-qPCR.

3.1   Case Selection

The pathology database of the Division of Oral Pathology, in Pathology and Laboratory Medicine of Schulich School of Medicine & Dentistry, Western University, was used to identify a total of 23 serial cases of benign GCTs from 2006-2016. Malignant cases were included. An additional 10 cases of Schwannoma were randomly selected from the database over the same time interval to be used as tissue control. We did not identify any instance of two separate GCTs biopsied in the oral cavity of the same individual. In the instance of the same lesion biopsied on more than one occasion, with an incisional biopsy followed by an excisional biopsy, the lesion was treated as a single case. Once cases were identified, we verified the availability of the Formalin-fixed, paraffin-embedded tissue specimens (FFPE) in the tissue archives and assessed that there was sufficient material for the completion of our proposed experiments. Confirmation of the histopathological diagnosis was made using H&E sections and light microscopy by the graduate student and an experienced Oral Pathologist (supervisor). Patient information collected included age, sex, and location of the lesion biopsied. Tables 1.1 and 1.2, summarize the demographic information for the 23 GCTs and 10 Schwannomas.

Table 1.1 Demographics and site of biopsy for Granular Cell Tumours

Case No.	Age	Sex	Site
1	41	Female	midright dorsum of tongue
2	33	Female	dorsum of tongue
3	15	Female	dorsum of tongue
4	43	Male	dorsum of tongue
5	20	female	right tongue
6	36	Male	dorsum of tongue
7	48	female	left posterior hard palate
8	50	Male	dorsum of tongue
9	37	female	left lateral border of tongue
10	55	female	right palatal mucosa
11	39	female	dorsum of tongue
12	21	female	right dorsum of tongue
13	52	male	right lateral border of tongue
14	48	male	right dorsum of tongue
15	46	male	right dorsum of tongue
16	35	female	right dorsum of tongue
17	63	female	left dorsum of tongue
18	55	female	left dorsum of tongue
19	37	male	dorsum of tongue
20	21	female	right lateral border of tongue
21	56	male	dorsum of tongue
22	58	male	right lateral ventral tongue
23	43	Female	left dorsal tongue

Table 1.2 Demographics and site of biopsy for Schwannomas.

Case No.	Age	Sex	Site
1	28	Male	buccal mucosa 37
2	21	Male	left dorsum of tongue
3	23	Male	right tip of tongue
4	41	Male	left buccal mucosa
5	16	Female	*** oral cavity
6	37	Female	lower lip mucosa
7	22	Male	lower lip mucosa
8	15	Male	left buccal vestibule
9	16	Male	dorsum of tongue
10	31	Male	Upper lip

*** *site of biopsy was unspecified, anatomically from the oral cavity*

3.2. Immunohistochemistry

GCTs and Schwannomas were stained for neural markers: S100, SOX10, NSE and GAP43; APC markers: HLA-DR, CD68, CD163, CD40 and CD11c. IHC for these antigens was performed at the London Health Sciences Centre, London Ontario, using Dako Autostainer Link 48. IHC staining for GAP43, CD40 and CD11c was completed in our laboratory at the Department of Pathology and Laboratory Medicine, Schulich School of Medicine & Dentistry, Western University. Sections processed by the University Hospital Pathology Laboratory. Table 2 provides a summary of the IHC antibodies used in this investigation.

Table 2. Summary of the IHC antibodies applied to the GCTs and Schwannomas

Antibody	Manufacture/ Cat#	Antibody type	Constituent tissue and Labelling Targets	Dilution
S100	Dako, Santa Clara CA IR50461-2	rabbit polyclonal	Neural tissues, S100B (strong) S100A1 and S100A6 (weak)	Automated
NSE	Dako, Santa Clara CA !R61261-2	mouse monoclonal	Neural tissues, γ-enolase subunit	Automated
SOX10	Santa Cruz Biotech, Dallas TX, sc-365692	mouse monoclonal	Neural tissues, SOX10 transcription factor	Automated
GAP43	Bio-Techne Canada, Oakville On, NB300-143	rabbit polyclonal	Regenerating neural tissues/growth cones, GAP43 intracellular growth protein/membrane protein	1/5000
HLA-DR	Dako, Santa Clara CA MO74601	Mouse monoclonal	APCs and lymphocytes, Alpha-chain of HLA-DR cell surface receptor	Automated
CD68	Dako, Santa Clara CA GA61361-2	Mouse monoclonal	Macrophage, lysosomal-associated membrane proteins	Automated
CD163	Vector laboratories, Burlingame CA VP-C374	Mouse monoclonal	Macrophage, hemoglobin-scavenger receptor	Automated
CD40	Abcam, Toronto ON, ab13545	Rabbit polyclonal	APCs, cell surface innate immune response costimulatory protein	1/1000
CD11c	Abcam, Toronto ON, ab52632	Rabbit monoclonal	APCs, cell surface fibrinogen receptor	1/300

3.2.1 Slide preparation

Five μm tissue sections of each case were cut from FFPE blocks using a microtome (Microm HM 325;GMI Inc., Ramsey, MN). Tissue sections were then transferred to a warm water bath and mounted onto positively-charged glass slides. The slides were left to dry overnight in an incubator at 37°C.

3.2.2 IHC staining protocols for GAP43, CD40 and CD11c

Sections of GCTs and Schwannomas, in addition to appropriate positive controls (Schwannoma for GAP43 and tonsil for CD40 and CD11c) and negative case controls, were used. The sections

were hydrated using standard serial ethanol gradient. Endogenous peroxidase activity was quenched with 3% hydrogen peroxide in methanol. Antigen retrieval was performed in citrate buffer (pH6) using a decloaking chamber (Biocare Medical, Pacheco, CA). The temperature profile used included 112.5°C for 90 seconds, then 90°C for 10 seconds. Sections were cooled using running tap water and then washed for 5 minutes in Phosphate-buffered Saline (PBS). Sections were placed in a humidified chamber and were blocked for 30 minutes with 2.5% horse serum. After 30 minutes, the horse serum was drained and primary antibodies were applied. Rabbit anti-human Gap43 antibody (cat no. NB300-143, Bio-Techne Canada Corporation, Oakville, ON) was applied at a 1/5000 dilution. Rabbit anti-human CD40 antibody (cat no. ab13545, Abcam, Toronto ON) was applied at a 1/1000 dilution. Rabbit anti-human CD11c (cat no. ab52632, Abcam, Toronto ON) was applied at a dilution of 1/300. Slides were incubated overnight at 4°C. Negative control included incubation of slides in 2.5% horse serum alone (no primary antibody).

The next day, sections were washed 3 times for 3 minutes each in PBS and then incubated with secondary antibody. ImmPRESS anti-Rabbit IgG peroxidase (cat No. VECTMP540150, MJS Biolynx, Brockville,ON) was used for GAP43 and CD11c detection for 30 minutes at room temperature. Avidin-Biotin Complex VECTASTAIN Elite ABC-HRP Kit (cat no. PK-7200, Vector Laboratories, Burlington, ON, Canada) was used for CD11c at room temperature for 30 minutes. Sections were then washed 3 times for 3 minutes each in PBS. To visualize the staining, sections were incubated with a 3,3'-Diaminobenzidine (DAB) peroxidase substrate kit (cat no VECTSK4100, MJS Biolynx, Brockville,ON) for up to 10 minutes. The sections were counterstained with Harris hematoxylin (Leica Biosystems Inc, Concord, ON). Sections were dehydrated through ascending alcohols, cleared with xylene and cover slipped using Cytoseal (Fisher Scientific, Toronto, ON) for microscopic examination.

3.3 Evaluation of immunostaining

All slides were examined under light microscopy and scored according the semiquantitative methods described below. In addition to manual scoring, 5 randomly selected cases of both GCTs and Schwannomas for the antibodies GAP43, CD68, HLA-DR, CD163, were subjected to digital analysis using QuPath.

3.3.1 Manual IHC scoring

Each IHC slide was evaluated under light microscopy by the graduate student author and an experienced Oral Pathologist utilizing a semiquantitative analysis described below. The negative and positive control sections were compared to their study section to ensure that DAB staining of the sections was representative of the primary antibody IHC target. During the manual scoring of granular cells, only the large polygonal cells that matched the histological description of the granular cells of GCTs were assessed. Regarding Schwannomas, given the presence of a capsule, analysis was restricted to spindle shaped cells within the capsule. The scoring criteria consisted of an objective analysis of the average number of cells that stained positive within representative high-powered fields for the given section. Staining intensity was subjectively scored relative to the appropriate positive controls. The scoring system used in this investigation are illustrated in Table 3.1 and 3.2.

Table 3.1 Staining Intensity. Semiquantitative scoring values for identifying stain intensity of GCTs and Schwannomas, relative to positive controls

Score	Staining intensity
0	Absent
1	Weak
2	Moderate
3	High

Table 3.2 Percentage of cells stained. Semiquantitative scoring values for identifying the percent of cells staining positive within representative high-powered fields

Score	Percent positive staining
0	0%
1	0-50%
2	>50%

3.3.2 IHC digital analysis.

Five cases of GCTs and Schwannomas underwent high resolution whole-slide imaging using the Aperio slide scanner at the Department of Pathology and Laboratory Medicine, London Health Science Center for GAP43, HLA-DR, CD163 and CD68. Images were then uploaded to QuPath (v0.1.2), a validated open source software for bioimage analysis. Images stained with the same IHC antibody (5 cases of GCT and 5 cases of Schwannoma) were grouped to create a multi-slide project. For each of the four multi-slide projects, the same workflow was followed. Pixel size of all images was verified to be less than 0.5x0.5 μm ensuring that images were of adequate resolution for analysis. Image type for all images was set to Brightfield (H-DAB). The polygon tool was then used to accurately trace the boundaries of the lesion/region of interest, defining an object for analysis for each image. A representative image was then selected to perform color deconvolution, setting the stain vectors for Hematoxylin, DAB, and the background. Automated cell detection was completed by identifying cell nuclei, via the hematoxylin optical density and nucleus size parameters. The cells boundaries were digitally determined via cell expansion parameters, relative to the nuclei of the cells in proximity. Positive cell detection was determined by the mean DAB optical density of the cell. A detection classifier was trained by adjusting the DAB optical density classification for low, medium and high intensities after visually selecting cells that had objectively low, medium and high staining intensities as a reference. The workflow for

the representative image was then used to write a script that was applied to all images in the multi-slide project. Data from cell detection was reported as percentage of cells detected and as an H-score. H-scores range from 0-300 and are calculated by 3x percentage of strong staining + 2x percentage of moderate staining + 1x percentage of weak staining (total ranging from 0 to 300).

Figure 1. Select images taken from QuPath digital file of GCT Case# 1. Immunoreactivity of anti-HLA-DR antibody detected by DAB optical density (brown color), counterstained with haematoxylin. Indeterminate magnification. a) demonstrating the object for cell detection defined by the red border. b) Demonstrating positive cell detection stratified by mean DAB optical density, blue= negative, yellow= low intensity, orange = medium intensity and red = high intensity.

a)   b)
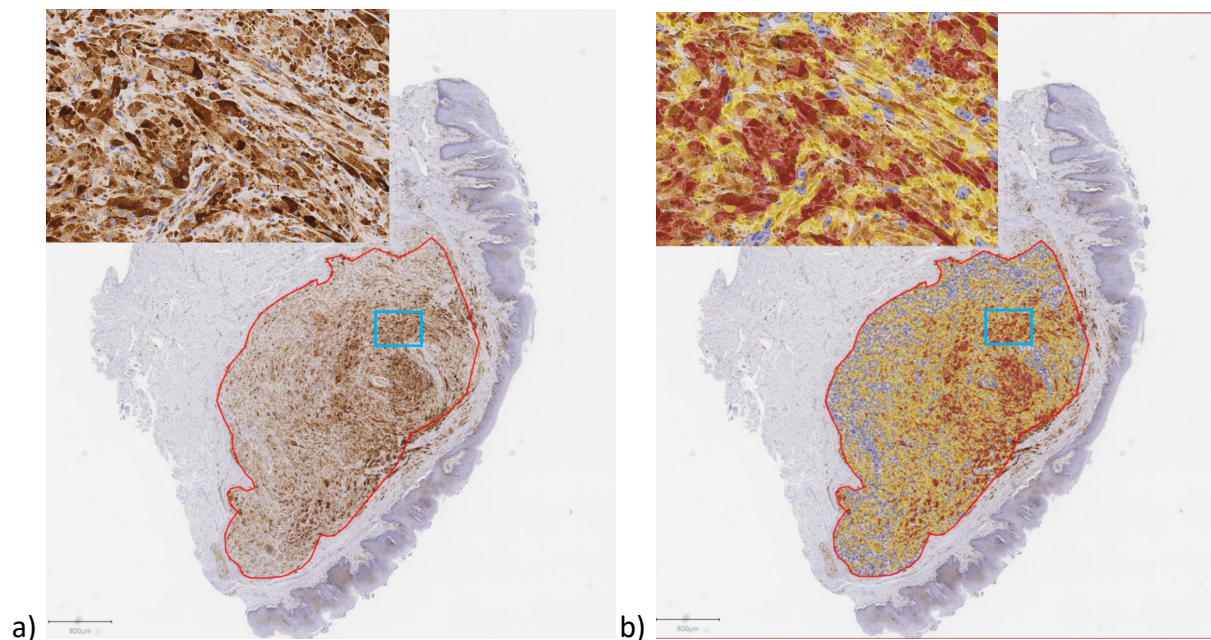
3.4 Statistical analysis of IHC results using semiquantitative and QuPath

Given that percent cells stained and stain intensity are both ordinal variables, a linear-by-linear association test was completed to assess for the correlation of the two variables between the pooled GCT and Schwannoma data resulting in a near perfect correlation. Due to the high level of correlation, only stain intensity was used for further statistical analysis, and results comparing staining intensity between GCTs and Schwannomas can be extrapolated to the percentage of cells staining. A Cochrane-Armitage test for trend using a generalized chi-squared test was used to compare the overall staining intensities for GCTs vs Schwannomas and for the 9 IHC antibodies used in this study with the ordered nominal variable (intensity) and a non-ordered nominal variable cell type. As multiple hypotheses were applied to the same data set, we applied a Bonferroni correction. Three of the IHC stains (S100, CD40 and CD11c) had no variability within their data set and were of equal values between GCTs and Schwannomas – these were not used when calculating the Bonferroni correction with m=6 ($\alpha_{bonferroni}$ =0.5/6)

Using the data generated by digital analysis, student t-tests, and Welch's t-test correction were performed to asses for differences between the H-scores of GCTs and Schwannomas. Again, a Bonferroni correction was used with m=4 ($\alpha_{bonferroni}$ 0.5/4). We also completed a Pearson correlation coefficient test, comparing the H-scores and the staining intensity for each individual IHC antibody.

3.5 Protocol for RT-qPCR

In this section, I will describe the protocols used for extracting RNA from FFPE tissues, the synthesis of cDNA from RNA, and methods for RT-qPCR to detect reactivity of CD68, Nestin, SOX2, SOX9, SOX10, NF2, GFAP, and β-Tub3.

3.5.1 Tissue preparation

Eleven FFPE blocks were assessed to have sufficient tumour material to proceed with RNA extraction. Tissue H&E was examined under light microscopy to identify a region of the tumour that demonstrated typical features of GCTs, and all attempts were made to exclude any non-tumour cells. The region of interest was marked on the H&E slide using a marking pen, and we identified the corresponding site of the FFPE block and obtained a 1 mm punch biopsy at a depth of 1mm. The tissue plug was then placed into 1.5 mL collection tube. We verified that the site of the punch biopsy was representative of the tumour by obtaining 5 μm tissue sections, of each respective case, from hydrated FFPE blocks using a microtome. H&E staining of these sections were completed, and the sections were visualized under the microscope confirming the accuracy of the tissue punches to be restricted to tumour tissue in all 11 cases.

3.5.2 Deparaffinization of tissue

Paraffin was removed from the specimens using the following procedures. First Xylene was added to the collection tubes, agitated on a vortex mixer (3 times for 4 seconds), and incubated for 2 minutes. The tubes were spun at 12000 x g for 2 minutes. The supernatant was discarded and the steps were repeated 3 times. We then repeated the process using 70% ethanol. Supernatant was removed from the tube and the tissue was incubated for 15 minutes at 55°C to ensure that the tissue plugs were dry.

3.5.3 RNA isolation

RNA isolation was completed using the High Pure FFPE RNA Micro Kit (Roche Applied Sciences, Mannheim, Germany, Cat # 04823125001). Tissue lysis buffer and 10% sodium dodecyl sulfate were added to the tissue plugs, followed by protein kinase K solution. Tubes were then agitated and incubated at 55°C for 3 hours. The cell lysate was extracted and placed into a RNA binding spin column. Each tube was then spun and the flow-through was discarded. DNase solution was

added, and the tubes were allowed to incubate 15 minutes at room temperature. Total RNA was then purified by rinsing the spin columns with a series of buffer solutions, centrifuging at 8000 x g for 5 minutes and discarding the supernatant each time. Elution buffer was added and allowed to incubate at room temperature for 1 minute. The RNA spin column was then centrifuged at 8000 x g for 1 minute. The RNA eluate was collected and used for RNA quantification.

3.5.4 RNA quantification

RNA concentration of the RNA eluate was measured using the Qubit Quan-iT RNA BR assay kit (Thermo Fisher Scientific Carlsbas, CA, USA, cat # Q10210) and Qubit Flurorometer. Qubit RNA BR reagent was diluted to 1:200 in Qubit RNA BR buffer. A total of 198 μL of prepared Qubit working solution and 2 μL of RNA eluent were added to clear 0.5 mL tubes. An additional 2 tubes were prepared by adding 10 μL Qubit standards to 190 μL of working solution and were used to calibrate the fluorometer to the standards. Concentration of RNA was then referenced to the prepared standards. RNA concentration in μg/mL was determined using the formula [QF = fluorescence reading]:

$$\text{RNA concentration} = QF * (200/\mu L \text{ sample added})$$

3.5.5 cDNA synthesis and RT-qPCR

In our study, 6 of 11 samples yielded sufficient RNA to proceed with complimentary DNA (cDNA) synthesis. Isolated RNA was transcribed to cDNA using the iScript cDNA Synthesis Kit (Bio-Rad Laboratories, Inc., Hercules, CA, Cat # 1708890). For each sample, 20 μL of cDNA mixture was prepared (4 μL 5x iScript reaction mix, 1 μL iScript reverse transcriptase, 100 ng RNA and balance of the volume as nuclease free H_2O). RT-qPCR reactions were carried out in 96 well arrays (Hard-Shell® Low-Profile Thin-Wall 96-Well Skirted PCR Plates, Bio-Rad, HSP-9601). Each well contained 10 μL RT² SYBR Green qPCR Mastermix (Bio-Rad, 330501), 2 μL primer (primer information in Table 4), 1 μL cDNA mix and 7 μL nuclease free water. We also used a No Template Control (NTC),

which contained 8 µL of nuclease free water, and no cDNA. The array was constructed with case # as the Y axis and RT-qPCR was completed over a total of 40 cycles of amplification. qPCR was performed in Bio-Rad CFX Connect. β-actin was used as housekeeping gene. Data was analyzed by ΔΔCT method using CFX Manager (Bio-Rad Laboratories).

Table 4. Summary of primers employed in RT-qPCR

Gene Assay	Vendor	Cat #	Amplicon Length	Exon-spanning
CD68	QIAGEN	QT00037184	73 bp	Y
NESTIN	QIAGEN	QT01015301	75 bp	Y
SOX2	QIAGEN	QT00237601	64 bp	N
SOX9	QIAGEN	QT00001498	111 bp	Y
SOX10	QIAGEN	QT01670326	145 bp	Y
NF2	QIAGEN	QT00030191	148 bp	Y
GFAP	QIAGEN	QT00081151	96 bp	Y
Beta-Actin	QIAGEN	QT01680476	104 bp	Y
Beta- TUB3	QIAGEN	QT00083713	78 bp	Y

CHAPTER 4

4.0 Results:

In this section, I will review our interpretation of the results obtained in the investigation of an APC phenotype using IHC techniques and a NCC developmental phenotype using RT-qPCR.

4.1 Demographics

The mean age for patients diagnosed with a biopsy-confirmed GCT was 41.4 ± 13.1. GCTs were most prevalent in the 4th-6th decades of life with 6 cases diagnosed in the 4th and 5th decade and 7 in the 6th decade (Figure 2.1). The mean age for patients with a biopsy proven Schwannoma was 25 ± 9. Lesions were most prevalent in the 3rd decade of life.

Figure 2.1 Distribution of patient age at the time of biopsy for GCTs and Schwannomas
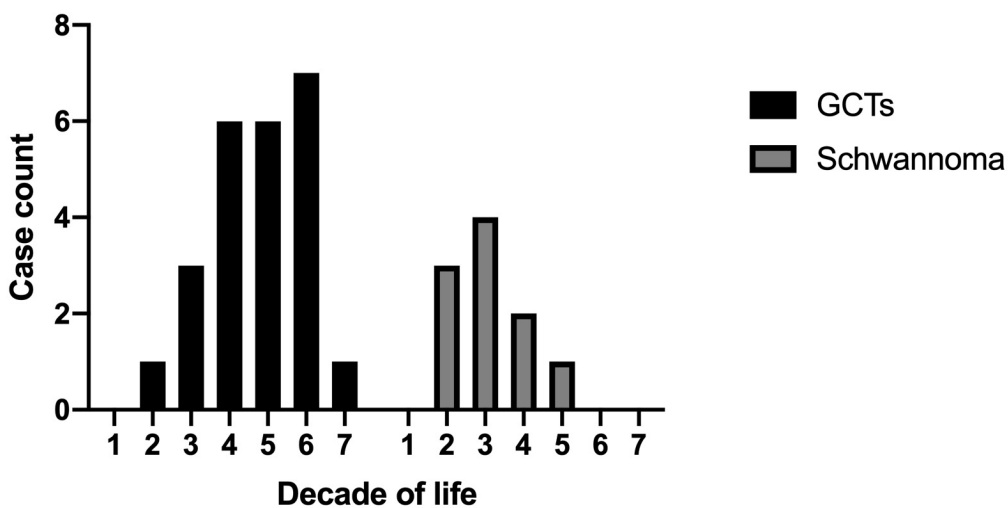
There were 14 cases of GCTs in females and 9 in males with a female:male ratio of 1.56:1 (Figure 2.2). There were 8 cases of Schwannomas in males and 2 in females with a male:female ratio of 4:1.

Figure 2.2 Sex distribution for GCTs and Schwannomas
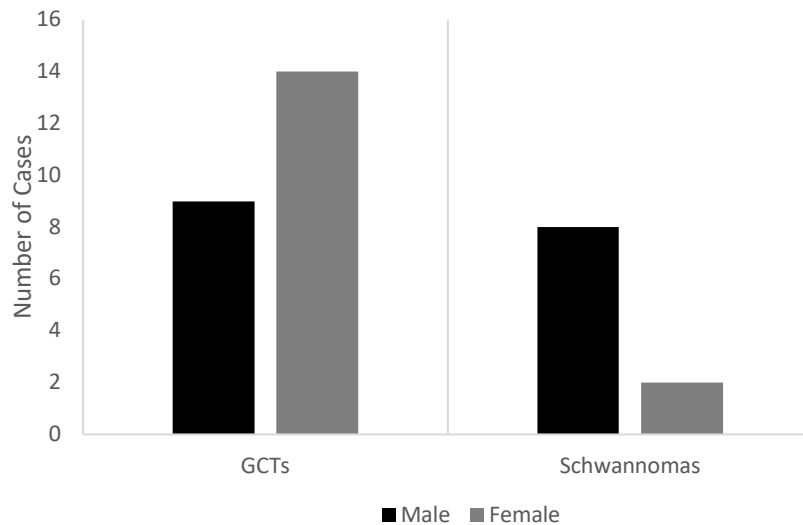
Incidence of anatomic location within the oral cavity are demonstrated below (Table 5.1 and 5.2). The most common location for GCTs was the dorsal tongue with 16/23 lesions or 69.5% of cases. There was no obvious anatomical site predilection for Schwannomas.

Table 5.1 Summary of anatomic location of GCTs

Anatomical site	Incidence
Dorsum of tongue	16
Lateral tongue	4
Ventral tongue	1
Hard palate	1
Soft palate	1

Table 5.2 Summary of anatomic location of Schwannomas

Anatomical site	Incidence
Buccal mucosa	3
Dorsum tongue	2
Lateral tongue	1
Lip	3
Undisclosed oral cavity	1

4.2 Qualitative evaluation of GCTs and Schwannomas

In this section, I will review the objective findings of each antibody employed in this investigation for both GCTs and Schwannomas.

4.2.1 Qualitative evaluation of S100 staining

S100 immunoreactivity was identified in both cytoplasm and nuclei of cells in GCTs and Schwannomas, although nuclear staining appeared to be greater than that of cytoplasm (Figure 3). Of note, when examining the spindle cells of Schwannomas, the staining was more punctate with bands of higher staining intensity in direct proximity to the nucleus, while cytoplasm staining of GCTs was more diffuse. Objectively, nearly all granular cells of GCT, and spindle cells of Schwannomas were found to stain positive with little to no variability in the staining intensity of positively staining cells.

Figure 3. **Immunohistochemical reactivity of S100 in GCTs and Schwannomas.**
Immunoreactivity was detected by DAB (brown colour). Images were taken using 200x original magnification. a) GCT stained with high intensity and diffusely in all cells, b) Schwannoma stained with high intensity in all cells with a punctate appearance
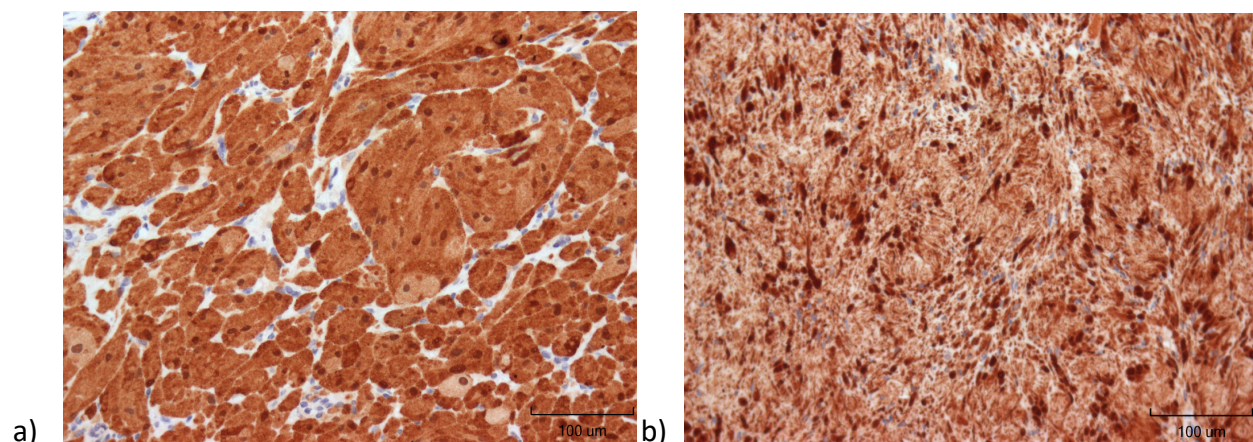
4.2.2 Qualitative evaluation of NSE staining

Objectively, there was a difference in the staining of NSE immunoreactivity between GCTs and Schwannomas. Staining of GCTs was restricted to the cytoplasm, while Schwannomas were found to have mostly cytoplasm staining although nuclear staining was seen in many cells (Figure 4). Nearly all GCT granular cells were found to stain positive and with high intensity. Within a given granular cell, no identifiable architecture could be identified but there were patchy regions that stained with higher intensity that the remainder of the cytoplasm. Most spindle cells of Schwannomas were found to stain positive, although cells with absent immunoreactivity were identified, certainly more than 50% of cells stained positive in all cases. In cases of Schwannoma that stained with medium intensity, the level of staining was relatively the same for all cells that stained positive in a given section. There was no architectural pattern of staining identified for the spindle cells.

Figure 4. **Immunohistochemical reactivity of NSE in GCTs and Schwannomas.**
Immunoreactivity was detected by DAB (brown colour). Images were taken using 200x original magnification. a) GCT stained with high intensity in the majority of cells B) Schwannoma stained positive with weak to moderate intensity in >50% of cells

a)   b)
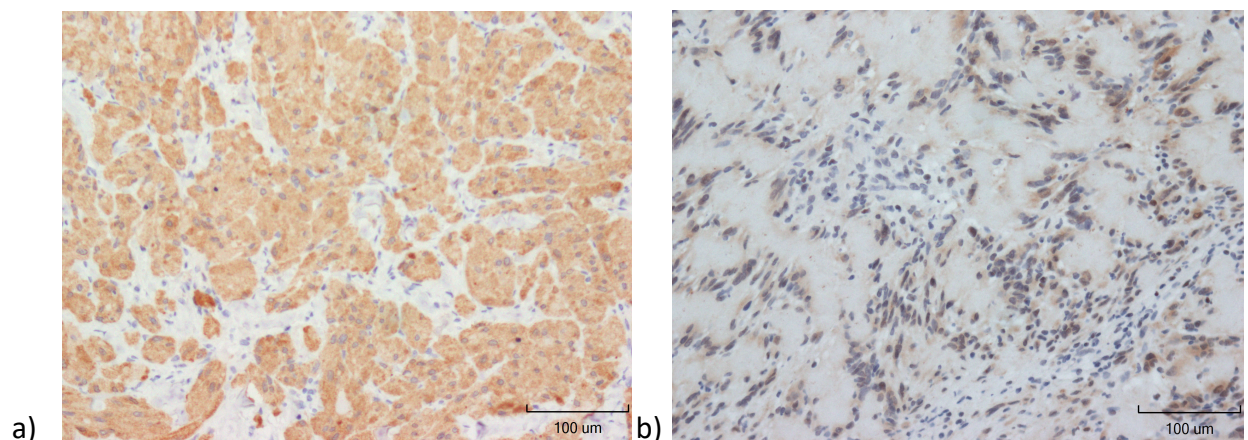
4.2.3 Qualitative evaluation of SOX10 staining

SOX10 immunoreactivity was restricted to the nucleus of GCTs and Schwannomas (Figure 5). Staining was of high intensity for all cells, and there was almost no variability in the staining intensity of cells in the same section. There was some background blushing that was seen on the Schwannoma sections, but not the GCTs, however it did not impact our analysis. There was one section of GCT, case #21, that had no immunoreactivity for SOX10 (data not shown). Given that all other cases stained with high intensity in almost all cells, we repeated IHC staining for case #21. Negative reactivity was also seen on the second section processed (data not shown). It should be noted that this section had freeze artifact, however immunoreactive staining for all other antibodies on this section were nearly identical to other sections for that particular antibody.

Figure 5. **Immunohistochemical reactivity of SOX10 in GCTs and Schwannomas.** Immunoreactivity was detected by DAB (brown colour). Images were taken using 200x original magnification. a) GCT, nucleus stained with high intensity in all cells b) Schwannoma, nucleus staining with high intensity in all cells
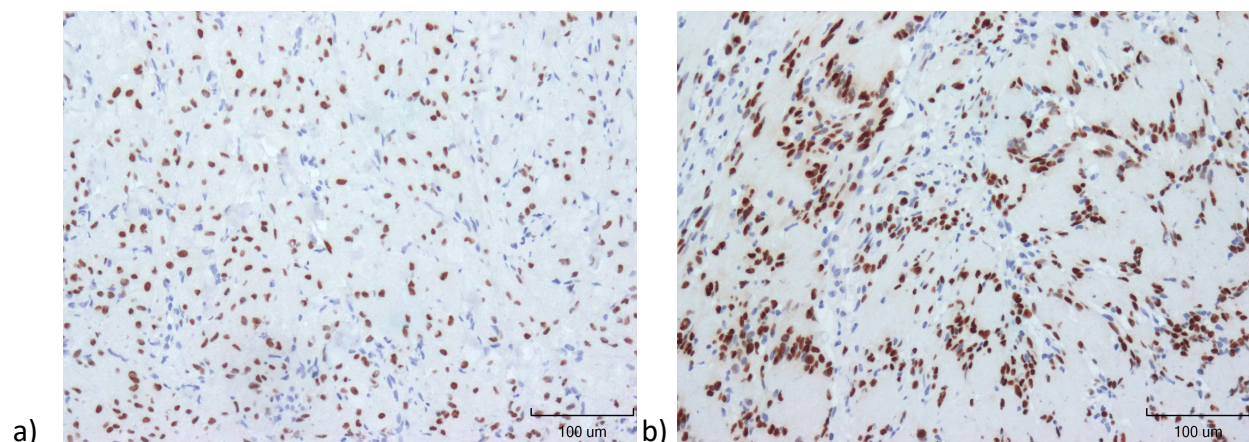
4.2.4 Qualitative evaluation of GAP43 staining

Objectively there was a difference between the immunoreactivity of GCTs and Schwannomas (Figure 6.1 and 6.2). Both GCT and Schwannoma immunoreactivity was found to be restricted to the cytoplasm. There was considerable variability in the staining intensity of the cells both when comparing sections of the same tumour and when comparing positive cells from the same section for both GCTs and Schwannomas. For GCTs, two different cell staining patterns were identified. Cells either stained mostly diffusely with sparse punctate staining, or cells stained mostly with a punctate pattern, and minimal diffuse cytoplasmic staining. Within a given section, granular cells tended to either demonstrate more punctate or more diffuse staining patterns. Staining of the Schwannomas was considerably different than that of GCTs. All positive spindle cells demonstrated diffuse cytoplasmic staining and a punctate pattern was not appreciated. Spindle cells found in the densely populated Antoni A areas were found to stain with high intensity. In contrast, the spindle cells of the Antoni B areas were either negative for GAP43 reactivity or stained with low to moderate intensity in less than 50% of the cells. This gave a patchy appearance to the Schwannoma GAP43 sections. During our semiquantitative analysis, sections with a higher percentage of Antoni A areas, relative the their Antoni B areas, scored higher than sections with a higher percentage of Antoni B relative to Antoni A areas. An unexpected finding was localized staining of some epithelial cells of the stratum basale, and blushing of the stratum spinosum was also seen for nearly all cases.

Figure 6.1 Immunohistochemical reactivity of GAP43 in GCTs and Schwannomas.

Immunoreactivity was detected by DAB (brown colour). Images were taken using 200x original magnification. a) GCT, stained with high intensity in all cells, mixed diffuse and punctate staining. B) Schwannoma, Antoni A regions stained with high intensity with a diffuse appearance, while Antoni B was weak or absent
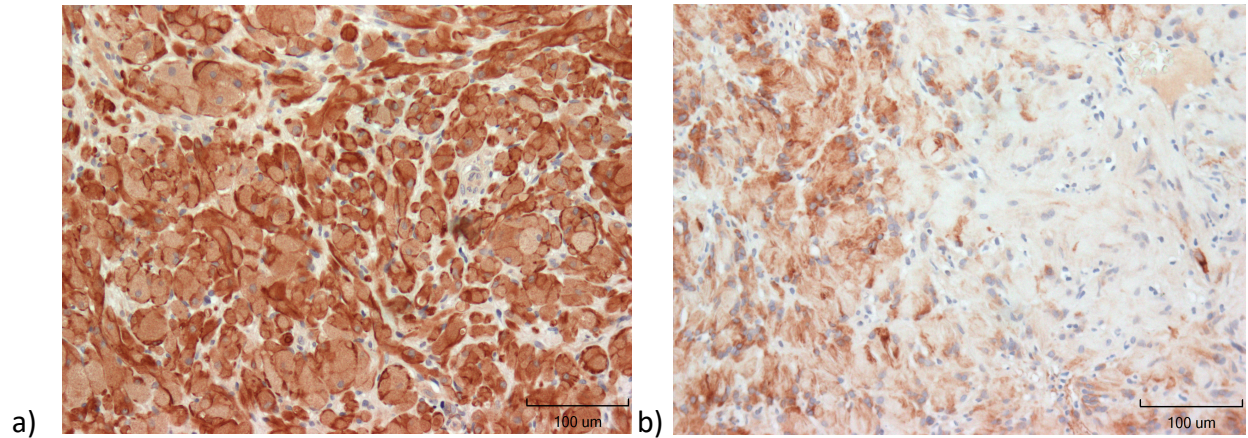
Figure 6.2 Immunohistochemical reactivity of GAP43 in Schwannomas.

Immunoreactivity was detected by DAB (brown colour). Image was taken using 20x original magnification. Antoni A regions stained with high intensity, while Antoni B stained with low intensity or negative staining
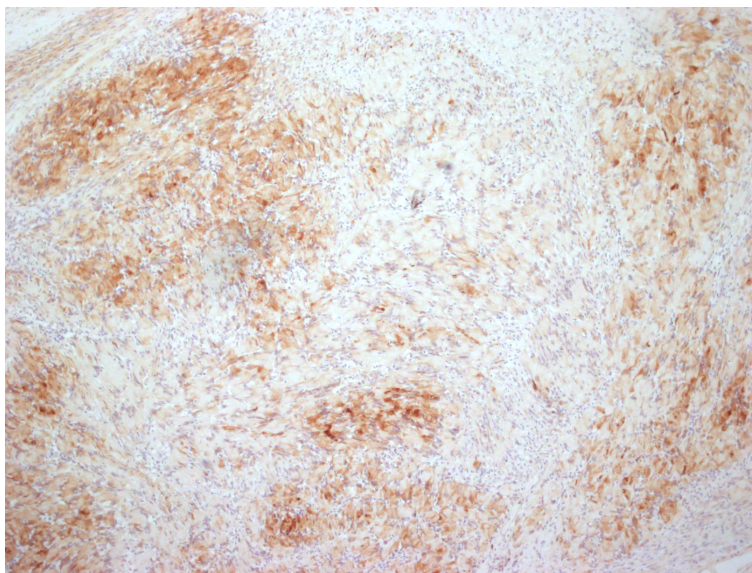
4.2.5 Qualitative evaluation of HLA-DR staining

Both GCTs and Schwannomas has similar staining for HLA-DR immunoreactivity (Figure 7). Staining was mostly restricted to the cytoplasm, with some nuclei appearing to stain positive for GCTs. Staining patterns were punctate on a diffuse background for both tumours. Nearly all granular cells of GCTs and spindle cells of Schwannomas stained positive with a high intensity, and there was minimal variability when comparing sections or cells of the same section for both tumours.

Figure 7. **Immunohistochemical reactivity of HLA-DR in GCTs and Schwannomas.** Immunoreactivity was detected by DAB (brown colour). Images were taken using 200x original magnification. a) GCT stained with high intensity and diffuse appearance B) Schwannoma stained with high intensity and diffuse appearance
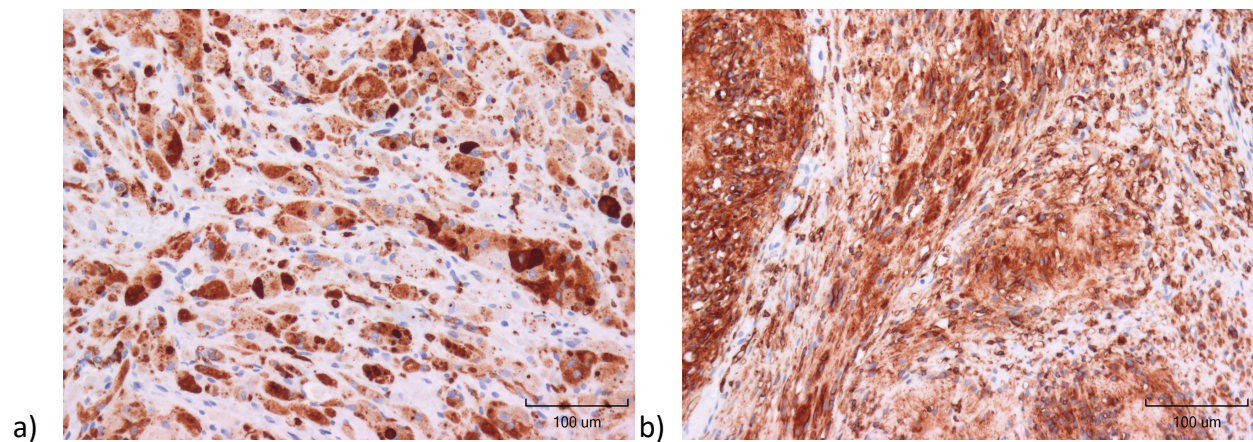
4.2.6 Qualitative evaluation of CD68 staining

There were considerable differences in the staining of CD68 immunoreactivity for GCTs and Schwannomas (Figure 8). Staining was restricted to the cytoplasm of both tumours. GCTs were found to stain with a punctate pattern on a light diffuse cytoplasmic background. All cells had similar staining intensity, both when comparing cells of a given section or when comparing section. Schwannoma staining was variable. One section was void of any appreciable staining for CD68 immunoreactivity. The other 9 sections had low to moderate staining. Some cells identified as positive had as few as one appreciable granule of staining, while other cells had more of a diffuse cytoplasm reactivity.

Figure 8. **Immunohistochemical reactivity of CD68 in GCTs and Schwannomas.**
Immunoreactivity was detected by DAB (brown colour). Images were taken using 200x original magnification. a) GCT stained with high intensity in all cells with a diffuse appearance. B) Schwannoma staining was negative
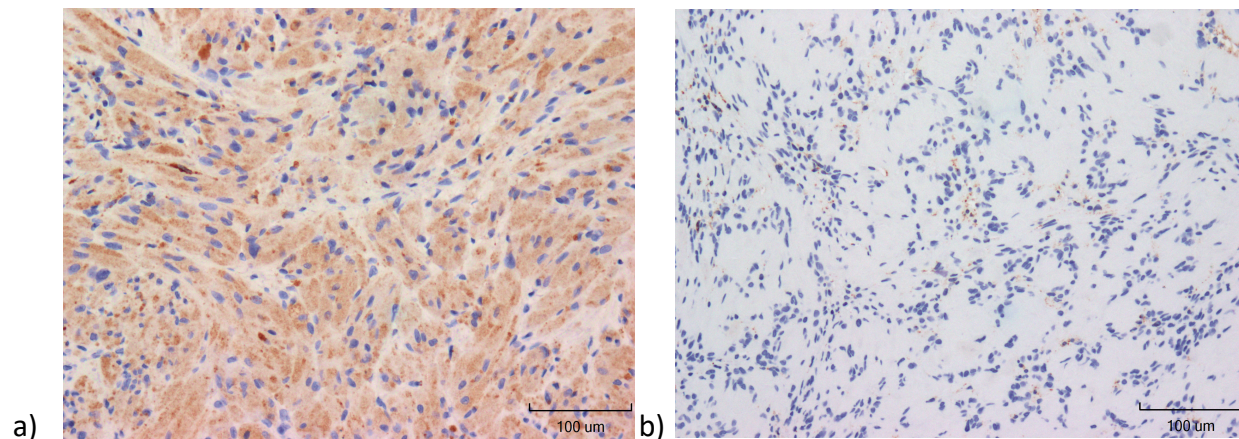
4.2.7 Qualitative evaluation of CD163 staining

Schwannomas were found to stain positive for CD63 with a high intensity in all sections, while GCT immunoreactivity was absent (Figure 9). Schwannoma staining was punctate for all cells, and staining was restricted to the cytoplasm. The number of granules varied between cells, but the majority of cells stained positive. On examination of the GCT sections, a number of cases demonstrated what appeared to be dendritic reactive for CD163, but they were not seen in all cases.

Figure 9. **Immunohistochemical reactivity of CD163 in GCTs and Schwannomas.**
Immunoreactivity was detected by DAB (brown colour). Images were taken using 200x original magnification. a) GCT staining was negative. B) Schwannoma stained with high intensity and punctate appearance in the majority of cells

a) 100 um b) 100 um
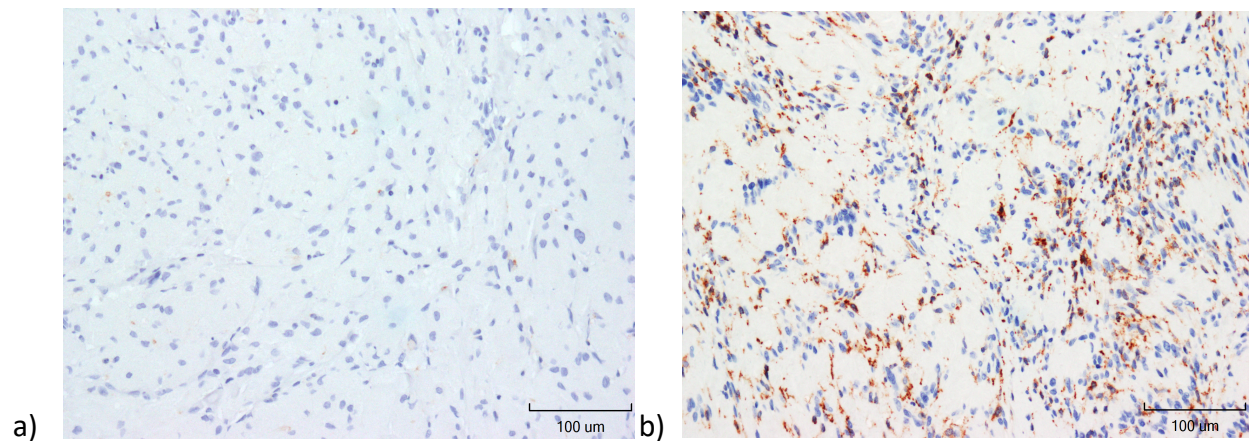
4.2.8 Qualitative evaluation of CD40 staining

Schwannomas and GCTs were both found to have no to scant staining of CD40 immunoreactivity (Figure 10). Some sections for both tumours had some cells with a dendritic appearance staining positive for CD40.

Figure 10. **Immunohistochemical reactivity of CD40 in GCTs and Schwannomas.**
Immunoreactivity was detected by DAB (brown colour). Images were taken using 200x original magnification. a) GCT staining was negative. B) Schwannoma staining was negative
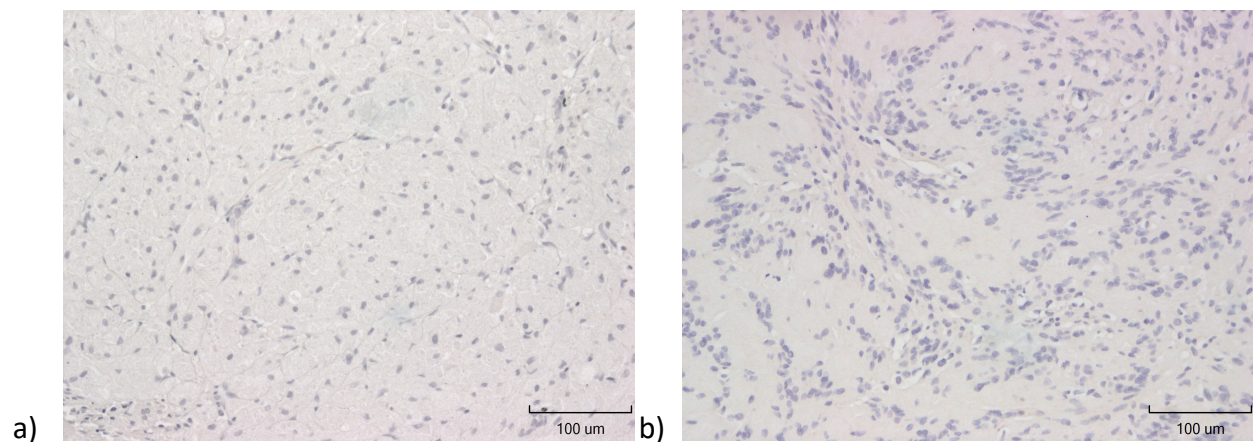
4.2.9 Qualitative evaluation of CD11c staining

Schwannomas and GCTs were both found to have no to scant staining of CD11c immunoreactivity (Figure 11). Some sections for both tumours had some cells with a dendritic appearance staining positive for CD11c.

Figure 11. **Immunohistochemical reactivity of CD11c in GCTs and Schwannomas.** Immunoreactivity was detected by DAB (brown colour). Images were taken using 200x original magnification. a) GCT staining was negative. B) Schwannoma staining was negative
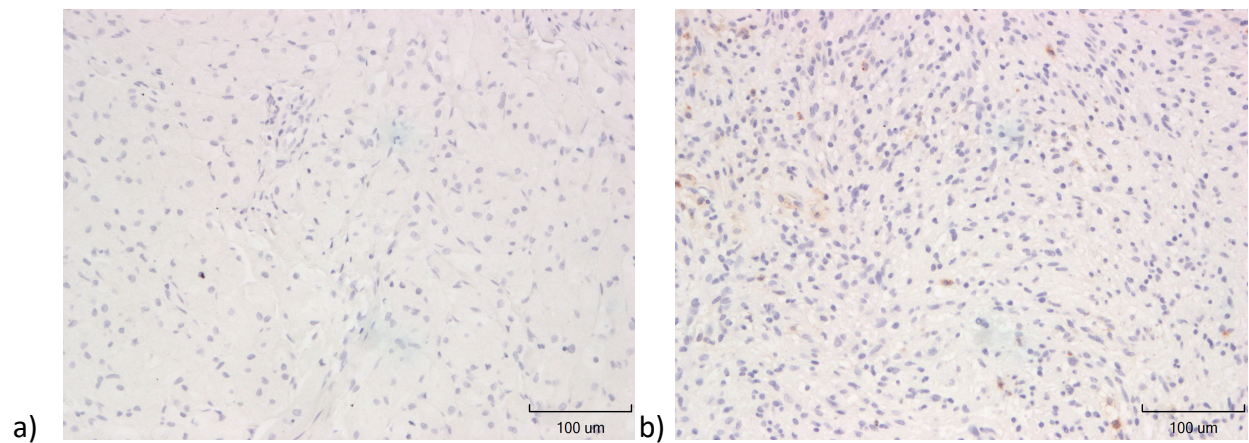
4.3 Semiquantitative Analysis using manual scoring.

Tables 6.1 and 6.2 show cumulative scores for percentage of cells stains and stain intensity for GCTs and Schwannomas. This data was used to complete statistical comparisons between GCTs and Schwannomas for our semiquantitative scoring system.

Table 6.1 Percentage of cells staining positivity for IHC reactivity in GCTs and Schwannomas.

Case 2 of GCT did not have a section for CD163 IHC

IHC antibody	Tumour type	0 (0%)	1 (>0≤50%)	2 (>50%)
S100	GCT	-	-	23
	Schwannoma	-	-	10
NSE	GCT	-	-	23
	Schwannoma	-	-	10
SOX10	GCT	1	-	22
	Schwannoma	-	-	10
GAP43	GCT	-	-	23
	Schwannoma	-	3	7
HLA-DR	GCT	-	-	23
	Schwannoma	-	-	10
CD68	GCT	-	-	23
	Schwannoma	1	6	3
CD163	GCT	22*	-	-
	Schwannoma	-	-	10
CD40	GCT	23	-	-
	Schwannoma	10	-	-
CD11c	GCT	23	-	-
	Schwannoma	10	-	-

Table 6.2. Objective assessment of mean DAB stain intensity in GCTs and Schwannomas

Case 2 of GCT did not have a section for CD163 IHC

IHC antibody		Absent	Low	Medium	High
S100	GCT	-	-	-	23
	Schwannoma	-	-	-	10
NSE	GCT	-	-	3	20
	Schwannoma	-	4	6	-
SOX10	GCT	1	-	-	22
	Schwannoma	-	-	-	10
GAP43	GCT	-	-	2	21
	Schwannoma	-	-	4	6
HLA-DR	GCT	-	-	6	17
	Schwannoma	-	-	4	6
CD68	GCT	-	-	17	6
	Schwannoma	1	6	3	-
CD163	GCT	22*	-	-	-
	Schwannoma	-	-	1	9
CD40	GCT	23	-	-	
	Schwannoma	10	-	-	
CD11c	GCT	23	-	-	
	Schwannoma	10	-	-	

4.3.1 Investigating the difference between intensity and percentage variables

A contingency table was constructed with the ordinal variable percentage cells staining as the x-variable and staining intensity as the y-variable. A linear-by-linear association test was completed. The p-value <0.0000000000000002, identifies that the two variables are almost perfectly correlated. We rejected the null hypothesis that there is no association between the variables: percent cells stained and cell stain intensity. Assuming the correlation between variables, we chose to complete further analysis using only the ordinal variable for staining intensity and can extrapolate our findings to percent cells staining.

4.3.2 Investigating the Difference between GCT and Schwannoma for all antibodies using data obtained from semiquantitatve method

For each antibody used, a chi-squared table was constructed using the ordinal variable (staining intensity) as the x-axis and nominal variable (cell type) as the y-axis. Given that we are performing multiple tests, a Bonferroni correction was applied. CD40, CD11c, and S100 antibody scoring was identical between GCTs and Schwannomas. Without variance between these three data sets, we were unable to complete a statistical analysis, but can assume that there is no statistical difference in the staining patters between GCTs and Schwannomas for the antibodies S100, CD40 and CD11c. Our Bonferoni correction was m = 6 (6 tests), and our new alpha value is $\alpha_{bonferroni}$ = 0.05/6 = 0.0083.

We found no statistical difference between the staining intensity for the antibodies SOX10 (p= 0.5), GAP43 (p= 0.03), HLA-DR (p = 0.4). As previously mentioned, statistical analysis was not completed for the antibodies S100, CD40 and CD11c, but without variance between their staining intensities there is no significant difference in the staining intensity for these antibodies (p= 1).

Significant higher stain intensity was identified for GCTs the antibodies NSE (p= 0.000008), CD68 (p = 0.0001) . CD163 had significantly higher stain intensity for Schwannomas (p= 0.00000007).

An additional Cochrane-Armitage test was completed to compare the cell staining intensity across all variable for GCTs and Schwannomas. The staining intensities were compiled into a single chi-squared table. A significant difference was identified between the overall staining intensities for GCTs and Schwannomas (α= 0.05, p=0.000004).

4.4 H-score analysis obtained from QuPath Bioimage analysis

As previously described, QuPath was used to digitally identify cells staining positive, which were then further stratified into low, medium and high staining intensities. In Table 7. data for percent cells staining positive and the h-score are provided.

Table 7. Summary of % cells staining positive and H-score obtained from QuPath Bioimage analysis.

Tissue type	GAP43		HLA-DR		CD68		CD163	
	% positive	H-score	% positive	H-score	% positive	H-score	% positive	H-score
GCT	81.79 +/- 10.95	121.39 +/- 52.18	78.63 +/- 12.4	142.90 +/- 77.26	88.52 +/- 11.42	188.11 +/-41.94	10.14 +/- 7.67	10.54 +/- 8.03
Schwannoma	32.86 +/- 15.12	38.53 +/- 20.50	83.00 +/- 16.67	168.16 +/- 89.49	24.07 +/- 10.2	27.7 +/- 13.13	68.43 +/- 15.22	90.11 +/- 35.34

4.4.1 Investigating the Difference between GCT and Schwannoma for GAP43, HLA-DR, CD68 and CD163 using H-score

During our statistical analysis, it became apparent that the distribution of H-score may follow a non-Gaussian distribution, however given the low case count it was difficult to perform an analysis of variance. We elected to proceed with both student's t-test for Gaussian distribution, and Welch's t-test for non-Gaussian distribution. Again, a Bonferroni correction was applied with $m = 4$ (4 tests) resulting in $\alpha_{bonferroni} = 0.05/4 = 0.0125$. Comparisons of H-score between GCT, and Schwannoma for GAP43, HLA-DR, CD68 and CD163 antibodies are demonstrated in Figures 12.1-12.4.

Figure 12.1 H-score for GCTs and Schwannomas for anti-GAP43 antibody, a) Statistical comparison using student's t-test ($\alpha = 0.0125$, p= 0.0108), b) Statistical analysis using Welch's t-test correction ($\alpha = 0.0125$, p= 0.0201) # p $\leq$ 0.0125

a)   b)
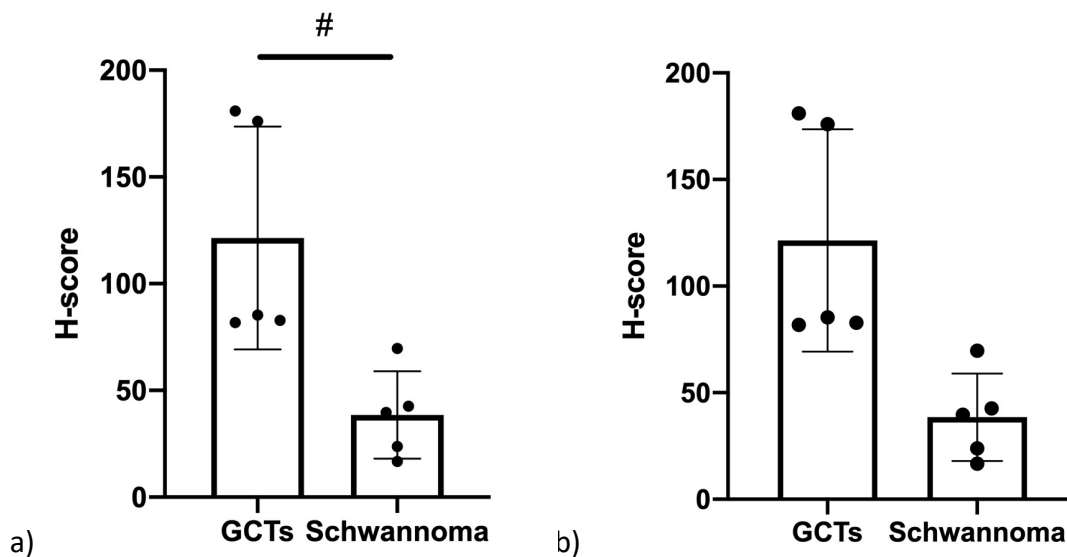
Figure 12.2. H-score for GCTs and Schwannomas for anti-HLA-DR antibody, a) Statistical comparison using student's t-test (α= 0.0125, p= 0.646), b) Statistical analysis using Welch's t-test correction (α= 0.0125, p= 0.646)
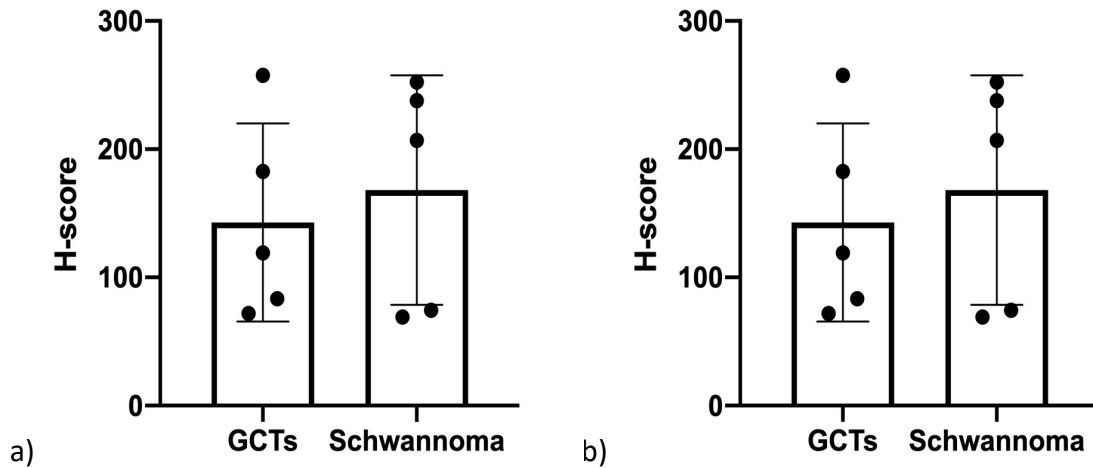
Figure 12.3. H-score for GCTs and Schwannomas for anti-CD163 antibody, a) Statistical comparison using student's t-test (α= 0.0125, p= 0.0012), b) Statistical analysis using Welch's t-test correction (α= 0.0125, p= 0.0062) # p $\leq$ 0.0125, ## p$\leq$ 0.005
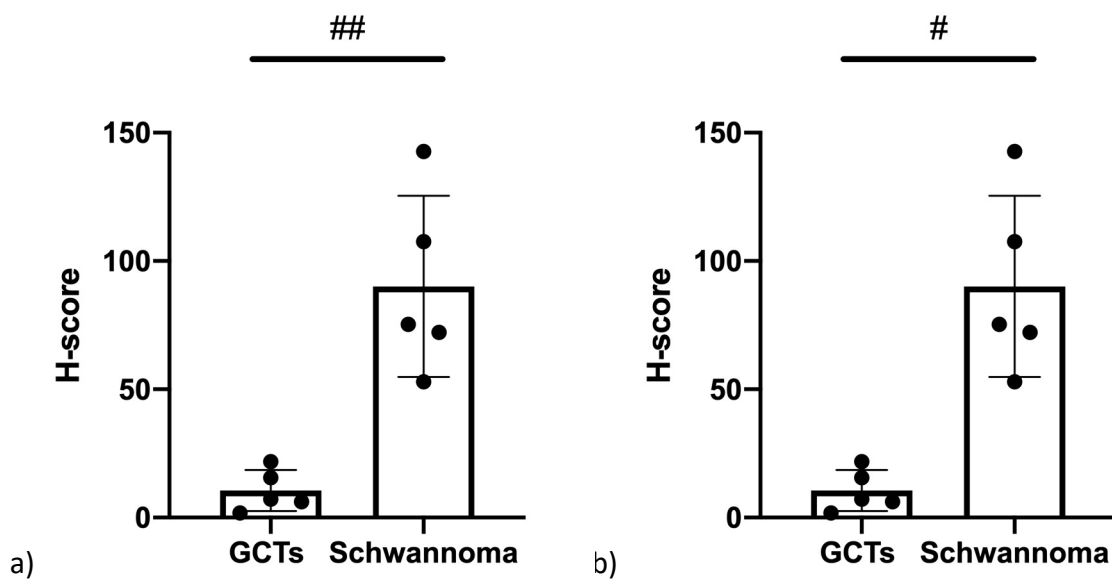
Figure 12.4. H-score for GCTs and Schwannomas for anti-CD68 antibody, a) Statistical comparison using student's t-test (α= 0.0125, p< 0.0001), b) Statistical analysis using Welch's t-test correction (α= 0.0125, p= 0.0006), ### p$\leq$ 0.001
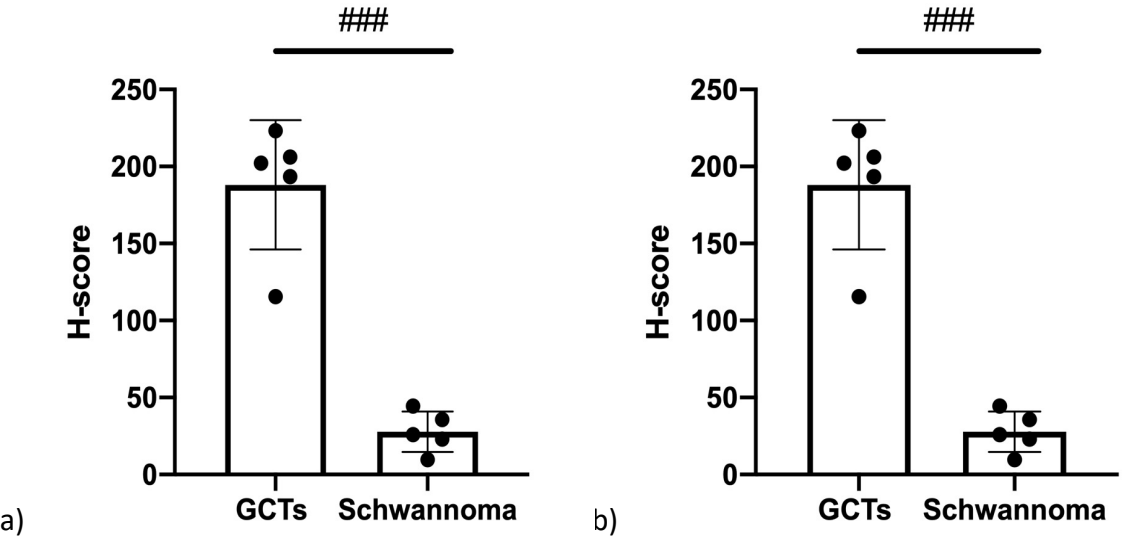
4.5 Comparing the manual scoring percentage of cell stained positive to digital bioimage analysis using QuPath

We compared the percentage cells staining for both manual and digital scoring using QuPath in Table 8. Statistical analysis was not performed for cell staining percentage. There appears to be a correlation between the Manual scoring percent cells staining positive and the positive staining cells in QuPath as the value of our semiquantitative manual score falls within the standard deviation obtained from positive cell detection using QuPath.

Table 8. Average percentage of cells staining positive for GCTS and Schwannomas. Summary of semiquantitative score using the average ordinal value for manual scoring of percent cells staining (0=0%, 1= >0≤50%, 2= >50%) and positive cell detection using QuPath

IHC Antibody	Tumour type	Manual scoring	QuPath
GAP43	GCT	2	81.79% +/- 10.94
	Schwannoma	1.7	32.86 +/- 15.12
HLA-DR	GCT	2	78.65 +/- 12.38
	Schwannoma	2	83.04 +/- 16.66
CD68	GCT	2	88.52 +/- 11.42
	Schwannoma	1.2	24.07 +/- 10.2
CD163	GCT	0	10.14 +/- 7.67
	Schwannoma	2	68.43 +/- 15.22

4.6 Comparing the manual intensity of cell staining to H-score

We compared the digital scoring (H-score) to manual scoring intensity of cell staining using Pearson's correlation coefficient and Pearson's correlation for continuous variables (T-test). Results are summarized in Table 9. All comparisons suggested statistically significant evidence that there was a near perfect correlation between the manual scoring of cell staining intensity

and the H-score derived from digital analysis using QuPath. A Bonferroni correction was not applied as the p-values for all analysis were extremely low.

Table 9. Summary of the comparison of cell stain intensity using manual semiquantitative scoring and H-score derived from QuPath

Antibody	Correlation (r)	95% CI	P-value
All tumours	0.906	0.827-0.949	0.000000000000001
GCTs only	0.903	0.767-0.961	0.00000005
Schwannomas only	0.9	0.759- 0.960	0.00000007
GAP43	0.92	0.689-0.981	0.0002
HLA-DR	0.961	0.841-0.991	0.000009
CD68	0.989	0.951-0.997	0.00000007
CD163	0.979	0.911-0.979	0.0000008

4.7 Results for RT-qPCR of GCTs

In this section, I will review the RNA data from the 11 FFPE sections, and RT-qPCR results for CD68, Nestin, SOX2, SOX9, SOX10, NF2, GFAP, β-Tub3. Transcripts were detected by SYBR fluorescence and reported as Cq values (threshold cycle). Statistical analysis was not performed.

4.7.1 RNA concentration obtained from FFPE blocks

Using the Qubit Quan-iT RNA BR assay kit and Qubit fluorometer, RNA concentration of the 11 selected cases of GCT were determined (Table 10). Sufficient RNA concentration to proceed with RT-qPCR was identified in 6/11 cases.

Table 10. Concentration of RNA extracted from FFPE tissue punches. *= RNA concentration insufficient to proceed with RT-qPCR*

Case #	RNA concentration (µg/mL)
1	**6.5**
3	17.4
6	4.24*
7	2.88*
8	**5.7**
15	**7.4**
16	Low*
17	2.2*
18	**10**
22	4.16*
23	**6.5**

4.7.2 Summary of Cq value obtained using RT-qPCR

RT-qPCR was used to detect the presence of cDNA, and reported as the Cq value, the replication cycle where signal was detected above baseline. No Statistical analysis was performed using the RT-qPCR data, results are observational/qualitative only.

β-actin was used as a housekeeping gene in this investigation to verify the integrity of mRNA obtained from FFPE tissues. β-actin mRNA was detected in 6/6 cases, and not in the NTC indicating that there was likely to be cDNA in sufficient quantity and quality for interpretation of the Cq results for the other 8 genes. It should be noted that case 18 and 23 showed high number of copies of cDNA synthesized. Raw Cq values for β-actin are summarized in table 11.1.

Table 11.1 Summary of B-actin transcripts reported as Cq value. -- fluorescence not detected

Case#	Cq
1	34.70
3	37.38
8	36.94
15	34.53
18	29.71
23	28.89
NTC	---

CD68 was identified in 5/6 specimens by RT-qPCR. Case #1 had no CD68 transcripts, despite staining densely positive in all granular cells using IHC. Cases 3, 8, 15, 18, and 23 were positive for CD68 mRNA. Raw Cq values for CD68 is summarized in table 11.2.

Table 11.2. Summary of CD68 transcripts reported as Cq value. -- fluorescence not detected

Case#	Cq
1	--
3	37.15
8	35.96
15	37.12
18	32.53
23	25.60
NTC	---

With exception of case # 23, including the NTC, none of the other cases showed detectable levels of SOX2, SOX9, SOX10, NF2 or Nestin. Transcripts were detected in cases #18 and 23 for β-Tub3, while all others were negative. No cases showed SOX2 or GFAP transcripts. Cq values for Case #23 are summarized in Table 11.3.

Table 11.3 Summary of Cq values for Case #23. -- fluorescence not detected

CD68	29.60
Nestin	39.02
SOX2	--
SOX9	36.18
SOX10	38.01
NF2	37.14
GFAP	--
Beta Actin	28.89
Beta TUB3	36.72

Chapter 5

5.0 Discussion

5.1 Clinical Features

The mean age of patients diagnosed with a GCT was 41.4 ± 13.1 years, with the highest prevalence in the 4th-6th decade, and the ratio of females to males was 1.6:1. The mean age of cases is within the standard deviation of the reported mean age from larger case series which ranges from 31-37 yrs old[4,5], and is consistent with the WHO epidemiological data on GCTs[8]. In our investigation, the sex ratio of females to males, was lower than the published ratio of the WHO of 2:1[8], however there was still a female predilection. We did not record race as this data was not readily available. For Schwannomas, we had a male: female ratio of 8:2 with a mean age of 25 ± 9 years. The mean age is consistent with the age of diagnosis for Schwannomas, however the expected sex predilection is 1:1. This would suggest that our sample has the potential for bias should sex play a role in gene expression.

All GCTs and Schwannomas were tissue taken from the oral cavity. The most common location for GCTs was the dorsal tongue at 69.5%, which is the most common location for GCTs in the oral cavity. There was no tissue predilection for Schwannomas. It is possible that GCTs of the oral cavity could express different proteins than their non craniofacial counterparts. This could make generalization of our report to non-oral cavity GCTs challenging. We recognize the lack of tissue availability, and as a result the absence of analysis of tissues from non-oral cavity sites, as a potential confound. There is no consensus if trauma plays a role in the formation of either GCTs or Schwannomas, however the anatomical location of tumours in regions that are frequently traumatized by the dentition suggests that trauma may play a role in the formation of both of these tumours.

5.2 Comparison between IHC cell stain intensity and H-score derived from QuPath

Recently, there has been an increased interest in using digital imaging analysis in both research and clinical applications as a method of both quantitatively detecting cells positive for immunoreactivity and objectively measuring staining intensity of positive cells. Stain intensity can give insight into relative protein content indicating increased activity of a target protein and its cellular function[182,183]. Traditionally, our lab has used semiquantitative analysis of immunoreactivity using traditional light microscopy. It was our intention during this project to initiate a method of digitally analyzing slides that could be used for future investigations. Our lab selected QuPath, a free open source digital bioimage analysis software that has been validated for its accuracy and reproducibility of results[184,185]. A benefit of using digital analysis is that one can create a workflow script that can be applied to all images in a project so that all images are analyzed with the same parameters. In our study, we completed Pearson Correlation Coefficient analysis, comparing H-score to cell stain intensity, for GAP43, HLA-DR, CD163 and CD68, and composites for each tumour and all sections. For all analysis, there was a near perfect correlation suggesting that there was no difference in the results obtained using each scoring methods. This can be interpreted as validating both methods of section analysis as a high H-score is predictive of a high semiquantitative score and vice versa. We recognize that our limited ability to have sections scanned using the Aperio scanner resulted in a low case count (5 sections of GCT and 5 sections of Schwannoma for each IHC antibody). However, given the high degree of correlation between H-score and our manual semiquantitative analysis of cell staining intensity our opinion is that the case count is adequate and representative of data we would obtain if we had digitized all sections included in the manual analysis.

5.3 Review of antibodies supporting a NCC origin of GCTs

While some of the antibodies employed in our investigation, NSE and S100, have had their specificity called into question, collectively this report provides a strong body of evidence to

support a NCC cell of origin for GCTs and the similarity of GCT and Schwannoma immunoreactivity would suggest that they likely develop from the same cell type. As expected, both GCTs and Schwannomas were found to stain with high intensity in all cells for S100 antibody.

Polyclonal S100 is one of the most commonly used antibodies employed by Pathologists to assist with differentiating spindle cell lesions originating from NCC and non-NCC origins. The S100 polyclonal antibody used in this investigation has highest specificity for S100B, but also low specificity to S100A1 and S100A6. S100A1 is abundant in skeletal muscle[119], while S100A6 is not cell specific but elevated levels have been associated with tumourigenesis of common malignancies and thought to be increased as a stress response[186]. There is copious evidence to suggest that neural and glial cells expresses a high level of S100 protein, particularly S100B in their healthy state[120]. It is also generally accepted that all benign and most malignant tumours originating from NCCs stain positive for polyclonal S100 immunoreactivity[120]. In contrast to the presumed specificity of S100B, a variety of tumours and cells originating from all germ layers can be induced to express S100 proteins particularly S100A8, S100A9, S100A12 and S100B as a result of oxidative stress and tissue inflammation[119]. The strong intensity of SOX10 immunoreactivity provides additional evidence of a NCC origin for GCTs, and is emerging as a more specific marker of NCC origin than S100. It is interesting to note that Case #21 was non-reactive for SOX10 immunoreactivity while staining with strong intensity in most cells for S100. Negative immunoreactivity to SOX10 was confirmed by repeating SOX10 IHC on a second section of case #21. SOX10 has been shown to stain positive for virtually all BPNST, however there are several reports identifying absence of SOX10 staining in MPNST in 30% of tumours, which can be problematic for pathologists in diagnosing malignant spindle cell lesions[187]. We were unable to find a case report identifying either peripheral benign or malignant GCTs that stained negative for SOX10 but positive for S100. Of note, central GCTs which are presumed to develop from an astrocyte origin and have virtually identical histological appearance to peripheral GCTs were found to stain negative for SOX10[188]. The SOX10 sections for case #21 were reviewed with two experienced pathologists. As a consequence of freeze artifact, the tumour architecture was distorted but the histological diagnosis of GCT was confirmed. The section also did not appear

to show evidence of malignant transformation. We considered excluding case #21 from our investigation but ultimately decided that the tissue was still interpretable for histopathology. Explanation for the lack of SOX10, in the context of the remainder of the staining profile of case #21, could either be that during tumourigenesis the tumour lost SOX10 expression, or that the lack of SOX10 staining was a consequence of freezing during tissue transport. In contrast, there are several case reports identifying GCTs to be negative for S100, but positive for SOX10 both from the oral cavity and other anatomical sites. It is unclear if these tumours referred to as primitive GCTs are derived from mesenchyme of a NCC origin that differs from traditional GCTs, or if these tumours have lost S100B expression[189]. While both GCTs and Schwannomas stained positive for NSE providing support of a NCC origin, an interesting finding of this investigation was that GCTs stained with higher intensity in a greater percentage of cells than Schwannomas for NSE. A higher intensity of NSE staining in GCTs may indicate that GCTs have a higher metabolic demand than Schwannomas as there are multiple reports that NSE is upregulated in both tumours derived from NCC and non-NCC derived turmors during inflammation and hypoxic stress.

This report is the first to identify GAP43 immunoreactivity of GCTs, with strong stain intensity in most granular cells. As of yet, their role in glial cells has yet to be determined, however there is evidence to suggest that they play a role in promoting outgrowth of neurites during development and also following nerve injury in growth cone formation[139]. It is interesting to note that GAP43 is expressed in RSC and SCP but not mature SC. Its expression also occurs late following nerve injury at 4 weeks which suggests that its expression occurs late in Wallerian degeneration following clearance of myelin debris[190]. In comparison to S100 and SOX10, GAP43 is a relatively newly discovered protein. It appears to be highly specific as a marker of neural and glial tissues. In contrast to S100 and SOX10, GAP43 expression is also retained in MPNST and has recently been suggested to have a higher sensitivity and specificity for NCC derived spindle cell malignancies than either S100 or SOX10[141]. Recent studies have identified GAP43 immunoreactivity in a variety of malignancies including papillary thyroid cancer[143], non-small cell lung cancer[144] and some breast cancers[145] calling into to question the presumed specificity of

GAP43 and suggesting that it has additional, yet to be determined roles in tumorigenesis. Additionally, tumours expressing GAP45 have a higher risk of intracranial metastasis[145]. GAP43 immunoreactivity provides new evidence that GCTs originate from NCC and provides the strongest evidence yet that GCTs likely develop from Schwann cells. It is also the first antibody to suggest that the granular cells of GCTs have a cell phenotype similar to RSC or SCP than mature SCs.

Another finding in this report that has not been described was the architecture of Schwannoma GAP43 staining. Immunoreactivity of the cell rich Antoni A region was found to stain with high intensity in most spindle cells, while the Antoni B region was found to stain with low intensity in less than 50% of the spindle cells. Antoni B regions are generally thought to be degenerated regions of Schwannomas associated with inflammation such as hyalinization, fibrosis, mucin inclusion, thrombosis, and macrophage and lymphocyte infiltration[93,98]. Greater staining of the Antoni A regions would suggest that GAP43 immunoreactivity and protein expression decreases as the spindle cells of Schwannomas begin to lose the architecture of Antoni A areas and transition to Antoni B areas. This would also suggest that the granular cells of GCTs are more similar to the spindle cells found in the Antoni A areas than the Antoni B areas.

5.4 Review of antibodies supporting an APC phenotype

Collectively, evidence from this investigation provides evidence of an APC phenotype or some APC-like features for GCTs. At the onset of our investigation, the function of the increased lysosome content of the granular cells were unknown, and it was unclear if GCTs were reactive lesions or tumours. Consistent with other reports, this investigation identified strong staining intensity in the majority of granular cells for CD68 antibody indicating that the granules are lysosomes. CD68 is generally accepted as a cell marker for tissues with phagocytic function such histiocytes, monocytes, giant cells, Kupffer cells, and osteoclasts, and it expression is thought to be regulated by a macrophage specific promoter gene[155,156]. It had been theorized that lysosomes of GCTs may indicate a phagocytic function of GCTs following nerve injury. The

presence of an abnormal number of lysosomes has now been explained by the work of Pareja et al, who have identified a novel mutation of the ATP6AP1 and ATP6AP2 genes coding V-ATPase accessory proteins which have roles in endosome acidification and transport[36]. The findings of Pareja et al. provide clear genetic evidence to explain the intensity of CD68 immunoreactivity, and confirm the theory that the accumulation of lysosomes is a result of altered lysosomal transport and function. Additional support of an APC phenotype for GCTs is from the strong intensity of immunoreactivity for HLA-DR. HLA-DR expression is associated with by APCs including B lymphocytes, activated T lymphocytes and professional APCs (monocytes, macrophage and dendritic cells). We had theorized that in combination with CD68 immunoreactivity, HLA-DR immunoreactivity would suggest that GCTs may be reactive in nature and have a role in antigen presentation during the innate immune response. This theory is disproven by evidence that the lysosomes of GCTs are non-functional and negative reactivity for the costimulatory molecule CD40 suggest that GCTs cannot participate in T-cell activation. Given that GCTs are thought to have malignant potential, it is plausible that HLA-DR expression serves a role in GCTs analogous to HLA-DR expression by melanomas. In melanomas, HLA-DR is thought to be associated with tumour-antigen presentation, tissue inflammation, and an immune response against tumour cells, and is a positive prognostic factor for survival[191]. A third explanation is that the presence of HLA-DR immunoreactivity may suggest an epithelial-mesenchymal transformation with HLA-DR immunoreactivity more indictive of tissue dedifferentiation and an APC phenotype rather than serving a role in antigen presentation. Finally, a fourth possible explanation is that expression of HLA-DR indicates tissue inflammation as HLA-DR expression has been reported in several cell populations including sinusoidal endothelial cells and hepatocytes, [150], respiratory epithelium and gastrointestinal epithelium[151] and conjunctiva[152] during tissue inflammatory responses. HLA-DR immunoreactivity has not been previously described in Schwannomas. At the onset of our investigation we presumed that HLA-DR would stain negative for immunoreactivity in the spindle cells of Schwannomas, however all sections of Schwannomas stained positive for HLA-DR with moderate to high intensity. This surprising finding could be explained by the same theories proposed for GCT HLA-DR expression. While immunoreactivity of Schwannomas to HLA-DR has not been reported, expression of HLA-

DR has been reported in gliomas and neuroblastomas[192]. In gliomas and neuroblastomas, HLA-DR expression is thought to be associated with increased tumour inflammation and patient outcomes are worse in tumours expressing higher levels of HLA-DR[192].

The negative immunoreactivity of GCTs for CD163, CD40 and CD11c do not provide support of an APC phenotype of GCTs. An interesting finding that has not been previously reported was the strong intensity of Schwannoma immunoreactivity for CD163. The upregulation of CD163 in Schwannomas could possibly be explained by a cell phenotype of the spindle cells of Schwannomas similar to the phagocytic phenotype of RSCs, and also serve as a marker of an inflammatory process. On sections of GCT we identified cells with a dendritic appearance that had reactivity to CD163. This supports inflammation within GCTs which could result in HLA-DR expression but does not provide support of an APC phenotype for GCTs.

5.5 Interpretation of raw RT-qPCR data

β-actin was used as a housekeeping gene to verify the integrity of mRNA obtained from FFPE tissues. Housekeeping transcripts were detected in 6/6 cases, and not in the NTC. Given the strong body of evidence of CD68 IHC immunoreactivity, we chose to investigate CD68 mRNA expression as a positive control, expecting that we would find high levels of CD68 mRNA present in all cases. CD68 mRNA was identified in 5/6 specimens. Case #1 did not show detectable CD68 mRNA, despite staining densely positive in all granular cells using IHC.

Case #23 demonstrated positivity for Nestin, SOX9, SOX10, NF2, and β-TUB3 transcripts. β-TUB3 gene expression indicates that there was likely neural tissue present in the cores obtained from the FFPE blocks making interpretation of RT-qPCR results of this case challenging.

Surprisingly SOX10 mRNA was only found in case 23 and not in 5/6 other cases. Lack of SOX10 cDNA is in stark contrast to previously published literature regarding GCT immunoreactivity to SOX10 and is inconsistent with the IHC findings of this investigation. Given that RT-qPCR is more

sensitive and specific that IHC, this result is perplexing. One possible theory is that SOX10 may be a stable protein, such that protein levels are detected despite low levels of mRNA. One other possible explanation is that SOX10 mRNA is more susceptible to degradation. Degradation could have occurred from chemical binding and degradation during formalin fixation and paraffin infiltration, or from poor tissue storage, as the FFPE blocks were stored at room temperature in an uncontrolled environment for as long as 12 years. Fragmented mRNA would still be detected using Qubit fluorescence. Without positive SOX10 transcript levels, it is challenging to draw conclusions from Nestin, SOX2, SOX9, SOX10, NF2 and GFAP mRNA data.

5.6 Other lesions with a granular appearance

Reviewing the literature identified greater than 40 soft tissue lesions of the head and neck region that are characterized by a granular appearance. These lesions include both malignant and benign entities derived from odontogenic, fibroblastic, histiocytic, myoblastic and neural cells of origin[193]. In this section, I will give a brief review of several of these entities and their presumed histogenesis. Similar to GCTs the cellular processes that lead to accumulation of lysosomes or other granular inclusions are mostly unknown.

A relatively rare lesion with near identical histological appearance to GCTs is the congenital epulis of newborn (CEN) or congenital granular epulis. Unlike GCTs, the most common location is the alveolar ridge with a predilection for the maxilla. While generally less than 1 cm in size, lesions can be larger resulting in feeding difficulties or possible airway obstruction[193]. On histology, CEN are characterized by large polygonal cells with eosinophilic granular cytoplasm arranged in clusters with scant connective tissue and atrophic mucosa without pseudoepitheliomatous hyperplasia. CEN can be differentiated from GCTs by their IHC profile. Evidence to suggest a differing cell of origin than GCTs are supported by the non-reactive IHC for s100, CD68, and p75 antibodies. In CEN the granules thought to represent lysosomes, have been found to stain positive for collagen suggesting they are of a myofibroblastic cell line of origin[194]. It is unclear if CEN are reactive lesions or tumours.

There are a group of tumours derived from odontogenic epithelium including, granular cell ameloblastoma (GCA), Central Granular cell odontogenic tumour (CGOT), granular cell ameloblastic fibroma (GCAF), calcifying epithelial odontogenic tumour, and granular cell odontogenic cyst[193]. Unlike GCTs, GCA tend to appear heterogenous with granular cell islands interspersed with an epithelial stroma. In GCA, granular change is indicative of an aggressive variant of ameloblastoma, and is concerning for malignant change, and metastasis. The granular cells demonstrate great variability in granule size and are thought to represent ancient change as they tend to be found centrally while the peripheral tumour architecture maintains a stellate reticulum pattern[193]. It is generally accepted that the granules ae lysosomes, although it is unclear if the granular cells are a result of ongoing phagocytosis or a change in cell morphology similar to GCTs. They are reactive for CD68, and cytokeratin, but non-reactive for s100, vimentin, and NSE refuting a NCC origin and supporting an epithelial origin[195]. The CGCOT has granular cells arranged in sheets and lobules interspersed with cords of odontogenic epithelium, without stellate reticulum. The granular cells are thought to originate from fibroblasts as on histology there appears to be a transformation from fibroblast at the periphery to granular cells centrally with an increased granular appearance thought to be lysosomes. Due to the rarity of the lesion the IHC profile has been poorly explored, but case series have identified that they stain for vimentin and CD68, but negative for S100 and NSE immunoreactivity. Collectively the histological and immunohistochemical findings are interpreted to suggest a mesenchymal transformation of fibroblasts similar to CEN[196]. Another group of lesions restricted to the head and neck region include benign and malignant salivary gland tumours.

Other soft tissue lesions that can arise in any region of the body that can have a granular cell change include, leiomyoma, rhabdomyoma, neurilemmona, dermatofibroma, and their associated sarcomas. Hodgkins' lymphoma also has cells with a granular appearance, as do some tumours of histiocytic origin such as langerhan histiocytosis and verruciform xanthoma[193]. There are also lesions that can metastasize to the head and neck including the granular cell variant of renal cell carcinoma, hepatocellular carcinoma, and breast adenocarcinomas that are

characterized by cells with a granular appearance. Granular cells can also be seen in melanomas and basal cell carcinomas[193]. It is important for the Pathologist to be aware of these other lesions when considering a histopathological diagnosis of GCT to ensure that patients receive the most appropriate course of treatment.

5.7 Limitations of this study

While digital analysis is likely more accurate than objective scoring methods, and certainly seems to be better at detecting small differences in staining intensity, there are several criticisms of whole slide analysis using QuPath. Firstly, cell detection relies on QuPath detecting cell nuclei and then using programed algorithms to determine the boundaries used for cell borders. While analysis of nucleus staining is highly accurate, the algorithmically calculated cytoplasmic expansion may not be truly representative of actual cell membranes and the contents of cell cytoplasm. This results in inaccuracies when analyzing IHC stains either restricted to the cytoplasm or those that stain both cytoplasm and the nucleus. Another concern identified during cell detection was that the nucleus diameter is set manually. If the diameter was set too high then nuclei of positive staining cells were missed in the analysis. In contrast when the nuclear diameter was set to capture the majority of positive cells there was incidence of nucleus fractioning based on variations of the optical density of the hematoxylin stain within the nucleus that were interpreted as separate nuclei by the QuPath algorithm. This resulted in an artificially increased number of cells detected in both positive and negative cells. During analysis we made the assumption that nucleus fractioning was the same for both positive cells and negative cells which would not affect the H-score as the formula for H-score is based on the percentage of cells staining positive at low medium and high intensity. A third concern identified during QuPath analysis was that when performing whole tumour analysis all cells with nuclei smaller than the programed diameter are identified during cell detection including those that are not of interest. It is possible to manually exclude individual cells from your assessment however for most of the tumours the cell count was greater than 50 000 cells, with some tumours having cell counts as high as 120 000. This error during digital analysis was most apparent during QuPath analysis of

GCT sections for CD163. During manual scoring it was evident that there were a number of cells that stained positive in sections of GCTs that had a dendritic appearance suggesting presence of inflammation within the tumour, while all granular cells appeared to stain negative for CD163 immunoreactivity. As an example, using QuPath case 11 had positive cell identification of 21% for CD163 while case 9 had only 1.6% positive cell identification. An alternative approach to whole slide imaging is to select regions of the tumour for analysis with a more manageable cell count, however this can result in selection bias if the chosen region is not representative of the entire tumour. Finally, as the thresholds for low, medium and high staining intensity corresponding to DAB optical density are entered manually interpretation of an H-score should only be made between tissues that were assessed using the same algorithm. Light microscopy of sections can suffer from analysis errors such as selecting fields that are not representative of the tumour, varying conditions such as microscope brightness, and errors in interpreting cell immunoreactivity could result in diagnostic or scoring errors. Recognize that DAB staining intensity can be relative to the duration that the tissue section is exposed to DAB during tissue processing, the use of subjective cell stain intensity as a measure of protein content is not a precise measure, and interpretation of cell function should be used cautiously. Additionally, while identifying cells that stain positive for an antigen is suggestive of upregulation of the protein, it is possible that there is cross reactivity between other proteins with a similar structure. Cross reactivity of SOX10 in GCTs must be questioned due to the absence of SOX10 mRNA. In light of a strong body of evidence that GCTs are immunoreactive for SOX10, we believe the absence of SOX10 mRNA may be due to technical issues.

5.8 Future work

Recognizing that mRNA extraction from FFPE is challenging and highly technique sensitive, it could be valuable to repeat our RT-qPCR experiments investigating a NCC developmental phenotype of GCTs using an alternative RNA isolation protocol. It would also be of value if either fresh tissue or fresh frozen tissue were available to allow for more predictable RNA extraction

and stability. Given the rarity of GCTs, and their benign presentation obtaining tissue before formalin fixation is unlikely.

It is important for pathologists to be aware of the rare and atypical variants of tumours that can have a granular cell appearance in order to make an accurate histopathological diagnosis given the similarity of the histology for many of these lesions. Correct identification requires appropriate use of IHC antibodies, and correlation with the clinical presentation, anatomic location and tissue architecture. Given that granular variants of many of these lesions are rare little is known about their tumourigenesis. Generally, the accumulation of lysosomes is thought to represent a mesenchymal change and dedifferentiation of the precursor cells with unknown significance. More work needs to be done to explore the variety of lesions that can occur with granular appearance. Specifically, it would be interesting to assess for mutations of lysosome formation, acidification and transportation using gene sequencing similar to the methods used to identify genetic mutations of ATP6AP1 and ATP6AP2 in GCTs. Given that the epidemiological data indicates a higher female predilection it would be interesting to investigate ATP6AP1 and ATP6AP2 gene expression of the inactivated X-allele. If ATP6AP1 and ATP6AP2 are co expressed by the X and Xi chromosomes it could be a possible explanation for the higher female predilection of GCTs.

Chapter 6

6 Conclusion

This study provides new evidence of a NCC cell of origin for GCTs, likely originating from SC lineage as supported by IHC immunoreactivity of GAP43. Specifically, GAP43 has been shown to be expressed by SCP and RSC, but not mature SC suggesting that the GCT phenotype is more similar to dedifferentiated SC than mature myelinating or non-myelinating SCs. We also provide additional evidence of an NCC of origin by IHC immunoreactivity to NCC markers S100, SOX10 and NSE. While we provided evidence of HLA-DR and CD68 immunoreactivity, other commonly used IHC antibodies supporting an APC phenotype CD163, CD40 and CD11c were non-reactive. Collectively the IHC evidence provides weak evidence of an APC phenotype for GCTs.

We have also provided new evidence of Schwannoma IHC immunoreactivity for CD163, suggesting either a phagocytic phenotype analogous to repair SCs or inflammation within the tumour. This report is also the first to describe the differences in the staining patters of Antoni A and Antoni B areas of Schwannomas for GAP43 providing support that Antoni B areas develop from degenerated Antoni A areas.

Unfortunately, we were not able to provide molecular evidence of a NCC origin or identify a developmental NCC phenotype of GCTs given the challenges faced during RT-qPCR. While PCR has higher specificity and sensitivity than IHC, the lack SOX10 transcripts raises questions about the methods used in RNA extraction and cDNA synthesis and the quality and quantity of RNA extracted. Reliable qPCR data would have allowed us to make conclusions about similarities of GCTs to SC developmental stages. Access to fresh or frozen tissue would improve the validity of RT-qPCR results and could provide definitive evidence of an NCC origin for GCTs.

As a result of the strong evidence that GCT tumourigenesis is from NCCs, most likely SCs, we propose that GCTs should be added to the PNST classification system. Additionally, as a granular cell appearance is not unique to GCTs we propose a name change to Granular Nerve Sheath Tumour which is more descriptive of this rare lesion.

Citations

1.   Ordonez NG, Mackay B. Granular Cell Tumor : A Review of the Pathology and Histogenesis. *Ultrastractural Pathol*. 1999;23:207-222. doi:10.1080/019131299281545

2.   Chow LTC, Chow MBCY. Intraneural granular cell tumor: Histologic spectrum and histogenetic implication. *J Cutan Pathol*. 2020;47(1):57-60. doi:10.1111/cup.13558

3.   Lack EE, Worsham RGF, Callihan MD, et al. Granular cell tumor: A clinicopathologic study of 110 patients. *J Surg Oncol*. 1980;13(4):301-316. doi:10.1002/jso.2930130405

4.   Vance III SF, Page Hudson Jr. R. Granular Cell Myoblastoma: Clinicopathologic Study of Forty-two Patients. *Am J Clin Pathol*. 1969;52(2):208-211. doi:10.1093/ajcp/52.2.208

5.   Khansur T, Balducci L, Tavassoli M. Granular cell tumor. Clinical spectrum of the benign and malignant entity. *Cancer*. 1987;60(2):220-222. doi:10.1002/1097-0142(19870715)60:2<220::aid-cncr2820600217>3.0.co;2-v

6.   Goodstein ML, Eisele DW, Hyams VJ, Kashima HK. Multiple synchronous granular cell tumors of the upper aerodigestive tract. *Otolaryngol Head Neck Surg*. 1990;103(4):664-668. doi:10.1177/019459989010300426

7.   Hatta J, Yanagihara M, Hasei M, Abe S, Tanabe H, Mochizuki T. Case of multiple cutaneous granular cell tumors. *J Dermatol*. 2009;36(9):504-507. doi:10.1111/j.1346-8138.2009.00684.x

8.   Speight PM. *World Health Organization Classification of Tumors: Pathology and Genetics of Head and Neck Tumors.* (Barnes L, Everson J, Reichart P SD, ed.). Jyon: IARCPress; 2005.

9.   Curtis R, Stewart HJS, Hall SM, Wilkin GP, Mirsky R, Jessent KR. GAP43 Is Expressed by Nonmyelin-forming Schwann Cells of the Peripheral Nervous System. 1992;116(6).

10.   Barakat M, Kar AA, Pourshahid S, et al. Gastrointestinal and biliary granular cell tumor: diagnosis and management. *Ann Gastroenterol*. 2018;31(4):439-447. doi:10.20524/aog.2018.0275

11.   Rivlin ME, Meeks GR, Ghafar MA, Lewin JR. Vulvar granular cell tumor. *World J Clin cases*. 2013;1(4):149-151. doi:10.12998/wjcc.v1.i4.149

12.   Gurzu S, Ciortea D, Tamasi A, et al. The immunohistochemical profile of granular cell (Abrikossoff) tumor suggests an endomesenchymal origin. *Arch Dermatol Res*. 2015;307(2):151-157. doi:10.1007/s00403-014-1505-3

13.   Porta N, Mazzitelli R, Cacciotti J, et al. A case report of a rare intramuscular granular cell tumor. *Diagn Pathol*. 2015;10(1):162. doi:10.1186/s13000-015-0390-1

14.   Worsaae N, Schwartz O, Pindborg JJ. Follow-up study of 14 oral granular cell tumors. *Int J Oral Surg*. 1979;8(2):133-139. doi:10.1016/S0300-9785(79)80008-3

15.   Ferreira JCB, Oton-Leite AF, Guidi R, Mendonca EF. Granular cell tumor mimicking a squamous cell carcinoma of the tongue: a case report. *BMC Res Notes*. 2017;10(1):14. doi:10.1186/s13104-016-2325-7

16. Toi PC, Siddaraju N, Basu D. Fine-needle aspiration cytology of granular cell tumor: A report of two cases. *J Cytol*. 2013;30(3):195-197. doi:10.4103/0970-9371.117641

17. Miller AS, Leifer C, Chen S-Y, Harwick RD. Oral granular-cell tumors: Report of twenty-five cases with electron microscopy. *Oral Surgery, Oral Med Oral Pathol*. 1977;44(2):227-237. doi:https://doi.org/10.1016/0030-4220(77)90273-0

18. Sobel HJ, Marquet E, Avrin E, Schwarz R. Granular cell myoblastoma. An electron microscopic and cytochemical study illustrating the genesis of granules and aging of myoblastoma cells. *Am J Pathol*. 1971;65(1):59-78.

19. Manara GC, De Panfilis G, Bacchi AB, et al. Fine structure of granular cell tumor of abrikossoff. *J Cutan Pathol*. 1981;8(4):277-282. doi:10.1111/j.1600-0560.1981.tb01012.x

20. Stewart CM, Watson RE, Eversole LR, Fischlschweiger W, Leider AS. Oral granular cell tumors: A clinicopathologic and immunocytochemical study. *Oral Surgery, Oral Med Oral Pathol*. 1988;65(4):427-435. doi:10.1016/0030-4220(88)90357-X

21. Mukai M. Immunohistochemical localization of S-100 protein and peripheral nerve myelin proteins (P2 protein, P0 protein) in granular cell tumors. *Am J Pathol*. 1983;112(2):139-146.

22. Musha A, Ogawa M, Yokoo S. Granular cell tumors of the tongue: Fibroma or Schwannoma. *Head Face Med*. 2018;14(1):1-7. doi:10.1186/s13005-017-0158-9

23. Nagel H, Hemmerlein B, Ruschenburg I, Huppe K, Droese M. The value of anti-calretinin antibody in the differential diagnosis of normal and reactive mesothelia versus metastatic tumors in effusion cytology. *Pathol Res Pract*. 1998;194(11):759-764. doi:10.1016/S0344-0338(98)80065-4

24. Campbell LK, Thomas JR, Lamps LW, Smoller BR, Folpe AL. Protein Gene Product 9.5 (PGP 9.5) Is Not a Specific Marker of Neural and Nerve Sheath Tumors: An Immunohistochemical Study of 95 Mesenchymal Neoplasms. *Mod Pathol*. 2003;16(10):963-969. doi:10.1097/01.MP.0000087088.88280.B0

25. Martins M, Anunciato de Jesus L, Fernandes K, Bussadori S, Taghloubi S, Martins MA. Intra-oral Schwannoma: Case report and literature review. *Indian J Dent Res*. 2009;20(1):121-125. doi:10.4103/0970-9290.49059

26. Shintaku M. Immunohistochemical localization of autophagosomal membrane-associated protein LC3 in granular cell tumor and Schwannoma. 2011:315-319. doi:10.1007/s00428-011-1104-z

27. Regezi JA, Zarbo RJ, Courtney RM, Crissman JD. Immunoreactivity of granular cell lesions of skin, mucosa, and jaw. *Cancer*. 1989;64(7):1455-1460. http://www.ncbi.nlm.nih.gov/pubmed/2776107. Accessed November 30, 2016.

28. Schrader KA, Nelson TN, De Luca A, Huntsman DG, McGillivray BC. Multiple granular cell tumors are an associated feature of LEOPARD syndrome caused by mutation in PTPN11. *Clin Genet*. 2009;75(2):185-189. doi:10.1111/j.1399-0004.2008.01100.x

29. Aragues IH, Dominguez MC, Blanco VP, Zubicaray BE, Fernandez RS. LEOPARD syndrome

and multiple granular cell tumors: An underreported association? *Indian J Dermatol Venereol Leprol*. 2016;82(1):77-79. doi:10.4103/0378-6323.171642

30. Castagna J, Clerc J, Dupond A-S, Laresche C. [Multiple granular cell tumours in a patient with Noonan's syndrome and juvenile myelomonocytic leukaemia]. *Ann Dermatol Venereol*. 2017;144(11):705-711. doi:10.1016/j.annder.2017.06.008

31. Moatamedi M, Derakhshan M. LEOPARD syndrome: a case report and literature review. *Clin Med*. 2019;19(Suppl 3):23. doi:10.7861/clinmedicine.19-3-s23

32. Turner AM. Noonan syndrome. *J Paediatr Child Health*. 2014;50(10):E14-20. doi:10.1111/j.1440-1754.2010.01970.x

33. Fragale A, Tartaglia M, Wu J, Gelb BD. Noonan syndrome-associated SHP2/PTPN11 mutants cause EGF-dependent prolonged GAB1 binding and sustained ERK2/MAPK1 activation. *Hum Mutat*. 2004;23(3):267-277. doi:10.1002/humu.20005

34. Franca JA, de Sousa SF, Moreira RG, et al. Sporadic granular cell tumours lack recurrent mutations in PTPN11, PTEN and other cancer-related genes. *J Clin Pathol*. 2018;71(1):93-94. doi:10.1136/jclinpath-2017-204849

35. Rifkin RH, Blocker SH, Palmer JO, Ternberg JL. Multiple granular cell tumors. A familial occurrence in children. *Arch Surg*. 1986;121(8):945-947. doi:10.1001/archsurg.1986.01400080091017

36. Pareja F, Brandes AH, Basili T, et al. Loss-of-function mutations in ATP6AP1 and ATP6AP2 in granular cell tumors. *Nat Commun*. 2018. doi:10.1038/s41467-018-05886-y

37. Jansen EJR, Timal S, Ryan M, et al. ATP6AP1 deficiency causes an immunodeficiency with hepatopathy, cognitive impairment and abnormal protein glycosylation. *Nat Commun*. 2016;7(May). doi:10.1038/ncomms11600

38. Sekimizu M, Yoshida A, Mitani S, et al. Frequent mutations of genes encoding vacuolar H + -ATPase components in granular cell tumors. *Genes Chromosom Cancer*. 2019;58(6):373-380. doi:10.1002/gcc.22727

39. Fanburg-Smith JC. Malignant granular cell tumor of soft tissue: diagnostic criteria and clinicopathologic correlation. *Am J Surg Pathol*. 1998;22(7):779-794. doi:10.1097/00000478-199807000-00001

40. Nasser H, Danforth RD, Sunbuli M, Dimitrijevic O. Malignant granular cell tumor: Case report with a novel karyotype and review of the literature. *Ann Diagn Pathol*. 2010;14(4):273-278. doi:10.1016/j.anndiagpath.2009.08.004

41. Jardines L, Cheung L, LiVolsi V, Hendrickson S, Brooks JJ. Malignant granular cell tumors: report of a case and review of the literature. *Surgery*. 1994;116(1):49-54.

42. Hemalatha A, Rajan P, Prasad C, Ambikavathy M. Red flag in granular cell tumors: Role of a pathologist. *Clin Cancer Investig J*. 2014;3(5):417-419. doi:10.4103/2278-0513.138069

43. Farma JM. Malignant granular cell tumor : Clinical features and long - term survival. 2018;(February):891-897. doi:10.1002/jso.25227

44. Krishnamurthy A, George R, Majhi U. Malignant Granular Cell Tumor of the Tongue: A

Clinico-Pathological Challenge. *Indian J Surg Oncol*. 2014;5(1):71-74. doi:10.1007/s13193-013-0283-2

45. Wei L, Liu S, Conroy J, et al. Whole-genome sequencing of a malignant granular cell tumor with metabolic response to pazopanib. *Mol Case Stud*. 2015;1(1):a000380. doi:10.1101/mcs.a000380

46. Yu X, Li Z, Shen J. BRD7: a novel tumor suppressor gene in different cancers. *Am J Transl Res*. 2016;8(2):742-748. https://pubmed.ncbi.nlm.nih.gov/27158366.

47. Sadler TW (Thomas W. *Langman's Medical Embryology*. 12th ed. Philadelphia: Wolters Kluwer Health/Lippincott Williams & Wilkins; 2012.

48. Bronner ME. NIH Public Access. 2013;138(September 2012):179-186. doi:10.1007/s00418-012-0999-z.Formation

49. Gilbert SF. *Developmental Biology*. Palgrave Macmillan; 2000. https://books.google.ca/books?id=NEpnQwAACAAJ.

50. Sommer. Neural crest-derived stem cells. *StemBook*. 2010:1-20. doi:10.3824/stembook.1.51.1

51. Henderson DJ, Copp AJ. Role of the extracellular matrix in neural crest cell migration. *J Anat*. 1997;191(4):507-515. doi:10.1017/S0021878297002896

52. Monk KR, Feltri ML, Taveggia C. New insights on schwann cell development. *Glia*. 2015;63(8):1376-1393. doi:10.1002/glia.22852

53. Woodhoo A, Sommer L. Development of the Schwann Cell Lineage : From the Neural Crest to the Myelinated Nerve. 2008;1490(May):1481-1490. doi:10.1002/glia.20723

54. Kim J, Lo L, Dormand E, Anderson DJ. SOX10 Maintains Multipotency and Inhibits Neuronal Differentiation of Neural Crest Stem Cells. 2003;38:17-31.

55. Britsch S, Goerich DE, Riethmacher D, et al. The transcription factor Sox10 is a key regulator of peripheral glial development. *Genes Dev*. 2001;15(1):66-78. doi:10.1101/gad.186601

56. Britsch S, Goerich DE, Riethmacher D, et al. The transcription factor Sox10 is a key regulator of peripheral glial development. 2001:66-78. doi:10.1101/gad.186601.precursors

57. Birchmeier C, Nave KA. Neuregulin-1, a key axonal signal that drives schwann cell growth and differentiation. *Glia*. 2008;56(14):1491-1497. doi:10.1002/glia.20753

58. Roberts SL, Dun X, Doddrell RDS, et al. Sox2 expression in Schwann cells inhibits myelination in vivo and induces influx of macrophages to the nerve. 2017:3114-3125. doi:10.1242/dev.150656

59. Hjerling-leffler J, Marmigère F, Heglind M, et al. The boundary cap : a source of neural crest stem cells that generate multiple sensory neuron subtypes. 2005:2623-2632. doi:10.1242/dev.01852

60. Cosgaya M, Chan JR, Shooter EM. The Neurotrophin Receptor p75 NTR as a Positive

Modulator of Myelination. 2002;298(November):1245-1249.

61.   Triolo D, Dina G, Lorenzetti I, et al. Loss of glial fibrillary acidic protein (GFAP) impairs Schwann cell proliferation and delays nerve regeneration after damage. *J Cell Sci*. 2006;119(19):3981 LP - 3993. doi:10.1242/jcs.03168

62.   Susuki K. Node of ranvier disruption as a cause of neurological diseases. *ASN Neuro*. 2013;5(3):209-219. doi:10.1042/AN20130025

63.   Salzer JL. Schwann Cell Myelination. 2015:1-26.

64.   Ghislain J, Charnay P. scientific report. 2006;7(1):2-8. doi:10.1038/sj.embor.7400573

65.   Jacob C, Lo P, Engler S, et al. HDAC1 and HDAC2 Control the Specification of Neural Crest Cells into Peripheral Glia. 2014;34(17):6112-6122. doi:10.1523/JNEUROSCI.5212-13.2014

66.   Boullerne AI. The history of myelin. *Exp Neurol*. 2016;283:431-445. doi:10.1016/j.expneurol.2016.06.005

67.   Corfas G, Velardez MO, Ko CP, Ratner N, Peles E. Mechanisms and roles of axon-Schwann cell interactions. *J Neurosci*. 2004;24(42):9250-9260. doi:10.1523/JNEUROSCI.3649-04.2004

68.   Poliak S, Gollan L, Salomon D, et al. Localization of Caspr2 in myelinated nerves depends on axon-glia interactions and the generation of barriers along the axon. *J Neurosci*. 2001;21(19):7568-7575. doi:10.1523/jneurosci.21-19-07568.2001

69.   Saher G, Quintes S, Möbius W, et al. Cholesterol regulates the endoplasmic reticulum exit of the major membrane protein P0 required for peripheral myelin compaction. *J Neurosci*. 2009;29(19):6094-6104. doi:10.1523/JNEUROSCI.0686-09.2009

70.   Raasakka A, Ruskamo S, Kowal J, et al. Molecular structure and function of myelin protein P0 in membrane stacking. *Sci Rep*. 2019;9(1):1-15. doi:10.1038/s41598-018-37009-4

71.   Morell P QR. *Characteristic Composition of Myelin In: Siegel GJ, Agranoff BW, Albers RW, et Al., Editors. Basic Neurochemistry: Molecular, Cellular and Medical Aspects.* 6th editio. Philadelphia: Lippincott-Raven; 1999. https://www.ncbi.nlm.nih.gov/books/NBK28221/.

72.   Viader A, Golden JP, Baloh RH, Schmidt RE, Hunter DA, Milbrandt J. Schwann cell mitochondrial metabolism supports long-term axonal survival and peripheral nerve function. *J Neurosci*. 2011;31(28):10128-10140. doi:10.1523/JNEUROSCI.0884-11.2011

73.   Jessen KR, Mirsky R. The success and failure of the schwann cell response to nerve injury. *Front Cell Neurosci*. 2019;13(February):1-14. doi:10.3389/fncel.2019.00033

74.   Hanani M. Satellite glial cells in sympathetic and parasympathetic ganglia: In search of function. *Brain Res Rev*. 2010;64(2):304-327. doi:10.1016/j.brainresrev.2010.04.009

75.   HALL S. Nerve Repair: A Neurobiologist's View. *J Hand Surg Am*. 2001;26(2):129-136. doi:10.1054/jhsb.2000.0497

76.   Allodi I, Udina E, Navarro X. Specificity of peripheral nerve regeneration: Interactions at the axon level. *Prog Neurobiol*. 2012;98(1):16-37. doi:10.1016/j.pneurobio.2012.05.005

77. Jessen KR, Mirsky R, Lloyd AC. Schwann cells: Development and role in nerve repair. *Cold Spring Harb Perspect Biol*. 2015;7(7):1-15. doi:10.1101/cshperspect.a020487

78. Svennigsen ÅF, Dahlin LB. Repair of the peripheral nerve-remyelination that works. *Brain Sci*. 2013;3(3):1182-1197. doi:10.3390/brainsci3031182

79. Doddrell RDS, Dun XP, Moate RM, Jessen KR, Mirsky R, Parkinson DB. Regulation of Schwann cell differentiation and proliferation by the Pax-3 transcription factor. *Glia*. 2012;60(9):1269-1278. doi:10.1002/glia.22346

80. Hoffman PN, Cleveland DW. Neurofilament and tubulin expression recapitulates the developmental program during axonal regeneration: Induction of a specific β-tubulin isotype. *Proc Natl Acad Sci U S A*. 1988;85(12):4530-4533. doi:10.1073/pnas.85.12.4530

81. Carroll SL. NIH Public Access. 2013;123(3):321-348. doi:10.1007/s00401-011-0928-6.Molecular

82. Rodriguez FJ, Folpe AL, Giannini C, Perry A. Pathology of peripheral nerve sheath tumors: diagnostic overview and update on selected diagnostic problems. *Acta Neuropathol*. 2012;123(3):295-319. doi:10.1007/s00401-012-0954-z

83. Staser K, Yang F-C, Clapp DW. Pathogenesis of Plexiform Neurofibroma: Tumor-Stromal/Hematopoietic Interactions in Tumor Progression. *Annu Rev Pathol Mech Dis*. 2012;7(1):469-495. doi:10.1146/annurev-pathol-011811-132441

84. Carroll SL. Molecular mechanisms promoting the pathogenesis of Schwann cell neoplasms. *Acta Neuropathol*. 2012;123(3):321-348. doi:10.1007/s00401-011-0928-6

85. Wolkenstein P, Zeller J, Revuz J, Ecosse E, Leplège A. Quality-of-Life Impairment in Neurofibromatosis Type 1: A Cross-sectional Study of 128 Cases. *Arch Dermatol*. 2001;137(11):1421-1425. doi:10.1001/archderm.137.11.1421

86. Xu GF, O'Connell P, Viskochil D, et al. The neurofibromatosis type 1 gene encodes a protein related to GAP. *Cell*. 1990;62(3):599-608. doi:10.1016/0092-8674(90)90024-9

87. Messiaen LM, Callens T, Mortier G, et al. Exhaustive mutation analysis of the NF1 gene allows identification of 95% of mutations and reveals a high frequency of unusual splicing defects. *Hum Mutat*. 2000;15(6):541-555. doi:doi:10.1002/1098-1004(200006)15:6<541::AID-HUMU6>3.0.CO;2-N

88. Perry A, Roth KA, Banerjee R, Fuller CE, Gutmann DH. NF1 Deletions in S-100 Protein-Positive and Negative Cells of Sporadic and Neurofibromatosis 1 (NF1)-Associated Plexiform Neurofibromas and Malignant Peripheral Nerve Sheath Tumors. *Am J Pathol*. 2001;159(1):57-61. doi:10.1016/S0002-9440(10)61673-2

89. Xu G, Lin B, Tanaka K, et al. The catalytic domain of the neurofibromatosis type 1 gene product stimulates ras GTPase and complements ira mutants of S. cerevisiae. *Cell*. 1990;63(4):835-841. doi:10.1016/0092-8674(90)90149-9

90. Sherman L, Atit R, Rosenbaum T, Cox A, Ratner N. Single Cell Ras-GTP Analysis Reveals Altered Ras Activity in a Subpopulation of Neurofibroma Schwann Cells but Not Fibroblasts. *J Biol Chem*. 2000;275:30740-30745. doi:10.1074/jbc.M001702200

91. Stonecypher MS, Byer SJ, Grizzle WE, Carroll SL. Activation of the neuregulin-1/ErbB signaling pathway promotes the proliferation of neoplastic Schwann cells in human malignant peripheral nerve sheath tumors. *Oncogene*. 2005;24(36):5589-5605. doi:10.1038/sj.onc.1208730

92. Fletcher JS, Pundavela J, Ratner N. After Nf1 loss in Schwann cells, inflammation drives neurofibroma formation. *Neuro-Oncology Adv*. 2019;(November 2019):1-10. doi:10.1093/noajnl/vdz045

93. Wippold FJ, Lubner M, Perrin RJ, Lämmle M, Perry A. Neuropathology for the neuroradiologist: Antoni A and Antoni B tissue patterns. *Am J Neuroradiol*. 2007;28(9):1633-1638. doi:10.3174/ajnr.A0682

94. Joshi R. Learning from eponyms: Jose Verocay and Verocay bodies, Antoni A and B areas, Nils Antoni and Schwannomas. *Indian Dermatol Online J*. 2012;3(3):215-219. doi:10.4103/2229-5178.101826

95. Palm SL, Furcht LT. Production of laminin and fibronectin by Schwannoma cells: cell-protein interactions in vitro and protein localization in peripheral nerve in vivo. *J Cell Biol*. 1983;96(5):1218-1226. doi:10.1083/jcb.96.5.1218

96. Reibel J, Wewer U, Albrechtsen R. The pattern of distribution of laminin in neurogenic tumors, granular cell tumors, and nevi of the oral mucosa. *Acta Pathol Microbiol Immunol Scand A*. 1985;93(2):41-47. doi:10.1111/j.1699-0463.1985.tb03918.x

97. Crist J, Hodge JR, Frick M, et al. Magnetic Resonance Imaging Appearance of Schwannomas from Head to Toe: A Pictorial Review. *J Clin Imaging Sci*. 2017;7:38. doi:10.4103/jcis.JCIS_40_17

98. Papiez J, Rojiani M V, Rojiani AM. Vascular alterations in Schwannoma. *Int J Clin Exp Pathol*. 2014;7(7):4032-4038. https://www.ncbi.nlm.nih.gov/pubmed/25120781.

99. Sian CS, Ryan SF. The ultrastructure of neurilemoma with emphasis on Antoni B tissue. *Hum Pathol*. 1981;12(2):145-160. doi:10.1016/s0046-8177(81)80102-5

100. Kanatas A, Mücke T, Houghton D, Mitchell DA. Schwannomas of the head and neck. *Oncol Rev*. 2009;3(2):107-111. doi:10.1007/s12156-009-0015-6

101. Antinheimo J, Sankila R, Carpén O, Pukkala E, Sainio M, Jääskeläinen J. Population-based analysis of sporadic and type 2 neurofibromatosis-associated meningiomas and Schwannomas. *Neurology*. 2000;54(1):71 LP - 71. doi:10.1212/WNL.54.1.71

102. Kleijwegt M, Ho V, Visser O, Godefroy W, van der Mey A. Real Incidence of Vestibular Schwannoma? Estimations From a National Registry. *Otol Neurotol Off Publ Am Otol Soc Am Neurotol Soc [and] Eur Acad Otol Neurotol*. 2016;37(9):1411-1417. doi:10.1097/MAO.0000000000001169

103. Salehinejad J, Sahebnasagh Z, Saghafi S, Sahebnasagh Z, Amiri N. Intraoral ancient Schwannoma: A systematic review of the case reports. *Dent Res J (Isfahan)*. 2017;14(2):87-96. https://www.ncbi.nlm.nih.gov/pubmed/28584531.

104. Wright BA, Jackson D. Neural tumors of the oral cavity. A review of the spectrum of

benign and malignant oral tumors of the oral cavity and jaws. *Oral Surg Oral Med Oral Pathol*. 1980;49(6):509-522. doi:10.1016/0030-4220(80)90075-4

105. Lee E-Y, Kim J-J, Seok H, Lee J-Y. Schwannoma of the tongue: a case report with review of literature. *Maxillofac Plast Reconstr Surg*. 2017;39(1):17. doi:10.1186/s40902-017-0116-2

106. Hanemann CO, Evans DG. News on the genetics, epidemiology, medical care and translational research of Schwannomas. *J Neurol*. 2006;253(12):1533-1541. doi:10.1007/s00415-006-0347-0

107. Ud Din N, Ahmad Z, Abdul-Ghafar J, Ahmed R. Hybrid peripheral nerve sheath tumors: Report of five cases and detailed review of literature. *BMC Cancer*. 2017;17(1):1-8. doi:10.1186/s12885-017-3350-1

108. Evans DGR. Neurofibromatosis type 2 (NF2): a clinical and molecular review. *Orphanet J Rare Dis*. 2009;4:16. doi:10.1186/1750-1172-4-16

109. Morrow KA, Shevde LA. Merlin: the wizard requires protein stability to function as a tumor suppressor. *Biochim Biophys Acta*. 2012;1826(2):400-406. doi:10.1016/j.bbcan.2012.06.005

110. Seizinger BR, Rouleau G, Ozelius LJ, et al. Common pathogenetic mechanism for three tumor types in bilateral acoustic neurofibromatosis. *Science (80-)*. 1987;236(4799):317 LP - 319. doi:10.1126/science.3105060

111. Stemmer-rachamimov A, Xu L, Gonzalez-agosti C, et al. Universal Absence of Merlin , but Not Other ERM Family Members , in Schwannomas. 1997;151(6):1649-1654.

112. McClatchey AI, Saotome I, Ramesh V, Gusella JF, Jacks T. The Nf2 tumor suppressor gene product is essential for extraembryonic development immediately prior to gastrulation. *Genes Dev*. 1997;11(10):1253-1265. doi:10.1101/gad.11.10.1253

113. Ahmad I, Yue WY, Fernando A, Clark JJ, Woodson EA, Hansen MR. p75NTR is highly expressed in vestibular Schwannomas and promotes cell survival by activating nuclear transcription factor κB. *Glia*. 2014;62(10):1699-1712. doi:10.1002/glia.22709

114. Cheng E, Hansen MR. Schwannomas provide insight into the role of p75(NTR) and merlin in Schwann cells following nerve injury and during regeneration. *Neural Regen Res*. 2016;11(1):73-74. doi:10.4103/1673-5374.175045

115. Ahmad I, Yue WY, Fernando A, Clark JJ, Woodson EA, Hansen MR. p75NTR is highly expressed in vestibular Schwannomas and promotes cell survival by activating nuclear transcription factor κB. *Glia*. 2014;62(10):1699-1712. doi:10.1002/glia.22709

116. Provenzano MJ, Minner SA, Zander K, et al. p75(NTR) expression and nuclear localization of p75(NTR) intracellular domain in spiral ganglion Schwann cells following deafness correlate with cell proliferation. *Mol Cell Neurosci*. 2011;47(4):306-315. doi:10.1016/j.mcn.2011.05.010

117. Smith D, Tweed C, Fernyhough P, Glazner GW. Nuclear factor-kappaB activation in axons and Schwann cells in experimental sciatic nerve injury and its role in modulating axon

regeneration: studies with etanercept. *J Neuropathol Exp Neurol*. 2009;68(6):691-700. doi:10.1097/NEN.0b013e3181a7c14e

118. Morrison H, Sherman LS, Legg J, et al. The NF2 tumor suppressor gene product, merlin, mediates contact inhibition of growth through interactions with CD44. *Genes Dev*. 2001;15(8):968-980. doi:10.1101/gad.189601

119. Donato R, Cannon BR, Sorci G, et al. Functions of S100 proteins. *Curr Mol Med*. 2013;13(1):24-57. doi:10.2174/1566524011307010024

120. Kuberappa PH, Bagalad BS, Ananthaneni A, Kiresur MA, Srinivas GV. Certainty of S100 from Physiology to Pathology. *J Clin Diagn Res*. 2016;10(6):ZE10-ZE15. doi:10.7860/JCDR/2016/17949.8022

121. Xia C, Braunstein Z, Toomey AC, Zhong J, Rao X. S100 Proteins As an Important Regulator of Macrophage Inflammation . *Front Immunol* . 2018;8:1908. https://www.frontiersin.org/article/10.3389/fimmu.2017.01908.

122. Sedaghat F, Notopoulos A. S100 protein family and its application in clinical practice. *Hippokratia*. 2008;12(4):198-204. https://www.ncbi.nlm.nih.gov/pubmed/19158963.

123. Weiss AP, Dorfman HD. S-100 protein in human cartilage lesions. *J Bone Joint Surg Am*. 1986;68(4):521-526.

124. Pleger ST, Most P, Katus HA. S100 proteins: A missing piece in the puzzle of heart failure? *Cardiovasc Res*. 2007;75(1):1-2. doi:10.1016/j.cardiores.2007.05.009

125. Mavrogenis A, Bianchi G, Stavropoulos N, Papagelopoulos P, Ruggieri P. Clinicopathological features, diagnosis and treatment of clear cell sarcoma/melanoma of soft parts. *Hippokratia*. 2013;17(4):298-302. https://www.ncbi.nlm.nih.gov/pubmed/25031505.

126. Aggarwal N, Pongpruttipan T, Patel S, et al. Expression of S100 Protein in CD4-positive T-cell Lymphomas Is Often Associated With T-cell Prolymphocytic Leukemia. *Am J Surg Pathol*. 2015;39(12):1679-1687. doi:10.1097/PAS.0000000000000496

127. Harmon CM, Brown N. Langerhans Cell Histiocytosis: A Clinicopathologic Review and Molecular Pathogenetic Update. *Arch Pathol Lab Med*. 2015;139(10):1211-1214. doi:10.5858/arpa.2015-0199-RA

128. Gogas H, Eggermont AMM, Hauschild A, et al. Biomarkers in melanoma. *Ann Oncol*. 2009;20(suppl_6):vi8-vi13. doi:10.1093/annonc/mdp251

129. Metgud R, Naik S, Patel S. Spindle cell lesions: A review on immunohistochemical markers. *J Cancer Res Ther*. 2017;13(3):412-418. doi:10.4103/0973-1482.176178

130. Karamchandani JR, Nielsen TO, van de Rijn M, West RB. Sox10 and S100 in the diagnosis of soft-tissue neoplasms. *Appl Immunohistochem Mol Morphol*. 2012;20(5):445-450. doi:10.1097/PAI.0b013e318244ff4b

131. Miettinen M, Mccue PA, Sarlomo-rikala M, et al. HHS Public Access. 2016;39(6):826-835. doi:10.1097/PAS.0000000000000398.Sox10

132. Peshavaria M, Day IN. Molecular structure of the human muscle-specific enolase gene

(ENO3). *Biochem J*. 1991;275 (Pt 2(Pt 2):427-433. doi:10.1042/bj2750427

133. Isgro MA, Bottoni P, Scatena R. Neuron-Specific Enolase as a Biomarker: Biochemical and Clinical Aspects. *Adv Exp Med Biol*. 2015;867:125-143. doi:10.1007/978-94-017-7215-0_9

134. Joseph J, Cruz-Sánchez FF, Carreras J. Enolase Activity and Isoenzyme Distribution in Human Brain Regions and Tumors. *J Neurochem*. 1996;66(6):2484-2490. doi:doi:10.1046/j.1471-4159.1996.66062484.x

135. Vinores SA, Herman MM, Rubinstein LJ. Electron-immunocytochemical localization of neuron-specific enolase in cytoplasm and on membranes of primary and metastatic cerebral tumours and on glial filaments of glioma cells. *Histopathology*. 1986;10(9):891-908. doi:10.1111/j.1365-2559.1986.tb02588.x

136. Didiasova M, Schaefer L, Wygrecka M. When Place Matters: Shuttling of Enolase-1 Across Cellular Compartments . *Front Cell Dev Biol* . 2019;7:61. https://www.frontiersin.org/article/10.3389/fcell.2019.00061.

137. Mjønes P, Sagatun L, Nordrum IS, Waldum HL. Neuron-Specific Enolase as an Immunohistochemical Marker Is Better Than Its Reputation. *J Histochem Cytochem*. 2017;65(12):687-703. doi:10.1369/0022155417733676

138. Perrone-Bizzozero NI, Neve RL, Irwin N, Lewis S, Fischer I, Benowitz LI. Post-transcriptional regulation of GAP-43 rnRNA levels during neuronal differentiation and nerve regeneration. *Mol Cell Neurosci*. 1991;2(5):402-409. doi:10.1016/1044-7431(91)90027-l

139. Denny JB. Molecular mechanisms, biological actions, and neuropharmacology of the growth-associated protein GAP-43. *Curr Neuropharmacol*. 2006;4(4):293-304. doi:10.2174/157015906778520782

140. Hung C, Lin C, Chang H, et al. Astrocytic GAP43 Induced by the TLR4 / NF- B / STAT3 Axis Attenuates Astrogliosis-Mediated Microglial Activation and Neurotoxicity. 2016;36(6):2027-2043. doi:10.1523/JNEUROSCI.3457-15.2016

141. Chen W, Chen P, Lu D, Lind AC, Dehner LP. Growth-associated protein 43 in differentiating peripheral nerve sheath tumors from other non-neural spindle cell neoplasms. 2014;1:184-193. doi:10.1038/modpathol.2013.128

142. Schmitd L, Beesley L, Russo N, et al. Redefining Perineural Invasion: Integration of Biology With Clinical Outcome. *Neoplasia*. 2018;20:657-667. doi:10.1016/j.neo.2018.04.005

143. Zheng C, Quan R-D, Wu C-Y, et al. Growth-associated protein 43 promotes thyroid cancer cell lines progression via epithelial-mesenchymal transition. *J Cell Mol Med*. 2019;23(12):7974-7984. doi:10.1111/jcmm.14460

144. Zhang F, Jin J, Wu J, et al. Abstract 1083: GAP43, a novel potential metastases promoter in non-small cell lung cancer. *Cancer Res*. 2018;78(13 Supplement):1083 LP - 1083. doi:10.1158/1538-7445.AM2018-1083

145. Klein A, Olendrowitz C, Schmutzler R, et al. Identification of brain- and bone-specific breast cancer metastasis genes. *Cancer Lett*. 2009;276(2):212-220.

doi:https://doi.org/10.1016/j.canlet.2008.11.017

146. Choo SY. The HLA system: genetics, immunology, clinical testing, and clinical implications. *Yonsei Med J*. 2007;48(1):11-23. doi:10.3349/ymj.2007.48.1.11

147. Bergstrom RT, Silverman DA, Chambers K, Kim JA. CD40 monoclonal antibody activation of antigen-presenting cells improves therapeutic efficacy of tumor-specific T cells. *Otolaryngol Head Neck Surg*. 2004;130(1):94-103. doi:10.1016/j.otohns.2003.09.007

148. Alberts B, Johnson A, Lewis J et al. *Molecular Biology of the Cell. Helper T Cell and Lymphocyte Activation*. 4th editio. New York: Garland Science https://www.ncbi.nlm.nih.gov/books/NBK26827/.

149. Patel AJ, Fuentebella J, Gernez Y, et al. Increased HLA-DR expression on tissue eosinophils in eosinophilic esophagitis. *J Pediatr Gastroenterol Nutr*. 2010;51(3):290-294. doi:10.1097/MPG.0b013e3181e083e7

150. Mehrfeld C, Zenner S, Kornek M, Lukacs-kornek V, Lukacs-kornek V. The Contribution of Non-Professional Antigen-Presenting Cells to immunity and Tolerance in the Liver. 2018;9(March):1-8. doi:10.3389/fimmu.2018.00635

151. Wosen JE, Mukhopadhyay D, Macaubas C, Mellins ED. Epithelial MHC Class II Expression and Its Role in Antigen Presentation in the Gastrointestinal and Respiratory Tracts. 2018;9(September):1-14. doi:10.3389/fimmu.2018.02144

152. Epstein SP, Gadaria-Rathod N, Wei Y, Maguire MG, Asbell PA. HLA-DR expression as a biomarker of inflammation for multicenter clinical trials of ocular surface disease. *Exp Eye Res*. 2013;111:95-104. doi:10.1016/j.exer.2013.03.018

153. Meyer Zu Horste G, Heidenreich H, Lehmann HC, et al. Expression of antigen processing and presenting molecules by Schwann cells in inflammatory neuropathies. *Glia*. 2010;58(1):80-92. doi:10.1002/glia.20903

154. Fan X, Liang J, Wu Z, Shan X, Qiao H, Jiang T. Expression of HLA-DR genes in gliomas : correlation with clinicopathological features and prognosis. 2017:1-9. doi:10.1186/s41016-017-0090-7

155. Chistiakov DA, Killingsworth MC, Myasoedova VA, Orekhov AN, Bobryshev Y V. CD68/macrosialin: not just a histochemical marker. *Lab Investig*. 2017;97(1):4-13. doi:10.1038/labinvest.2016.116

156. Gottfried E, Kunz-Schughart LA, Weber A, et al. Expression of CD68 in non-myeloid cell types. *Scand J Immunol*. 2008;67(5):453-463. doi:10.1111/j.1365-3083.2008.02091.x

157. Demirel O, Jan I, Wolters D, et al. The lysosomal polypeptide transporter TAPL is stabilized by interaction with LAMP-1 and LAMP-2. *J Cell Sci*. 2012;125(Pt 18):4230-4240. doi:10.1242/jcs.087346

158. Amanzada A, Malik IA, Blaschke M, et al. Identification of CD68(+) neutrophil granulocytes in in vitro model of acute inflammation and inflammatory bowel disease. *Int J Clin Exp Pathol*. 2013;6(4):561-570.

159. Gloghini A, Rizzo A, Zanette I, et al. KP1/CD68 expression in malignant neoplasms

including lymphomas, sarcomas, and carcinomas. *Am J Clin Pathol*. 1995;103(4):425-431. doi:10.1093/ajcp/103.4.425

160. Kurtin PJ, Bonin DM. Immunohistochemical demonstration of the lysosome-associated glycoprotein CD68 (KP-1) in granular cell tumors and Schwannomas. *Hum Pathol*. 1994;25(11):1172-1178. doi:10.1016/0046-8177(94)90033-7

161. TOS APDEI, DOGLIONI C, LAURINO L, FLETCHER CDM. KP1 (CD68) expression in benign neural tumours. Further evidence of its low specificity as a histiocytic/myeloid marker. *Histopathology*. 1993;23(2):185-187. doi:10.1111/j.1365-2559.1993.tb00478.x

162. Etzerodt A, Moestrup SK. CD163 and inflammation: biological, diagnostic, and therapeutic aspects. *Antioxid Redox Signal*. 2013;18(17):2352-2363. doi:10.1089/ars.2012.4834

163. Kristiansen M, Graversen JH, Jacobsen C, et al. Identification of the haemoglobin scavenger receptor. *Nature*. 2001;409(6817):198-201. doi:10.1038/35051594

164. Van Gorp H, Delputte PL, Nauwynck HJ. Scavenger receptor CD163, a Jack-of-all-trades and potential target for cell-directed therapy. *Mol Immunol*. 2010;47(7-8):1650-1660. doi:10.1016/j.molimm.2010.02.008

165. Liu R, Cao S, Hua Y, Keep RF, Huang Y, Xi G. CD163 Expression in Neurons After Experimental Intracerebral Hemorrhage. *Stroke*. 2017;48(5):1369-1375. doi:10.1161/STROKEAHA.117.016850

166. Chatzigeorgiou A, Lyberi M, Chatzilymperis G, Nezos A, Kamper E. CD40/CD40L signaling and its implication in health and disease. *BioFactors*. 2009;35(6):474-483. doi:10.1002/biof.62

167. Qualai J, Li L-X, Cantero J, et al. Expression of CD11c Is Associated with Unconventional Activated T Cell Subsets with High Migratory Potential. *PLoS One*. 2016;11(4):e0154253. https://doi.org/10.1371/journal.pone.0154253.

168. Wu J, Wu H, An J, Ballantyne CM, Cyster JG. Critical role of integrin CD11c in splenic dendritic cell capture of missing-self CD47 cells to induce adaptive immunity. *Proc Natl Acad Sci*. 2018;115(26):6786 LP - 6791. doi:10.1073/pnas.1805542115

169. Rizzino A. Sox2 and Oct-3/4: a versatile pair of master regulators that orchestrate the self-renewal and pluripotency of embryonic stem cells. *Wiley Interdiscip Rev Syst Biol Med*. 2009;1(2):228-236. doi:10.1002/wsbm.12

170. Feng R, Wen J. Overview of the roles of Sox2 in stem cell and development. *Biol Chem*. 2015;396(8):883-891. doi:10.1515/hsz-2014-0317

171. Balakrishnan A, Stykel MG, Touahri Y, Stratton JA, Biernaskie J, Schuurmans C. Temporal Analysis of Gene Expression in the Murine Schwann Cell Lineage and the Acutely Injured Postnatal Nerve. *PLoS One*. 2016;11(4):e0153256. https://doi.org/10.1371/journal.pone.0153256.

172. Adameyko I, Lallemend F, Furlan A, et al. Sox2 and Mitf cross-regulatory interactions consolidate progenitor and melanocyte lineages in the cranial neural crest. *Development*.

2012;139(2):397 LP - 410. doi:10.1242/dev.065581

173. Liu K, Lin B, Zhao M, et al. The multiple roles for Sox2 in stem cell maintenance and tumorigenesis. *Cell Signal*. 2013;25(5):1264-1271. doi:10.1016/j.cellsig.2013.02.013

174. Jo A, Denduluri S, Zhang B, et al. The versatile functions of Sox9 in development, stem cells, and human diseases. *Genes Dis*. 2014;1(2):149-161. doi:10.1016/j.gendis.2014.09.004

175. Cheung M, Briscoe J. Neural crest development is regulated by the transcription factor Sox9. *Development*. 2003;130(23):5681 LP - 5693. doi:10.1242/dev.00808

176. Michalczyk K, Ziman M. Nestin structure and predicted function in cellular cytoskeletal organisation. *Histol Histopathol*. 2005;20(2):665-671. doi:10.14670/HH-20.665

177. Erinanç H, Göktürk HS, Kanat Ünler G, Karagülle E. Utility of Nestin immunohistochemistry in the diagnosis of granular cell tumor. *Arch Clin Exp Med*. 2018;3(3):160-164. doi:10.25000/acem.436429

178. Kim H-S, Lee J, Lee DY, et al. Schwann Cell Precursors from Human Pluripotent Stem Cells as a Potential Therapeutic Target for Myelin Repair. *Stem Cell Reports*. 2017;8(6):1714-1726. doi:https://doi.org/10.1016/j.stemcr.2017.04.011

179. Katsetos CD, Del Valle L, Geddes JF, et al. Localization of the Neuronal Class III β-Tubulin in Oligodendrogliomas: Comparison with Ki-67 Proliferative Index and 1p/19q Status. *J Neuropathol Exp Neurol*. 2002;61(4):307-320. doi:10.1093/jnen/61.4.307

180. Lebok P, Öztürk M, Heilenkötter U, et al. High levels of class III β-tubulin expression are associated with aggressive tumor features in breast cancer. *Oncol Lett*. 2016;11(3):1987-1994. doi:10.3892/ol.2016.4206

181. Silver N, Best S, Jiang J, Thein SL. Selection of housekeeping genes for gene expression studies in human reticulocytes using real-time PCR. *BMC Mol Biol*. 2006;7(1):33. doi:10.1186/1471-2199-7-33

182. Jensen K, Krusenstjerna-Hafstrøm R, Lohse J, Petersen KH, Derand H. A novel quantitative immunohistochemistry method for precise protein measurements directly in formalin-fixed, paraffin-embedded specimens: analytical performance measuring HER2. *Mod Pathol*. 2017;30(2):180-193. doi:10.1038/modpathol.2016.176

183. Hwang JTK, Gu YR, Shen M, et al. Individualized five-year risk assessment for oral premalignant lesion progression to cancer. *Oral Surg Oral Med Oral Pathol Oral Radiol*. 2017;123(3):374-381. doi:10.1016/j.oooo.2016.11.004

184. Loughrey MB, Bankhead P, Coleman HG, et al. Validation of the systematic scoring of immunohistochemically stained tumour tissue microarrays using QuPath digital image analysis. *Histopathology*. 2018;73(2):327-338. doi:10.1111/his.13516

185. Bankhead P, Loughrey MB, Fernández JA, et al. QuPath: Open source software for digital pathology image analysis. *Sci Rep*. 2017;7(1):16878. doi:10.1038/s41598-017-17204-5

186. Lyu X-J, Li H-Z, Ma X, et al. Elevated S100A6 (Calcyclin) enhances tumorigenesis and suppresses CXCL14-induced apoptosis in clear cell renal cell carcinoma. *Oncotarget*.

2015;6(9):6656-6669. doi:10.18632/oncotarget.3169

187. Kang Y, Pekmezci M, Folpe AL, Ersen A, Horvai AE. Diagnostic utility of SOX10 to distinguish malignant peripheral nerve sheath tumor from synovial sarcoma, including intraneural synovial sarcoma. *Mod Pathol an Off J United States Can Acad Pathol Inc*. 2014;27(1):55-61. doi:10.1038/modpathol.2013.115

188. Wisell J, Kleinschmidt-DeMasters BK. Sox10 nuclear immunostaining lacks diagnostic utility for CNS granular cell tumors. *J Neuropathol Exp Neurol*. 2014;73(1):98-100. doi:10.1097/NEN.0000000000000025

189. Solomon LW. S-100 Negative Granular Cell Tumor of the Oral Cavity. *Head Neck Pathol*. 2018;10(3):367-373. doi:10.1007/s12105-015-0673-6

190. Curtis R, Stewart HJ, Hall SM, Wilkin GP, Mirsky R, Jessen KR. GAP-43 is expressed by nonmyelin-forming Schwann cells of the peripheral nervous system. *J Cell Biol*. 1992;116(6):1455-1464. doi:10.1083/jcb.116.6.1455

191. Chen Y-Y, Chang W-A, Lin E-S, Chen Y-J, Kuo P-L. Expressions of HLA Class II Genes in Cutaneous Melanoma Were Associated with Clinical Outcome: Bioinformatics Approaches and Systematic Analysis of Public Microarray and RNA-Seq Datasets. *Diagnostics (Basel, Switzerland)*. 2019;9(2):59. doi:10.3390/diagnostics9020059

192. de Muralt B, de Tribolet N, Diserens AC, Stavrou D, Mach JP, Carrel S. Phenotyping of 60 cultured human gliomas and 34 other neuroectodermal tumors by means of monoclonal antibodies against glioma, melanoma and HLA-DR antigens. *Eur J Cancer Clin Oncol*. 1985;21(2):207-216. doi:10.1016/0277-5379(85)90175-0

193. Yogesh TL, Sowmya S V. Granules in Granular Cell Lesions of the Head and Neck : A Review. 2011;2011(1). doi:10.5402/2011/215251

194. Aparna HG, Jayanth BS, Shashidara R, Jaishankar P. Congenital epulis in a newborn: a case report, immunoprofiling and review of literature. *Ethiop J Health Sci*. 2014;24(4):359-362. doi:10.4314/ejhs.v24i4.12

195. Nikitakis NG, Tzerbos F, Triantafyllou K, Papadimas C, Sklavounou A. Granular cell ameloblastoma: an unusual histological subtype report and review of literature. *J oral Maxillofac Res*. 2011;1(4):e3-e3. doi:10.5037/jomr.2010.1403

196. Sarode SC, Sarode GS, Vaidya K. Central granular cell odontogenic tumor: a systematic review. *J Oral Pathol Med*. 2014;43(3):167-176. doi:10.1111/jop.12085

Appendix:

Manual scoring of anti-S100 antibody for GCT

Case #	Intensity	Percentage
1	3	2
2	3	2
3	3	2
4	3	2
5	3	2
6	3	2
7	3	2
8	3	2
9	3	2
10	3	2
11	3	2
12	3	2
13	3	2
14	3	2
15	3	2
16	3	2
17	3	2
18	3	2
19	3	2
20	3	2
21	3	2
22	3	2
23	3	2

Manual scoring of anti-SOX10 antibody for GCT

Case #	intensity	Percentage
1	3	2
2	3	2
3	3	2
4	3	2
5	3	2
6	3	2
7	3	2
8	3	2
9	3	2
10	3	2
11	3	2
12	3	2
13	3	2
14	3	2
15	3	2
16	3	2
17	3	2
18	3	2
19	3	2
20	3	2
21	0	0
22	3	2
23	3	2

Manual scoring for anti-NSE antibody for GCT

Case #	intensity	Percentage
1	3	2
2	3	2
3	3	2
4	2	2
5	3	2
6	3	2
7	3	2
8	3	2
9	3	2
10	3	2
11	3	2
12	3	2
13	3	2
14	2	2
15	3	2
16	3	2
17	3	2
18	3	2
19	2	2
20	3	2
21	3	2
22	3	2
23	3	2

Manual scoring for anti-GAP43 antibody for GCT

Case #	intensity	Percentage
1	3	2
2	3	2
3	3	2
4	3	2
5	2	2
6	3	2
7	2	2
8	3	2
9	3	2
10	3	2
11	3	2
12	3	2
13	3	2
14	3	2
15	3	2
16	3	2
17	3	2
18	3	2
19	3	2
20	3	2
21	3	2
22	3	2
23	3	2

Manual scoring for anti-CD68 antibody for GCT

Case #	intensity	Percentage
1	2	2
2	2	2
3	2	2
4	2	2
5	2	2
6	2	2
7	2	2
8	2	2
9	3	2
10	2	2
11	3	2
12	3	2
13	2	2
14	2	2
15	2	2
16	2	2
17	2	2
18	3	2
19	2	2
20	2	2
21	2	2
22	3	2
23	3	2

Manual scoring for anti-CD68 antibody for GCT

Case #	intensity	Percentage
1	2	2
2	2	2
3	2	2
4	2	2
5	2	2
6	2	2
7	2	2
8	2	2
9	3	2
10	2	2
11	3	2
12	3	2
13	2	2
14	2	2
15	2	2
16	2	2
17	2	2
18	3	2
19	2	2
20	2	2
21	2	2
22	3	2
23	3	2

Manual scoring for anti-HLA-DR antibody for GCT

Case #	intensity	Percentage
1	2	2
2	3	2
3	3	2
4	3	2
5	3	2
6	2	2
7	3	2
8	3	2
9	2	2
10	3	2
11	2	2
12	3	2
13	3	2
14	3	2
15	2	2
16	2	2
17	3	2
18	3	2
19	3	2
20	3	2
21	3	2
22	3	2
23	3	2

Manual scoring for anti-cd163 antibody for GCT

Case #	intensity	Percentage
1	0	0
2	--	--
3	0	0
4	0	0
5	0	0
6	0	0
7	0	0
8	0	0
9	0	0
10	0	0
11	0	0
12	0	0
13	0	0
14	0	0
15	0	0
16	0	0
17	0	0
18	0	0
19	0	0
20	0	0
21	0	0
22	0	0
23	0	0

Manual scoring for anti-cd40 antibody for GCT

Case #	intensity	Percentage
1	0	0
2	--	--
3	0	0
4	0	0
5	0	0
6	0	0
7	0	0
8	0	0
9	0	0
10	0	0
11	0	0
12	0	0
13	0	0
14	0	0
15	0	0
16	0	0
17	0	0
18	0	0
19	0	0
20	0	0
21	0	0
22	0	0
23	0	0

Manual scoring for anti-cd11c antibody for GCT

Case #	intensity	Percentage
1	0	0
2	--	--
3	0	0
4	0	0
5	0	0
6	0	0
7	0	0
8	0	0
9	0	0
10	0	0
11	0	0
12	0	0
13	0	0
14	0	0
15	0	0
16	0	0
17	0	0
18	0	0
19	0	0
20	0	0
21	0	0
22	0	0
23	0	0

Manual scoring for anti-S100 antibody for Schwannoma

Case #	intensity	Percentage
1	3	2
2	3	2
3	3	2
4	3	2
5	3	2
6	3	2
7	3	2
8	3	2
9	3	2
10	3	2

Manual scoring for anti-SOX10 antibody for Schwannoma

Case #	intensity	Percentage
1	3	2
2	3	2
3	3	2
4	3	2
5	3	2
6	3	2
7	3	2
8	3	2
9	3	2
10	3	2

Manual scoring for anti-NSE antibody for Schwannoma

Case #	intensity	Percentage
1	2	2
2	2	2
3	1	1
4	2	2
5	1	1
6	2	2
7	2	2
8	1	1
9	2	2
10	1	2

Manual scoring for anti-GAP43 antibody for Schwannoma

Case #	intensity	Percentage
1	3	2
2	3	2
3	2	1
4	2	1
5	2	2
6	3	2
7	3	2
8	3	2
9	3	2
10	2	1

Manual scoring for anti-CD68 antibody for Schwannoma

Case #	intensity	Percentage
1	1	1
2	2	1
3	1	1
4	1	1
5	2	2
6	1	2
7	0	0
8	1	1
9	1	1
10	2	2

Manual scoring for anti-HLA-DR antibody for Schwannoma

Case #	intensity	Percentage
1	3	2
2	3	2
3	2	2
4	3	2
5	3	2
6	2	2
7	2	2
8	2	2
9	3	2
10	3	2

Manual scoring for anti-CD163 antibody for Schwannoma

Case #	intensity	Percentage
1	3	2
2	3	2
3	3	2
4	3	2
5	3	2
6	2	2
7	3	2
8	3	2
9	3	2
10	3	2

Manual scoring for anti-CD40 antibody for Schwannoma

Case #	intensity	Percentage
1	0	0
2	0	0
3	0	0
4	0	0
5	0	0
6	0	0
7	0	0
8	0	0
9	0	0
10	0	0

Manual scoring for anti-CD11c antibody for Schwannoma

Case #	intensity	Percentage
1	0	0
2	0	0
3	0	0
4	0	0
5	0	0
6	0	0
7	0	0
8	0	0
9	0	0
10	0	0

H-score and percent staining positive for anti-GAP43 antibody in GCTs using QuPath digital analysis

Case #	Positive %	H-score
1	95.15	180.98
9	91.97	176.03
10	76.08	85.31
11	71.26	82.84
14	74.47	81.81

H-score and percent staining positive for anti-CD68 antibody in GCTs using QuPath digital analysis

Case #	Positive %	H-score
1	91.61	193.53
9	88.81	206.05
10	99.32	223.23

11	93.58	202.14
14	69.29	115.59

H-score and percent staining positive for anti-HLA-DR antibody in GCTs using QuPath digital analysis

Case #	Positive %	H-score
1	71.39	119.12
9	71.09	83.27
10	84.1	182.64
11	98.01	257.53
14	68.67	71.92

H-score and percent staining positive for anti-CD163 antibody in GCTs using QuPath digital analysis

Case #	Positive %	H-score
1	6.195	6.217
9	1.814	1.87
10	14.57	15.58
11	21.14	21.84
14	6.981	7.204

H-score and percent staining positive for anti-GAP43 antibody in Schwannomas using QuPath digital analysis

Case #	Positive %	H-score
1	32.65	39.7
3	21.87	23.82
4	16.33	16.77
5	38.51	42.68

8	54.96	69.71

H-score and percent staining positive for anti-CD68 antibody in Schwannomas using QuPath digital analysis

Case #	Positive %	H-score
1	22.7	25.92
3	32.21	35.75
4	21.66	23.06
5	34.8	44.38
8	8.978	9.756

H-score and percent staining positive for anti-HLA-DR antibody in Schwannomas using QuPath digital analysis

Case #	Positive %	H-score
1	90.65	206.92
3	96.58	252.26
4	58.17	69.14
5	95.89	237.94
8	73.73	74.42

H-score and percent staining positive for anti-CD163 antibody in Schwannomas using QuPath digital analysis

Case #	Positive %	H-score
1	77.5	107.57
3	57.54	72.13
4	64.44	75.29
5	89.96	142.66
8	52.73	52.89

Curriculum Vitae

7 EDUCATION

2015 – present	**Oral and maxillofacial Surgery resident,** Schulich School of Medicine and Dentistry, London Health Science Centre, London Ontario
2016 – 2020	**MD,** Schulich School of Medicine and Dentistry, Western University London Ontario
2015 – present	**Masters in pathology candidate,** Western University Schulich School of Medicine and Dentistry Faculty of Pathology
2013 – 2014	**General Practice Residency,** Foothills Medical Centre, Calgary, Alberta
2009 – 2013	**DMD (honours),** University of Manitoba Faculty of Dentistry, Winnipeg, Manitoba
2010 – 2013	**B.Sc. dent,** University of Manitoba Faculty of Dentistry, Winnipeg, Manitoba
2006 – 2009	**B.Sc. Biopsychology (Gold medal winner and honours),** University of Winnipeg, Winnipeg Manitoba

8 EMPLOYMENT

2014 – 2015	**General dentist,** Dental Choice**,** Calgary Alberta
2014	**Locum tenancy,** Foothills Medical Centre Dental clinic, providing clinic supervision to general practice dental residents
2014	**Surgical Assistant at Calgary Health Regional** to Dr. Miller Smith, Dr. Graham Cobb and Dr. Brett Hebijanic
2014	**Surgical assistant** at South Calgary Oral and maxillofacial, private OMFS clinic, Calgary Alberta

9 SCHOLARSHIPS AND AWARDS

2013   **Graduate with Honours**, achieved a minimum cumulative G.P.A. of 3.8

2012   **Dean's Honours**: achieved a minimum sessional G.P.A. of 3.8

Dr. Jack King Memorial Scholarship: top mark in Periodontology, Oral diagnosis and Radiology

Dr. J.B. Rumberg and Dr. H Rumberg Memorial Prize: top mark in Oral diagnosis and Radiology

2011   **Endowment Fund Scholarship in Dentistry**: high academic achievement while demonstrating communication and leadership skills

Dr. John M. Grahame Scholarship: best combines scholastic achievement, general character and participation in extra-curricular activities.

Winnipeg Police association scholarship: high academic standing

2010   **Dean's Honours**: achieved a minimum sessional G.P.A. of 3.8

Leonard Krueger Scholarship: high academic standing,

Wilhelm Kristjianson scholarship: A student of Icelandic descent with good academic standing that displays qualities of leadership and community service

Winnipeg Police association scholarship: high academic standing

2006-2009 University of Winnipeg entrance scholarship 2006
University of Winnipeg academic merit scholarship 2007, 2008
Winnipeg police association scholarship 2006, 2007, 2008

PUBLICATIONS

1. Rogala B, Kerr Z, Shimizu M, (2018) Septic Arthritis of the Temporomandibular Joint in a 10 Year Old: A Case Report and Literature Review, Journal of Oral and Maxillofacial Surgery, *in press April 2019*

2. Rogala B, Li Y, Li S, Chen X, Kirouac GJ (2012) Effects of a Post-Shock Injection of the Kappa Opioid Receptor Antagonist Norbinaltorphimine (norBNI) on Fear and Anxiety in Rats. PLoS ONE 7(11)

3. Aujla H, Hutton C, Rogala B,(2013) Assessing Anxiety and Reward- Related Behaviors Following Alcohol Administration or Chronic Stress. J Alcoholism Drug Depend 1:136

CITATIONS OF ACADEMIC PRESENTATIONS

1. Rogala B, Concomitant facial and cervical spine fractures in the geriatric population. 2018 Ontario Society of Oral and Maxillofacial Surgeons residents night.

2. Rogala B, Jackson- Boeters, Khan Z, Lapointe H, Darling M. Phenotype of granular cell tumours. 2018 Western university Schulich school of medicine and dentistry department of Pathology research day.

3. Rogala B, Jackson- Boeters, Khan Z, Lapointe H, Darling M. Investigating the etiology and phenotype of granular cell tumours. 2017 Western university Schulich school of medicine and dentistry department of Pathology research day.

4. Rogala B, Li Y, Chen XY, Li S, and Kirouac GJ. Effects of inactivation of kappa opioid receptors with norBNI on sensitized fear following a single episode of footshock in rats. Neuroscience, 2011.

5. Rogala B, Li Y, Chen XY, Li S, and Kirouac GJ. Effects of inactivation of kappa opioid receptors with norBNI on sensitized fear following a single episode of footshock in rats. 2012 Midwest Dental Student Research Conference, 2012.

6. Ben Rogala, Yonghui Li, Xiaoyu Chen, Sa Li, Gilbert Kirouac. Effects of inactivation of kappa opioid receptors on fear sensitization in a rat model of posttraumatic stress disorder. Manitoba Chapter of Society for Neuroscience, 2011

7. Ben Rogala, Yonghui Li, Xiaoyu Chen, Sa Li, Gilbert Kirouac. Effects of inactivation of kappa opioid receptors on fear sensitization in a rat model of posttraumatic stress disorder. University of Manitoba Undergraduate Research poster competition, 2011

8. Rogala B, Li Y, Chen XY, Li S, and Kirouac GJ. Effects of inactivation of kappa opioid receptors with norBNI on sensitized fear following a single episode of footshock in rats. Manitoba Dentistry Association , 2012.

RESEARCH GRANTS

1. **CAOMS Research support grant,** Canadian Association of Oral and Maxillofacial Surgeons foundation for continuing education and research in support of a master's thesis

2. **Natural Science and Engineering Research Council of Canada (NSERC) undergraduate student research grant**. Prestigious undergraduate grant for promising young researchers

ADDITONAL TRAINING

- **2018, AOCMF North America, Orbit fundamentals**
    - o Didactic and practical application of trauma and reconstruction of orbit and midface trauma
- **2017, AOCMF North America, management of facial trauma**
    - o Didactic and practical introduction to approaches to facial trauma

- **2014 Certification from ADA&C continuing education for oral, nitrous and single agent intraperitoneal sedation**
- **Advanced Cardiac Life Support 2020**
- **Pediatric Advanced Life support 2019**
- **Advanced traumatic Life support 2013**

- **Esthetic Alliance Program** in dental implant esthetics 2014
- Hands on Synthes Matrix and Sawbone workshops 2014 2018
- Hands on training for restoring Nobel biocare implants 2014, 2016, 2017, 2018
- Hands on training for restoring Denstply Astra implants 2014, 2018

PROFESSIONAL ORGANIZATIONS

- Canadian Association of Oral and Maxillofacial Surgeons resident member
- Ontario Dental Association
- Royal College of Dental Surgeons of Ontario

ACADEMIC INVOLVEMENT

- 2012-2013 Communications director, Manitoba Dental Students Association
- 2010-2011 Class president and a member of the student faculty council
- 2010- 2013 Students Research Group at the University of Manitoba Faculty of Dentistry
- 2011- 2013 member of the ADEA coSRF

INTERESTS

- Member of Balance Point Triathlon club in London Ontario
- Member of East Side Riders cycling club
- Member of Schulich School of Medicine and Dentistry hockey team